3D PRINTED ANTENNAS: METALIZED PLASTIC

By

Mohd Ifwat Mohd Ghazali

A THESIS

Submitted to
Michigan State University
in partial fulfilment of requirements
for the degree of

Electrical Engineering – Master of Science

2014

ABSTRACT

3D PRINTED ANTENNAS: METALIZED PLASTIC

By

Mohd Ifwat Mohd Ghazali

This thesis introduces the use of 3D printed plastic structures for the fabrication of antenna structures. Use of 3D printing technology allows for a simple fabrication technique that is faster and low cost compared with traditional microfabrication approaches. Two Vivaldi antenna designs are studied first: i) a simple notch antenna with a radiating slot line cavity and ii) a corrugated Vivaldi with a partially covered cavity. The corrugations help increase the bandwidth and gain of the Vivaldi antenna. The antennas show an extremely wide bandwidth of approximately 13 GHz and have a gain maximum of approximately 12dB. Further modifications were made by adding bilateral pieces and dielectric focal lens at the radiating end. A larger bandwidth and higher gain was attained. The dielectric guiding structure in the aperture helps to further improve the gain both at the lower frequency and higher frequency regions. The integration of dielectrics in the antenna design is readily achieved using 3D printing. Apart from the above Vivaldi antenna designs, three other antenna designs were also studied. This includes a dielectric loaded monopole antenna, a patch antenna and a reconfigurable Lego-like antenna. Complex 3D antenna structures and novel antenna designs that use a combination of dielectric and metal regions are studied and these structures can readily be fabricated using 3D printing.

ACKNOWLEDGEMENTS

First and foremost, I praise God, the almighty for providing me the strength and His blessing in completing this thesis. I was able to complete this thesis work with assistance and guidance from several individuals. I would like to take this opportunity by thanking all who contributed in the completion of this thesis.

I would like to express my deepest gratitude to my advisor, Dr. Premjeet Chahal, for his excellent motivation, wisdom, commitment and patience. His invaluable help of constructive comments and suggestions throughout the experimental and thesis works have contributed to the success of this research.

Secondly, I would like to thank the committee members, Dr. Edward Rothwell and Dr. Nelson Sepúlveda for their advice and detailed review of my thesis and providing me great feedback on my research work.

I sincerely thank all my colleagues in the TESLA group, in particular Kyoung Youl Park, Joshua Myers, Xianbo Yang, Amanpreet Kaur, Nophadon Wiwatcharagoses, Jennifer Byford and Eleazar Gutierrez for their kindness, help, encouragement and for their valuable feedback. Also, I would like to acknowledge all of my colleagues from Electromagnetic Research Group for their help during this research work. I also like to thank Brian Wright for helping me fabricates all the 3D printed structures without his help I would not have been able to complete this work.

I am grateful to the Malaysian Government and Islamic Science University of Malaysia for making it possible for me to study here through a generous fellowship.

Last but not least, my deepest gratitude to my parents, Mohd Ghazali Omar and Noraini Ismail, my parents-in law, Sheikh Mohd Nasir Sheikh Hassan and Hanizah Abu

Hassan and also my brothers and sisters especially Mohd Amin Ghazali for their endless love, prayers and encouragement. Also not forgetting my beautiful wife, Raihan Farhanah Mohamad Hassan who is always there to encourage me and stand by me through good and bad times. I would like to use this opportunity to thank every person who in some way has helped me in making this thesis a reality.

TABLE OF CONTENTS

LIST OF FIGURES

CHAPTER 1

Literature Review

1.1 Introduction and Background

Components with three-dimensional (3D) structure have gained significant interest in recent years. As the technology progresses rapidly, the electronic industry has become one of the main users of 3D component as an integral part of the system or sub-system. The competitiveness of the market to manufacture quality products, catering to individual costumers and at the same time provide dense functionality are the main driving forces leading to interest in this field. This allows the development of multifunctional, compact, miniaturize and light weight devices to be created in order to satisfy the need of the market either for high end technology applications or low cost electronics (e.g, single use RFID technologies). This need and challenge has led to a significant advancement in 3D manufacturing technology for a range of applications. In particular, the advances have been made to design and fabricate 3D physical prototypes rapidly. To date, major emphasis has been to design structures to provide mechanical properties. However, this technology has advanced significantly that 3D fabricated structures can now be adapted to carry out electrical functionality. In particular, 3D technology holds significant potential in the design of antenna structures that provide improved performance as complex 3D structures unimaginable can be easily fabricated. This chapter first gives a brief background on 3D printing and its potential application in the design of electronic circuit components. In particular, the benefits and challenges associated with the adoption of 3D printing of antenna structures.

1.2 Introduction to 3D Printing Technology

Before 3D printing technology existed, thousands of years back humans created 3D objects by all sorts of methods. The original purpose of 3D object was to design sharp objects or pattern material that will be used for hunting and daily usage for survival. Material that was largely used to create 3D object is called hammerstone which is shown in Figure 1.1 [1]. The hammerstone is a hammer like tool that was used to chip away stone and bone to create different 3D objects or tools and the method is called flint knapping [2]-[3]. Such material that was to produce arrowhead, axes and prehistoric knife for hunting while plates and cup for dinnerware. This technique evolved over time and is familiarly called sculpturing. The development of sculpturing evolved to a more sophisticated form which began to use a combination of different materials and tools. The Greeks used chisel to sculpture 3D object as special human body structure out of ceramic and stone while clay was used to design pottery which is usually molded by hand. This technique requires expertise to design complex structure and shape. As centuries passed, the approaches and tools to sculpture 3D objects have evolved to the atomic level. Now humans have a vast range of tools (albeit some are expensive) and materials that can be utilized to grow structures whereby the location of every atom inside a structure can be precisely controlled. To achieve this level of precision on a routine basis still requires significant advancement in technology. One area that has advanced significantly and is easily assemble is the sculpturing of objects using robotics coupled with thin layer film deposition, etching or molding in a precise area location.

Furthermore, the base structure onto which this molding takes places does not have to be planar.

The modern method of creating 3D objects is by using computers to control sawing, turning, drilling and milling machines [4]-[8]. The subtraction process uses blocks of material and carves away until the desired shape is achieved. Figure 1.2 shows an illustration of a subtraction process. The conventional methods have many disadvantages based on the expensive tools required and the loss of material wasted in the process. Beside subtraction methods, there are other conventional methods such as formative methods as a process for creating 3D objects. One of the processes that uses a formative method is an injection molding technique [9]-[12]. 3D objects are created by injecting a liquid material in into a mold under pressure where it fills all the voids and spaces. The material then hardens inside the mold which is then removed from the mold, see illustration in Figure 1.3. For low batch fabrication, this process is very time consuming and expensive in term of the equipment and material used. The major cost factor is the design and fabrication of the mold structure.

Over the past few decades, people have become more aware of the capability of 3D printing technologies often referred to as additive manufacturing. Some have dubbed 3D printing technology to be the next big innovation of this generation. 3D printing methods are a technique of producing a physical model of an object from a digital model. The ability to do so is by creating layer by layer material in the additive process. Layering of many thin films builds up which in the end becomes a 3D object. This technology is similar to having a paper printer on every office desk. This ability allows for rapid prototyping of an object with limitless design, and the control to design and fabricate is given to individual users. This technique eliminates many factors such as using excessive and expensive machinery or the use of adhesive material that is used to combine the parts and even reduce the waste material.

Figure 1.1 Hammerstone used in prehistoric time where the bottom three was made by modern archeology while the top three stone was found in Lizard Man Village, Arizona [1].

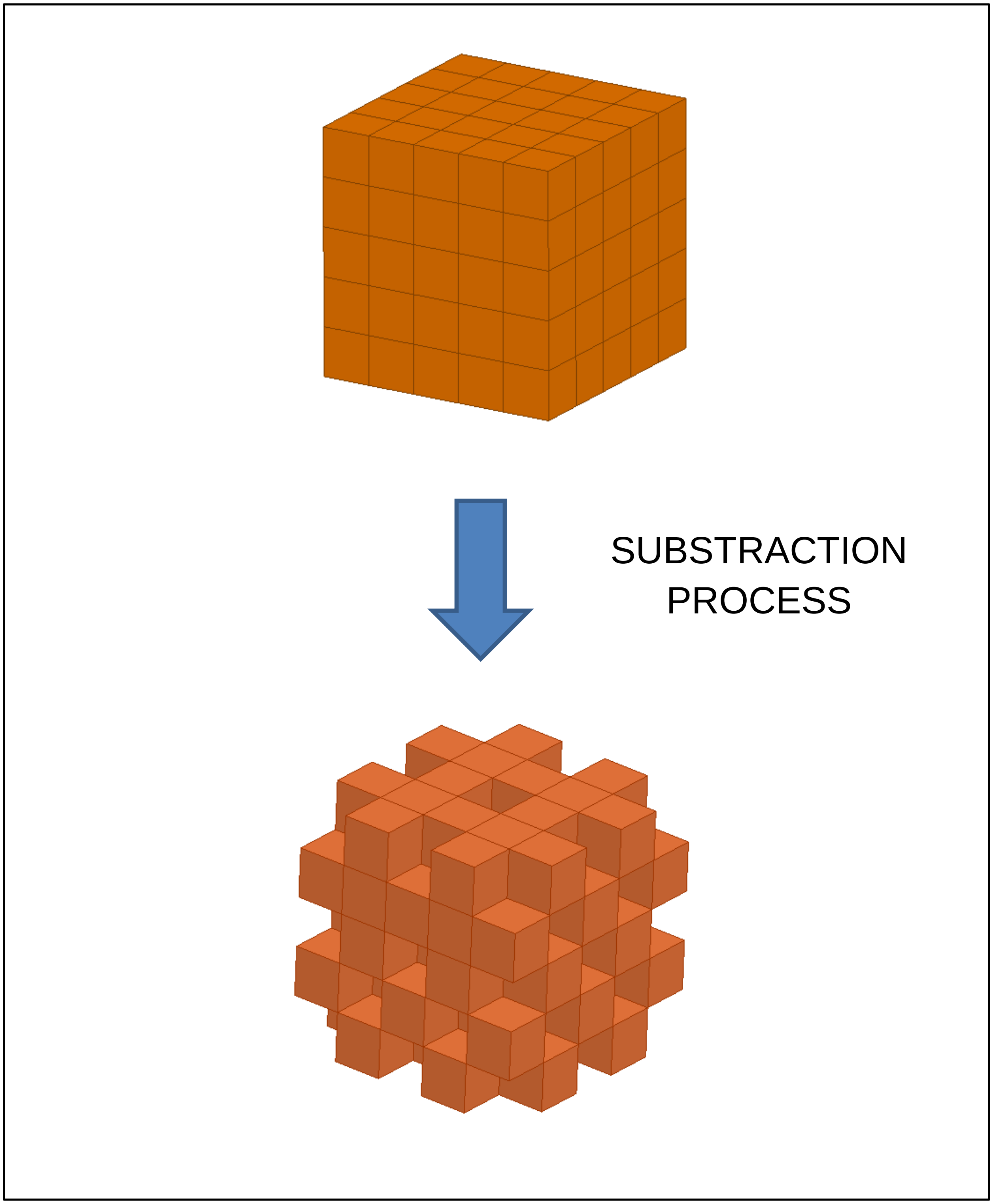

Figure 1.2 Illustration of a material that involve in subtraction process.

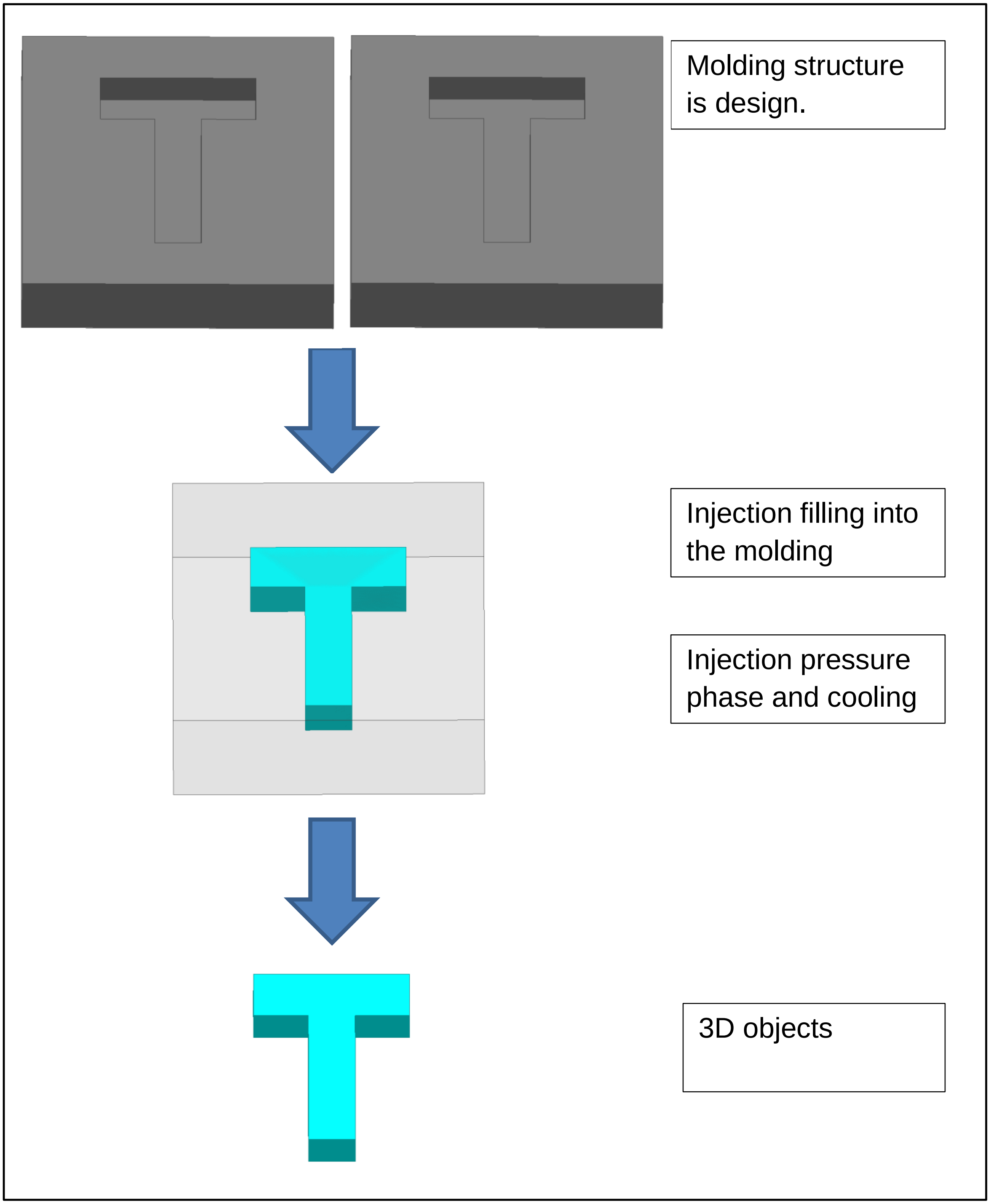

Figure 1.3 Simple illustration of 3D object design by using injection molding method.

1.3 History of 3D Printing Technology

3D printing technology was first introduced in the 1980's for rapid prototyping. The main goal of the technology was to build a prototype of an object in order to test the concept of the product that will be manufactured after preliminary tests. The first report of the concept was introduced by Hideo Kodama of Nagoya Municipal Industrial Research Institutes. He was using photopolymer to create rapid prototypes and published a paper under the title, "Automatic method for fabricating a three-dimensional plastic model with photo-hardening polymer," in 1981 and the schematic of the process is shown in Figure 1.4 [13]-[14]. The method uses a layer by layer technique and exposes the photopolymer area with UV light source to cure the polymer resulting in a 3D object. Further elaborating on the method, Charles W. Hull produced a method called laser lithography or better known as Stereolithography (SLA) in 1984 and the schematic of the process is shown in Figure 1.5 [15]-[16]. This technique uses a computer to deposit a polymer and instantaneously exposes the polymer to a source of UV light. The materials form an adhesive layer on each other allowing them to stick and form the desirable object or design. He was the first to patent this 3D printing process, and was given the credit as the first inventor of 3D printing devices. The technologies progressed rapidly, leading to many different methods for producing 3D printed objects. These methods include digital light processing (DLP), Laser Sintering or Laser Melting, Fused Deposition Model (FDM), Freeform Fabrication (FFF), Binder Jetting, Material Jetting, Selective Deposition Lamination (SDL) and Electron Beam Melting (EBM) 3D printing [16]-[23].

With all the capability presented by 3D printing, manufacturing industries have taken 3D printing to a new level. The first objective of 3D printing was merely creating a prototype of an object in order to test the functionality. However, 3D printing is now creating objects that can be used as end products. Any idea imaginable in a solid shape object that can be drawn or designed in a computer can be transformed in to a physical structure by merely using 3D printing machines. This technology has opened up a vast spectrum of applications in all sorts of fields. Many fields have taken advantage of the capability of 3D printing in order to improve and innovate in their respective fields.

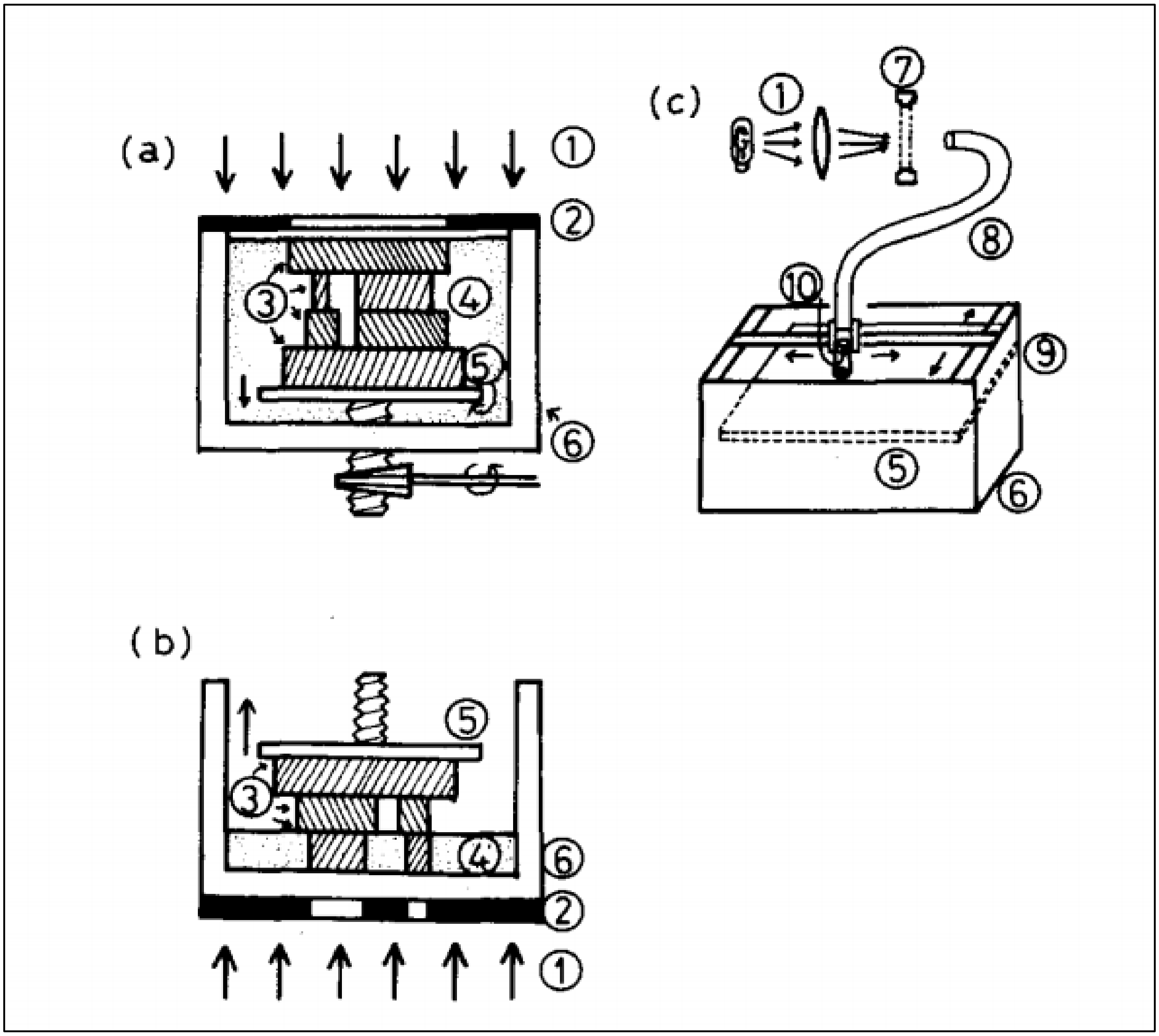

Figure 1.4 Schematic sketches of three types of apparatus constructed in the present work [13].

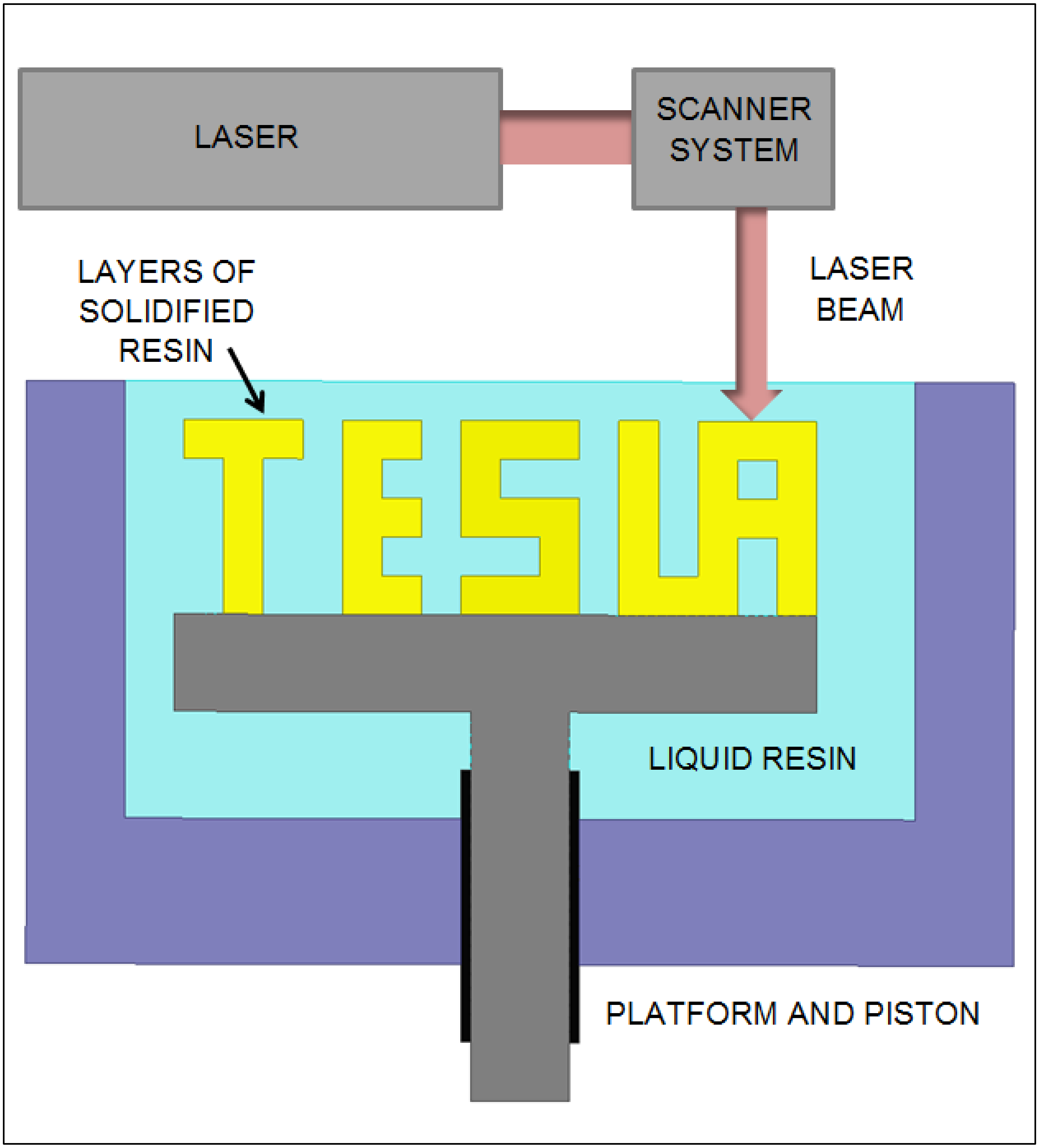

Figure 1.5 Stereolithography apparatus.

1.4 Applications of 3D Printing Technology

The medical field is one of the fields that are taking advantage of the potential of 3D printing. Custom made devices to aid patients are being made using 3D printing such as prosthetic limbs and hearing aids. As 3D printing has evolved, the uses in the medical field have also evolved. 3D printings technology are now used for replicating bones, parts of the body such as ears, skull and even reproducing tissue and organ can be seen in Figure 1.6 [24]-[26]. The main challenge in medical field is to create body parts as close as possible to the natural structure. In one example, a research paper shows the construction of recreating artificial aortic valve using 3D printing technology. As we know recreating human parts is very complex [27]. The way the paper shows is that the used 3D printing technology using material made out of polymer based call poly-ethylene glycol-diacrylate with hydrogels supplemented with alginate. They successfully fabricated anatomical scaffolds which resembles the mechanical function of aortic valve. This paper showed that 3D printing can be done by using different polymer which is able to interact safely with the cells and produce a functional aortic valve can be seen in Figure 1.7 [27].

Other than the medical fields, the automotive sector is one of the earliest users of 3D printing. Automotive industry requires manufacturing individual parts of the car and then assembling them together in an assembly line. Sometimes improvement must be made in order to upgrade the car to improve their quality. 3D printing was employed to make custom parts, to make prototypes and make replacement parts [28]-[30]. One of the new innovations of 3D printing in automotive is creating the whole car using 3D printing. The first 3D printed car was made by Local Motors, see Figure 1.8. The constructed 3D printed car is considered as the new manufacturing method and will be the way of manufacturing cars and parts in the future [31]. Significant advancements in 3D printing technology are still needed to be able to print metal and plastic parts simultaneously.

As stated earlier, plastic was the main source of 3D printing material. The technology is now expanding into printing different materials (e.g., metals, ceramics, etc.). One of the most interesting materials used in 3D printing is edible food substance. The conventional way of creating 3D printed chocolates was by using a cast technique, where the chocolates in a liquid form were poured into the cast and left to be solidified. But with 3D printing technology, the creation of 3D printed chocolates can be simplified and the vast design can be made. This has open up new applications of 3D printing technology in the sector by providing easy customizable 3D printing chocolates and the example can be seen in Figure 1.9 which showcase a chocolate with a face like shape was develop by a group of researcher from University of Exeter [32]. The concept was the same in creating plastic 3D printed object where layer by layer of chocolate was stack onto of each other to create the 3D objects. Based on this development, further research was done to create 3D printing edible food. Different type of food that was able to be done using 3D printing is cookies, mash potato waffles, candy and sugar frosting [33]-[35].

One of the more shocking uses of this technology is the creation of weaponry. The ability of creating weapons using 3D printing was demonstrated by a company called Solid Concept. They were capable of manufacturing a functional rifle using a 3D printer [36]-[38]. Fashion designers have been well known for the expertise in designing unique and complex design structure. High skill set is required to shape and mold accessories in the desirable shape. The modern designer uses 3D printing technology to promote futuristic style that might be the new way of designing clothes. This allows the more creativity in designing because complex shape and design can be easily manufactured. Some of the design is shown in Figure 1.11 to shows 3D printed capability to create clothing and accessories [39].

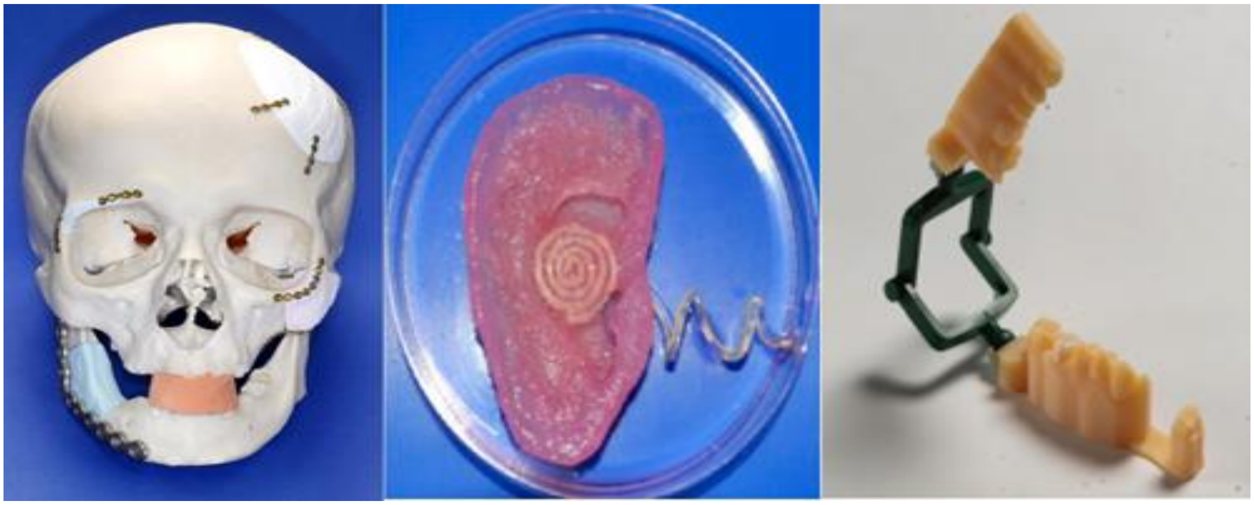

Figure 1.6 Example of 3D printing technology capabilities in medical field [24]-[26].

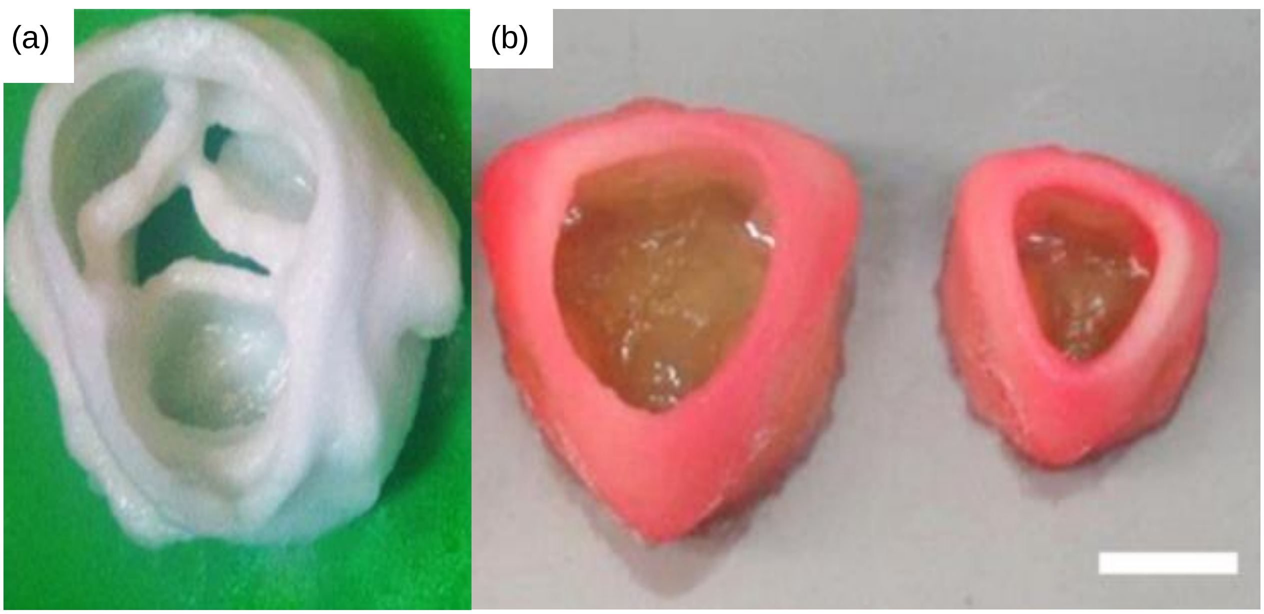

Figure 1.7 3D printed (a) structure of aortic valve and (b) combination of 3D printed aortic valve with hydrogels binding [27].

Figure 1.8 World’s First 3-D printed car [31].

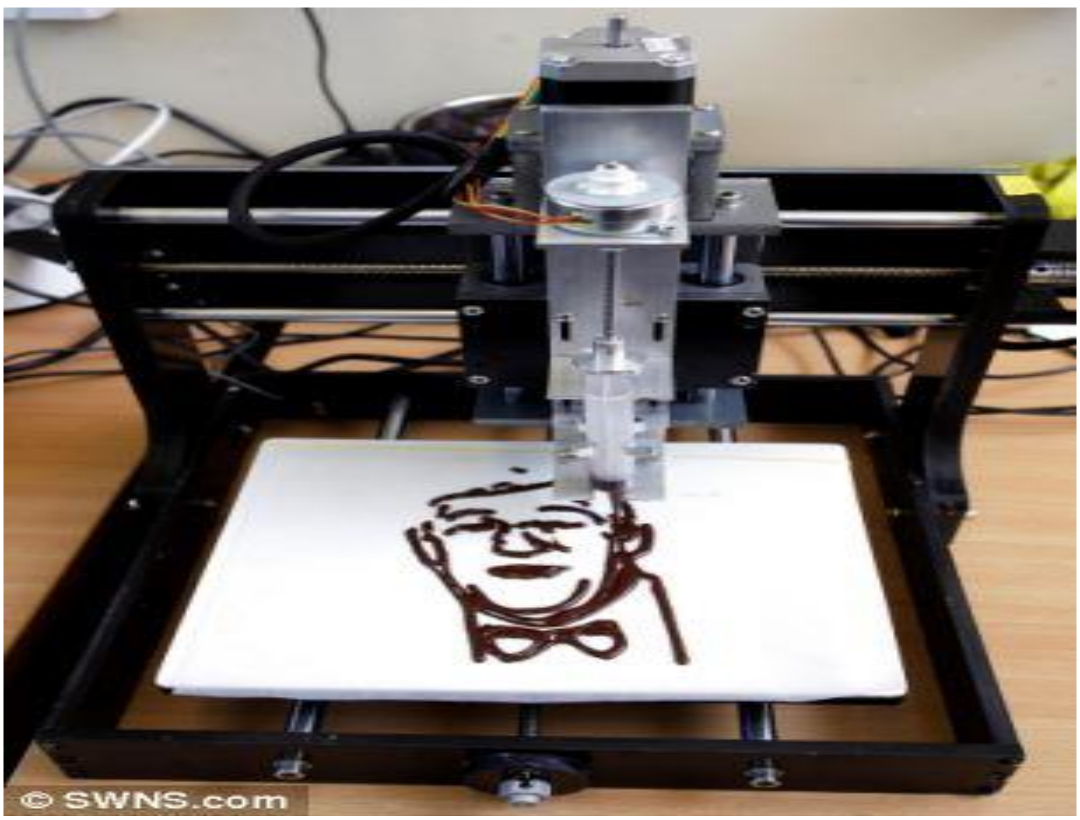

Figure 1.9 3D printed custom made chocolate [32].

Figure 1.10 3D printed gun component made from ABS plastic [38].

Figure 1.11 Necklace and shoes are some of the custom fashion elements that can be made using 3D printed technology [39].

1.5 Electronic Applications

The main focus of this thesis is to show the applicability of 3D printing for the fabrication of electronic components; in particular, antenna elements. Over the last few decades, there has been growing interest in the fabrication of 3D components that allows new functionality and high density integration. Hand-held electronic devices nowadays have become ultra-compact, miniaturize, light-weight and having multi-functionality in the systems. In a typical electronic system, the components are fabricated separately from the housing of the system. However, with recent advances in 3D printing these two can be readily be integrated together leading to the design of high density and complex systems.

The research on the development of compact and miniaturized electronic devices has long been developed. More than 30 years of research have been done to fabricate circuitry to a smaller level scale. In order to obtain such small scale devices a technique called microfabrication technology is commonly used [40]. Microfabrication technology consists of several processes in order to fabricate devices. The process uses lithography process, deposition of materials, pattering of the desire pattern and the etching process which is shown in Figure 1.12. Each process has their own techniques that changes depend of the desire application for the devices. With the advantage of making smaller devices using microfabrciation, applications in integrated circuitry, microfluidic, microsensors and microelemechanical systems (MEMs) was developed [41]-[44]. This allows compact and miniaturizing of devices to be done. However, there is a lot of limitation in using this technique such as the precision is based on the technical ability of the person fabricating and the technology used in the fabrication process as well as the time needed for fabrication takes a longer time [45]. In this case in does not allows the ability to fabricate the whole devices as the enclosure of the circuitry is done independently.

From weight point of view, different types of materials have been synthesized to give components a more feather like weight. One of the most popular materials used in devices nowadays is graphene. Graphene is a thin carbon layer that has many benefits properties such as the strength and durability of the material as well as the light weight aspect [46]-[47]. Graphene has been use in devices for the capability of integrating circuitry in order to enhance the performance and the efficiency of device as well as being used as an enclosure or shielding from electromagnetic waves [48]-[51] . However, the disadvantage of graphene is that it is very expensive due to the limitation in production of high quality material [52]. Furthermore, it does not give the ability to integrate multiple systems in a graphene form devices.

On the other hand, little have been done in designing multifunctional electronic devices that have the ability to multitask by incorporating all the functions into one package. The conventional way of designing multifunctional electronic devices is by building the component separately and assembling it to form the whole device which will take longer to produce and consumes more space.

The main goal of multifunctional electronic devices is to give a more affordable cost, trim down the manufacturing time, and simpler way to manufacture, compactness, combining the functionality into one, light weight and also maintaining the capability to operate well. There are several ways that has been developed to do so. One of the new technologies is 3D integration. 3D integration is a system where layer by layer of active devices are stack and interconnect with one another [53]. The main advantage of this technique is the ability to minimize the work space area by stacking the components by using vias in the z direction (vertical). Significant research is being carried out and tremendous progress has been made in 3D integration such as 3D packaging technology, monolithic 3D integration circuits and wafer to wafer 3D integration circuits [54]-[56]. However, several disadvantages arise due to the risk of having defect during fabrication, the accuracy depends on the sophistication of the machinery especially alignment, the complexity in designing and also the overall cost of manufacturing [57]-[58].

As an alternative, electrical engineering community has adapted the concept of 3D printing because of its simplicity, rapid prototyping, and the ability of print many types of materials at low temperatures on a host of substrates. These manufacturing methods have led to creating new devices and applications. Initially, 3D printing machines were used to merely generate enclosures and packaging elements for electronic devices. The conventional way of packaging electronic devices requires the use of molding material or using metal sheets or plastic to provide an enclosure and protection. However, the expensive molds have to be redesigned every time there is a change in package design or custom designs are necessary. Recently, 3D printing has drastically changed this concept. Companies now have the ability to manufacture packages in all sorts of shape and sizes depending on their needs as well as reducing the time and manufacturing cost.

Other usage of 3D printing is by integrating circuit designs on to packaging such as a substrate or any form of surface that can be printed on [59]-[61]. The conventional way of fabricating electromagnetic structure on a substrates requires careful procedure which include the photoresist application, exposure and developing of photoresist to UV light and lastly the etching of photoresist [62]. This leads to the rise in cost and time spent in fabricating and not to mention the fabrication must be done in a controlled environment due to the sensitivity of the photoresist. Along with these previous requirements there is a need to use potentially hazardous chemicals. An alternative way is by using 3D printing techniques to print the structure directly on to the circuit board or other suitable substrates can be illustrated in Figure 1.13. This application is useful for building circuitry on a compact space such as in aerospace, communication such as cell phone and electronics sensors [63]-[66].

A new implementation of 3D printing within electrical engineering is its use to develop new methods of fabricating antennas. The conventional way of fabricating a 3D antenna depends of the configuration of the antenna. For example a horn antenna is made by cutting out template of coppers or other conductive material and constructing them it in a specific dimension needed for the specific application. The template sheet is then joined together by soldering the pieces. The front end of the antenna is then combined together with the waveguide to form a horn antenna. Another way of fabrication involves subtracting the 3D antenna from a bulk of metal to the desired shape of the antenna. Both of the conventional techniques require sophisticated machinery which increases the cost of production and material waste. As an example, horn antennas have been fabricated using 3D printing technology. Theses antennas show the performance and the functionality to be as close as the standard horn antenna that is produced using conventional labor intensive machining processes [67]. Other type of antenna that used 3D printing method for fabricating is electrically small spherical wire antenna. This 3D printed antenna shows the capability of having similar characteristic with a well-known folded spherical helix antenna [68]. Both antennas are shown in Figure 1.14. Although these early results have shown the benefit of using 3D printing in place of conventional fabrication approaches, there is significant potential in using 3D printing to design novel antenna structures. New structures that can improve antenna performance and also new designs that would be difficult to achieve using conventional fabrication approaches are possible through 3D printing. The next section outlines the objective and motivation of this thesis work.

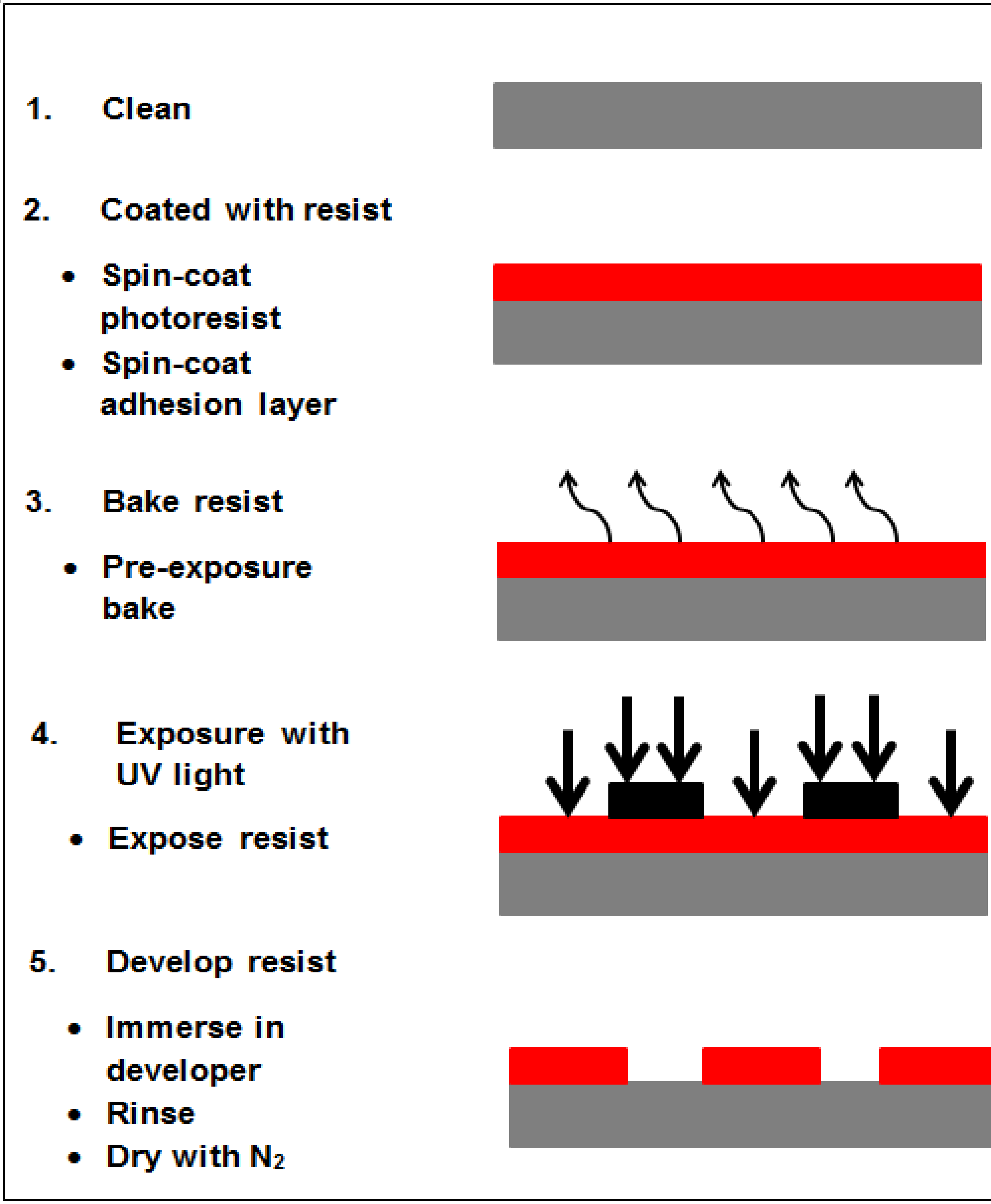

Figure 1.12 Microfabrication process flow.

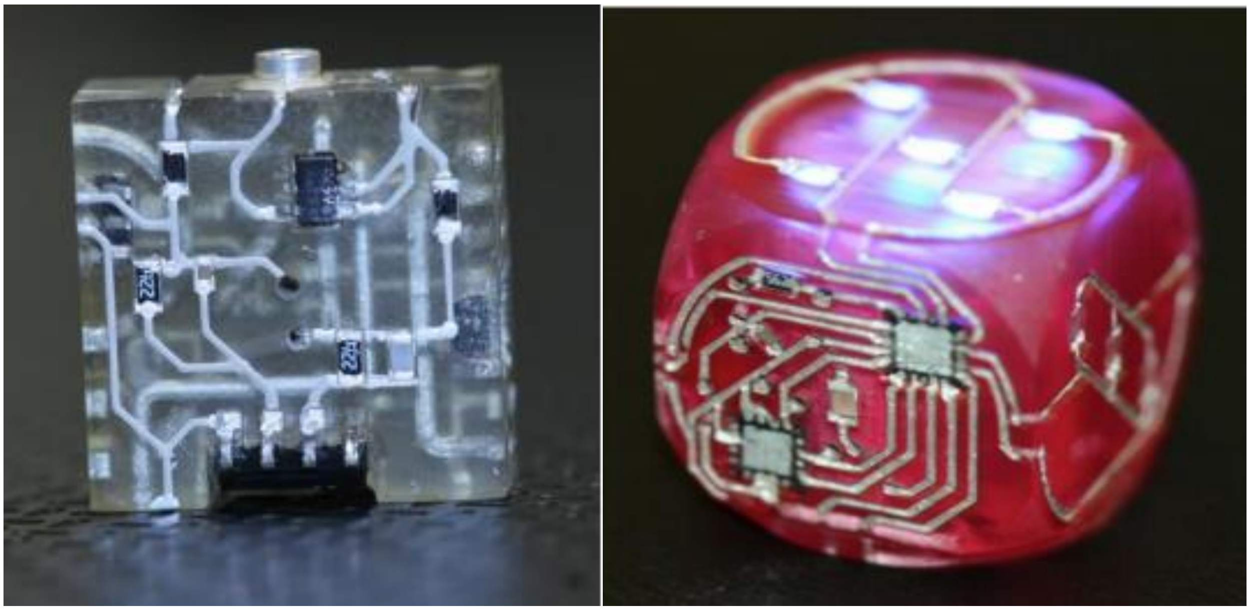

Figure 1.13 3D printed signal conditioning circuit and Electronic circuit mechanically designed into substrate [61].

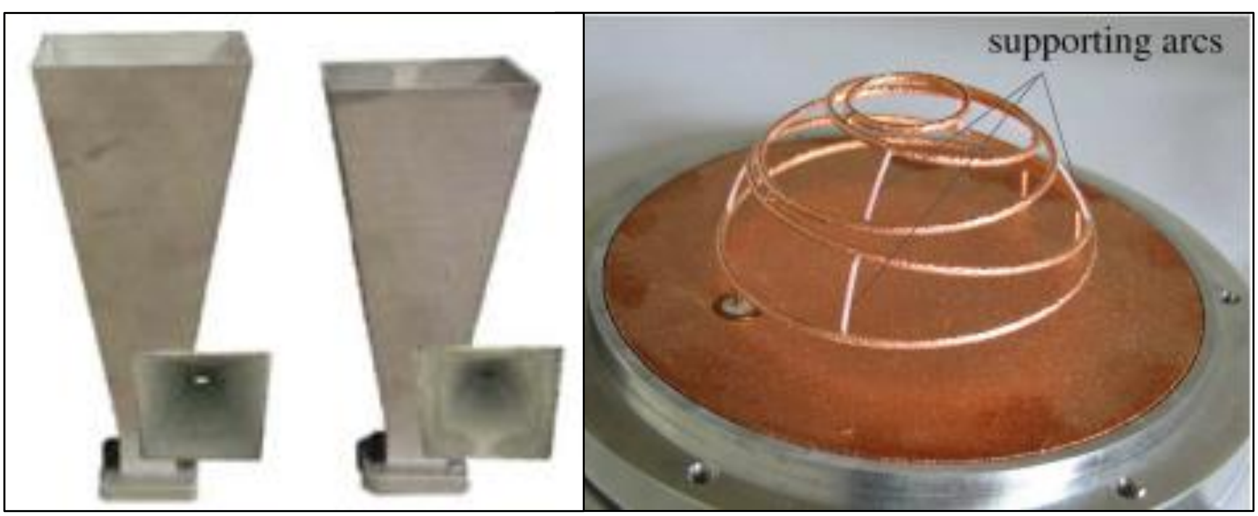

Figure 1.14 3D printed horns and spherical wire antenna [67]-[68].

1.6 Motivation and Objectives

In recent years, the interest towards wireless communication has become a topic of significant interest due to growing wireless applications. Antennas are an essential part of these wireless systems. Antenna designs are complex and they need to meet requirement for functionality or application, bandwidth, gain, efficiency, coupled with need to meet high reliability and low cost manufacturing. Various techniques have been applied in the fabrication of antennas. However, very little work has been reported in open literature on the design and fabrication of antennas utilizing 3D printing technology. The main focus of this thesis is to develop an alternative way to fabricated microwave antennas using low cost processes. In particular, the goal of this thesis is to design and demonstrate 3D printed wide band microwave antennas.

A Vivaldi antenna design was chosen in order to prove the concept that wide band high frequency operating antenna can be fabricated using 3D printing technology. Furthermore, Vivaldi antenna has high gain, symmetrical radiation pattern as well as excellent directivity due to the end-fire nature of the antenna. Also, Vivaldi can be designed to have a 3D physical structure which can be used to improve its performance. One of the major challenges with 3D printing is that a separate feed is required to excite the antenna that cannot be directly printed. Thus, a novel feed technique was devised for the antenna designs of this work. In this work, first a simple Vivaldi antenna was designed and fabricated and then improved based on the flexibility provided by 3D fabrication. This includes the physical structure as well as the ability to combine localized metal and dielectric regions within an antenna to achieve novel designs.

Apart from Vivaldi antennas, other antennas are also studied in this thesis work. This includes a patch antenna and a reconfigurable monopole antenna. The 3D printed dielectric is studied as a substrate for the patch antenna. 3D fabricated dielectric loading elements are also studied to change the resonant frequency of the monopole antenna. Additionally, a reconfigurable Lego like antenna will be presented in this thesis. This antenna demonstrates the concept of an interchangeable antenna element through the use of a combination of dielectric and metallic granules (Lego like blocks). This thesis presents both simulation results and measured results and these results are discussed in detail.

1.7 Thesis Layout

As a proof of concept, Chapter 2 will show the capability of building Vivaldi antenna using 3D printing technology. The performance of the antenna is based on the antenna parameters such as frequency operation (bandwidth), voltage standing wave ratio (VSWR), radiation pattern, beamwidth and gain of the antenna. This chapter shows that the performance of the Vivaldi antenna can be improved compared to conventional designs

In chapter 3, the concept of integrating a dielectric focusing element in Vivaldi antennas is introduced that can readily be fabricated using 3D printing. It shows that 3D printing readily allows integration of complex 3D dielectric and metallic parts which provides additional flexibility in antenna design. This chapter shows new Vivaldi antenna designs with enhanced performance. Also, novel antenna designs are presented that shows that tunable antennas can be designed using 3D printing.

Lastly, chapter 4 concludes the work of this thesis and also gives a brief outline of potential future work that can be carried out in the area of antenna designs using 3D printing technology.

CHAPTER 2

3D Printed Vivaldi Antenna

2.1 Introduction

Antennas have become an essential component in modern day electronics for a variety of applications including wireless communications, wireless sensors, RFIDs, military radar, and biomedical imaging [69]-[70]. A number of antenna parameters are important for these applications, such as antenna size, bandwidth, gain, and cost. Antenna bandwidth is of particular interest in a variety of applications. There are several types of well-known wideband antennas, such as horn, biconical, helical, and sleeve antennas [71]. There is also a significant effort in the research community to develop novel wideband antennas. In particular, much work has been done in the development of ultra-wideband antennas (UWB). UWB antennas are defined as any antenna with a bandwidth greater than at least 30 % of its center frequency [72]. However, due to recent FCC regulations allowing the transmission of low power signals from 3.1 to 10.6 GHz, there has been a particular interest in developing antennas with enough bandwidth to cover the entire range [73].

While antenna bandwidth is of particular interest for many communication systems, the gain of the antenna is equally important. Designing an antenna which combines a wide operating bandwidth with high-gain that is also compact in size, low-cost, and simple to fabricate is a challenge. One such antenna that combines many of these parameters is the Vivaldi antenna.

The Vivaldi antenna was first introduced by B.J. Gibson in [74] as an alternative wideband antenna. A traditional Vivaldi antenna contains an exponential tapered slot, and acts like end-fire travelling wave antenna. Based on its end-fire characteristic, the Vivaldi antenna has a high-gain, consistent radiation pattern over a large frequency range. Theoretically, a Vivaldi antenna can have infinite bandwidth; however, in [75] a traditional type Vivaldi antenna is shown to operate over a frequency bandwidth of approximately 4.9 GHz with center frequency of 2.45 GHz. When designing and fabricating a Vivaldi antenna, several methods have been suggested, the most common of which is a planar structure fabricated on a dielectric substrate [76]-[78]. While these methods produce a high-gain and wideband Vivaldi antenna, they can be difficult to feed and difficult to fabricate. Recently, 3D printed manufacturing processes have become very popular in the research community due to their ability to build precise geometric models of complex designs [79]-[81]. 3D printing also shows much promise in antenna design, as the fabrication process will be much faster, simpler, and very low cost. Additionally, the rigidity and flexibility of the structure allow a reliable antenna to be built. However, most 3D printed antennas in the current literature are printed directly from metal, as opposed to using a dielectric host structure [82]-[83]. Here, two high-gains, wideband Vivaldi antennas are made from a metalized-polymer 3D printed material. The first Vivaldi antenna consists of a simple slot-line design with a radiating cavity. The second antenna introduces a corrugated slot with a partially covered cavity, which is shown to increase the gain and bandwidth of the antenna. The antennas are designed using the commercial FEM solver HFSS and assumed made entirely of copper. Each design is 3D printed with a VeroWhite (ABS, Acrylonitrile butadiene styrene) plastic-polymer, and metalized with a thin layer of copper (1μm). The antennas are fed with a simple 50 coaxial cable through a slot that is printed in the design. Finally, the reflection coefficient and radiation parameters of each of the antennas are measured, showing a low reflection coefficient and high gain over a wide frequency band. The simulated and measured results show that these antennas will find application in low-cost UWB communication systems.

2.2 Antenna Design and Simulation

In this section, the design and simulation of the 3D printed Vivaldi antennas is presented. First, a conventional slot-line Vivaldi is introduced, followed by a modified corrugated structure. Solid copper is used to model the antennas, as it is assumed that the thickness of the copper will be negligible in the performance of the antenna. ANSYS HFSS is used to simulate the reflection coefficient and radiation patterns of the antennas.

For the initial slotline Vivaldi antenna, certain design parameters are important in deciding the performances of the antenna. The impedance of the antenna is dictated by the radius of the cavity which acts as a quarter-wave matching circuit in conjunction with the slotline. The tapering of the slot also acts as a smooth impedance transition between the 50 feed and the free space wave impedance. The physical dimension of the slotline Vivaldi antenna is shown in Figure 2.1. The relevant dimensions of the antenna are as follows: the width (W) is 37 mm, length (L) is 107 mm and the thickness (T) is 4.5 mm. The diameter (D) of the cavity is 22.1 mm and the slotline gap (S) is equal to 1.1mm. Finally, the position distance of the coaxial cable to the cavity (P) is 1.17 mm which is the optimize position. Figure 2.2 shows the reflection coefficient and also the voltage standing wave ratio (VSWR). In the graph it shows that the S11 has a large bandwidth from 3.39 to 19.55 GHz. However there was a discontinuity between 4.33 GHz until 4.72 GHz. It may be resulted in an impedance mismatch. The next Figure 2.3 shows the gain versus frequencies. While the slotline Vivaldi antenna provides a high-gain and very large bandwidth, the reflection coefficient can sometimes dip below an acceptable level intermittently throughout its frequency range.

One possible solution is to introduce corrugated edges into slotline of the Vivaldi antennas. The tapered slotline improves the impedance matching at the discontinuous frequencies, increasing the overall bandwidth. The regions where the discontinuities earlier in the simple notch Vivaldi have been better impedance match due to the addition of the corrugated elements. The corrugated edges act as a longer path resulting in a bigger aperture causing a better S11 at lower frequencies [84]. In addition, this design introduces a partially covered cavity which decreases the back-lobe of the radiation pattern increasing the overall gain of the antenna. The geometry of this design is shown in Figure 2.4, with a spacing gap (G) of 1mm, and corrugation periodicity (M) of 4mm, and cover spacing (C) of 18mm. The reflection coefficient was simulated to shows the changes that were due to the corrugated element shown in Figure 2.5. The maximum gain of both antennas as a function of frequency is shown in Figure 2.6. In both cases, the maximum gain occurs in the E-plane. As expected, the gain of the corrugated Vivaldi antenna is increased, especially in the lower frequency regime. However, both antennas have a very high gain over a large frequency range. The comparison was made between the simple notch Vivaldi and Corrugated Vivaldi for reflection coefficient and gain versus frequency are shown in Figure 2.7 and Figure 2.8 respectively.

In order to ensure the approximation of using solid copper to simulate the antennas is a valid assumption, the unmodified slotline antenna is simulated entirely made of copper and with a lossy-dielectric covered in a thin layer of copper. The dielectric used in the case has a $\varepsilon_r = 3.0$ and a $\tan \delta = .02$. The copper thickness for the dielectric case is modeled as 1.0 µm thick. Figure 2.9 shows the maximum gain of the antenna versus frequency for both cases. As expected, there is very little difference in the gain for both cases.

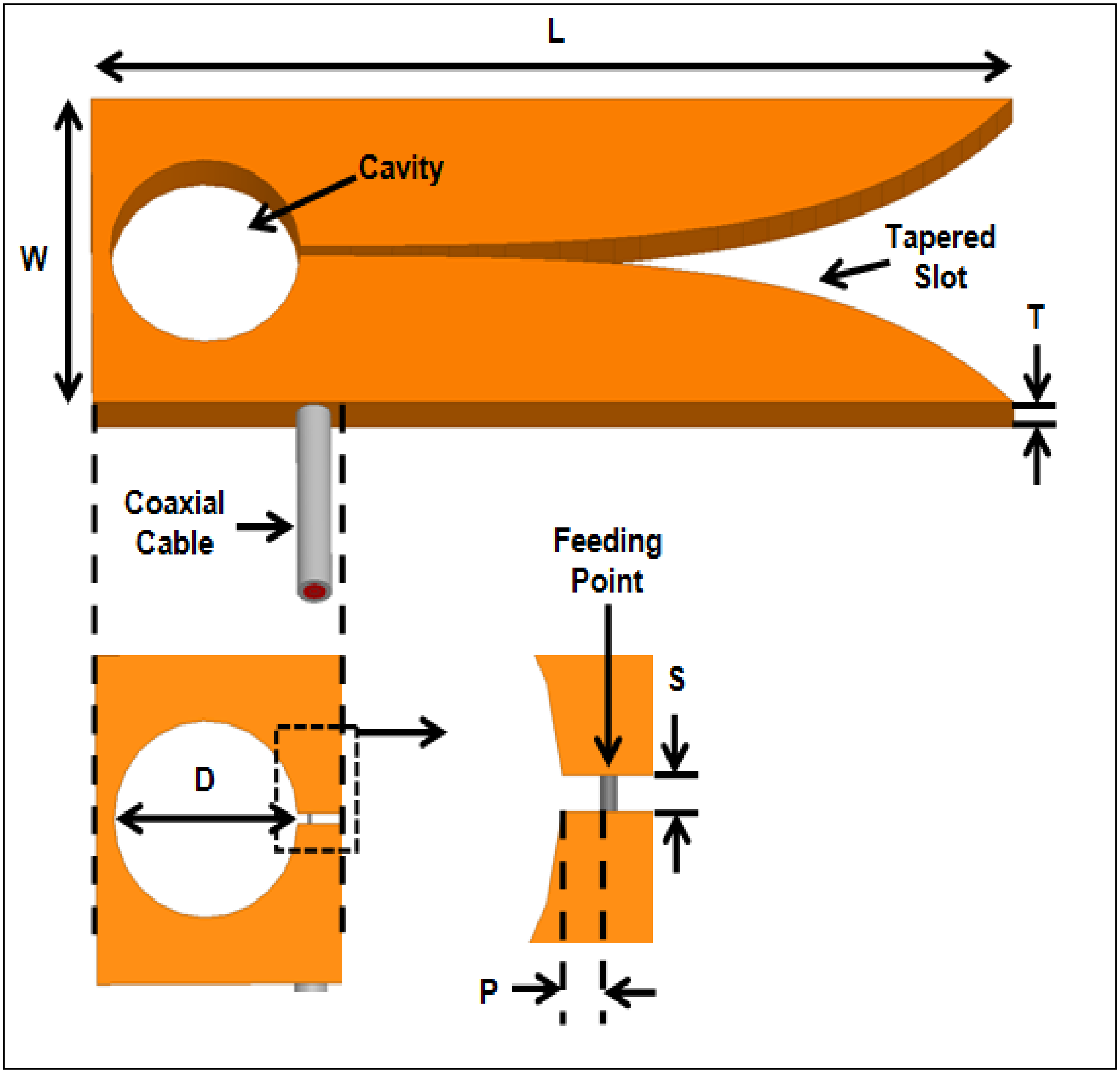

Figure 2.1 Design Parameters of the Simple Notch Vivaldi.

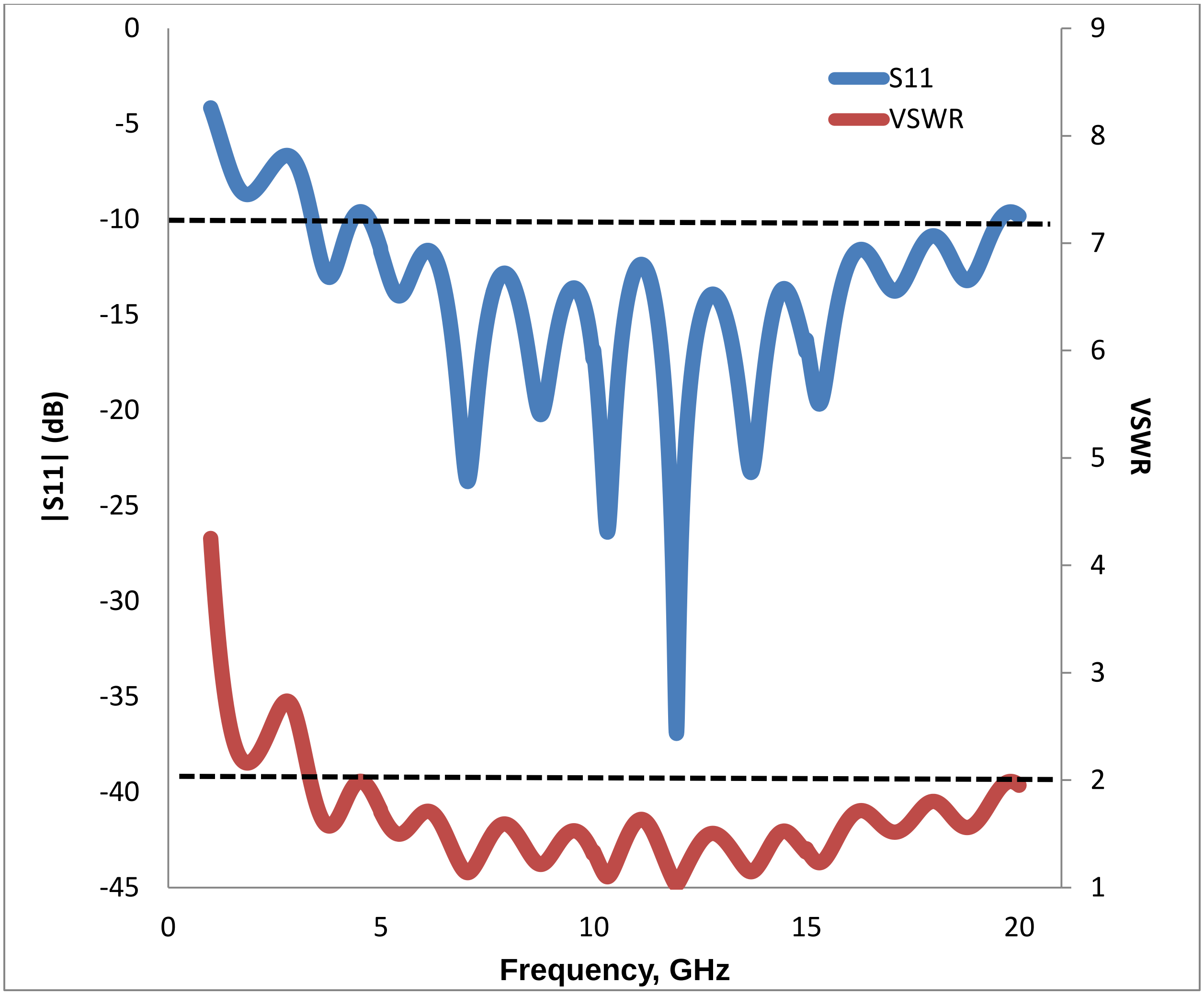

Figure 2.2 Simulated S11 and VSWR for Simple Notch Vivaldi.

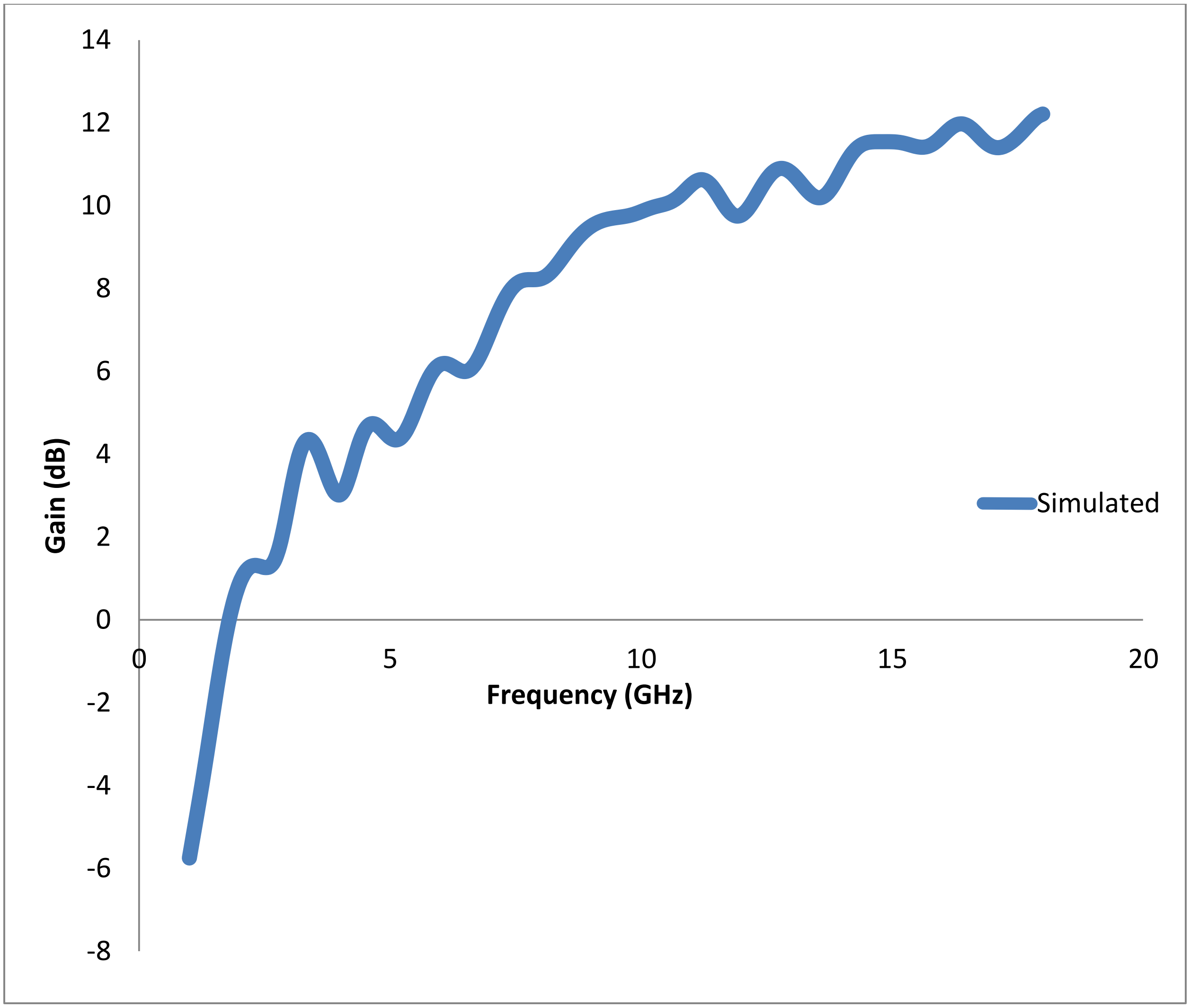

Figure 2.3 Simulated Gains versus Frequency of Simple Notch Vivaldi.

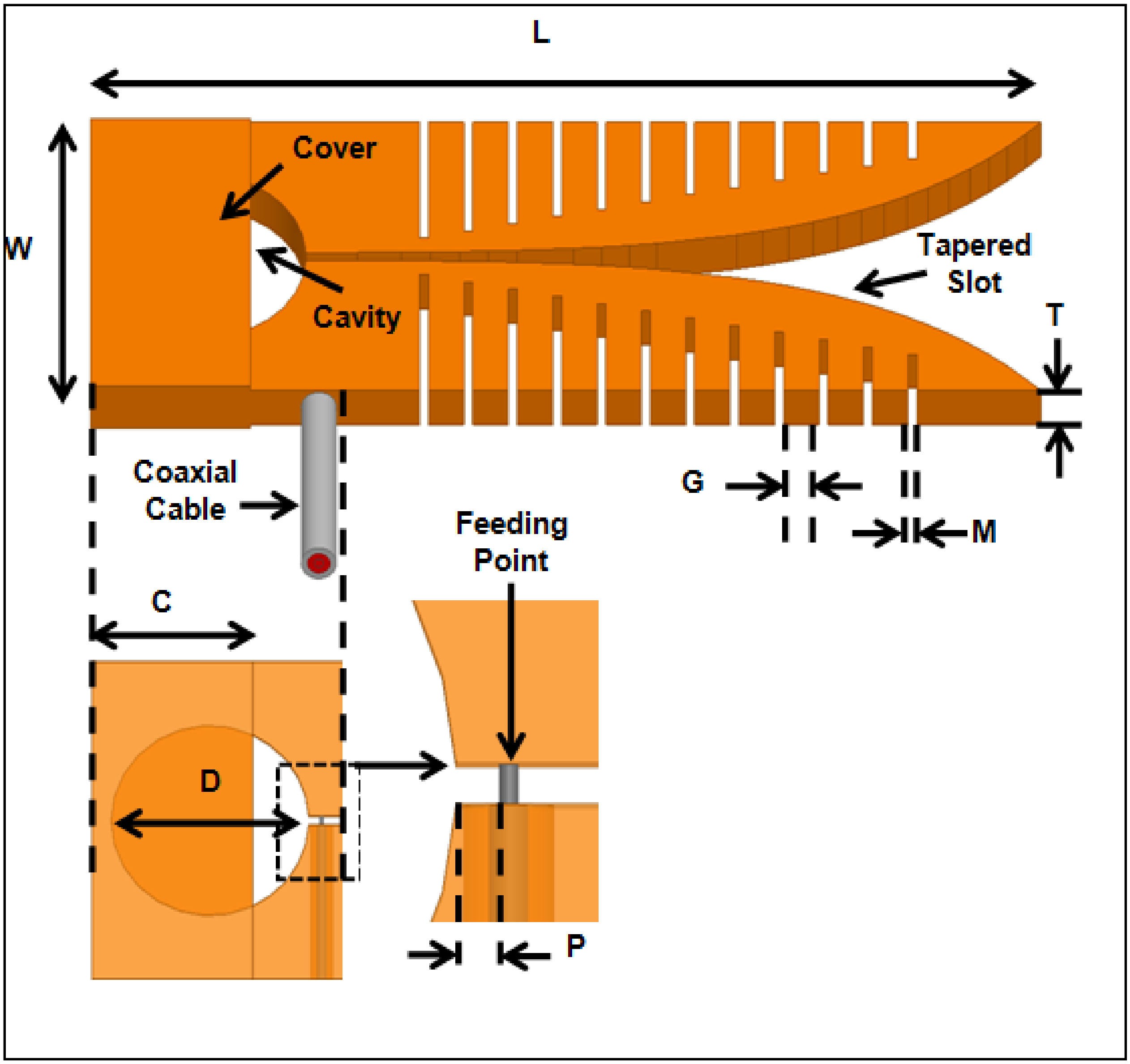

Figure 2.4 Design Parameters of the Corrugated Vivaldi.

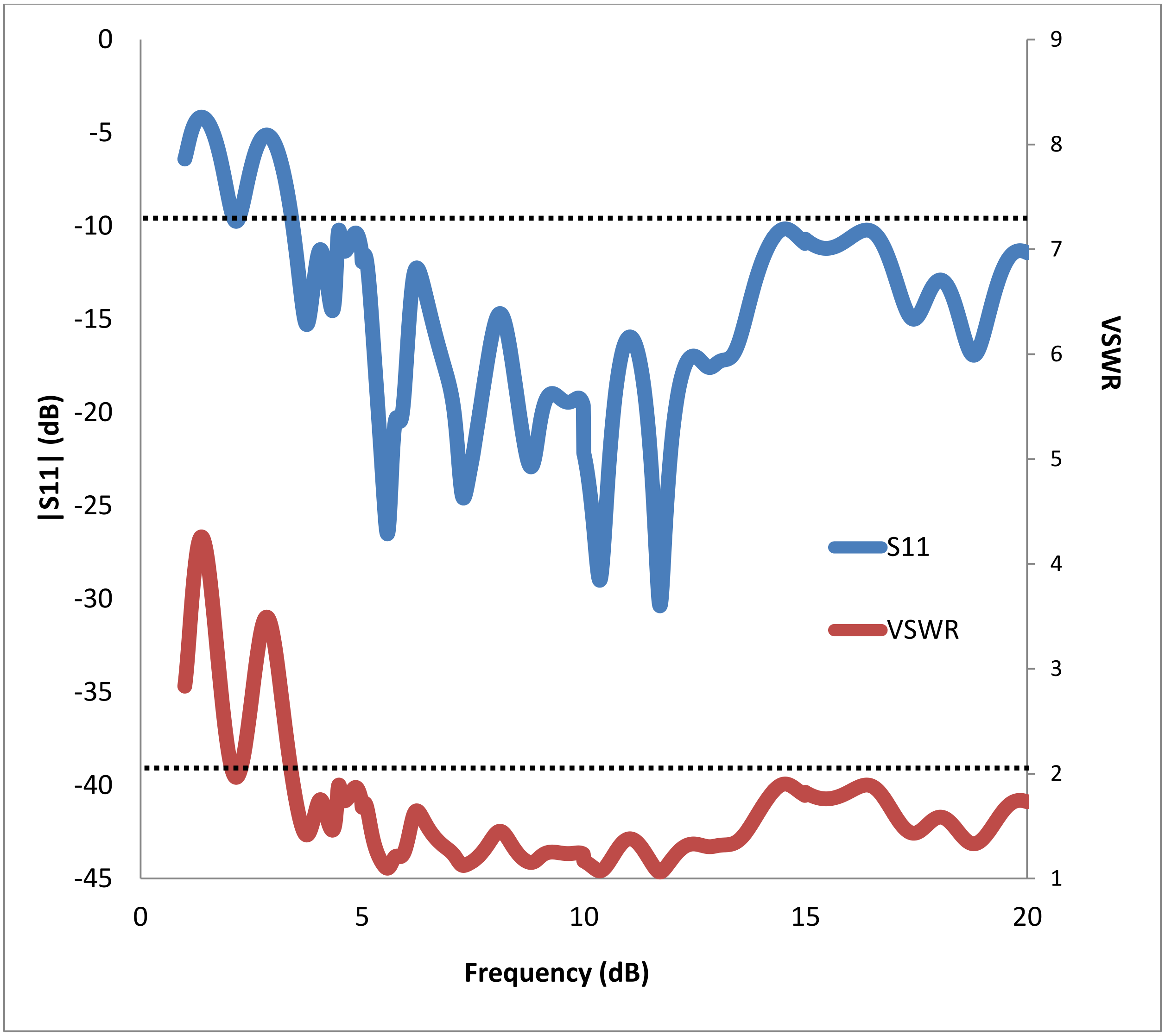

Figure 2.5 Simulated S11 and VSWR for Corrugated Vivaldi.

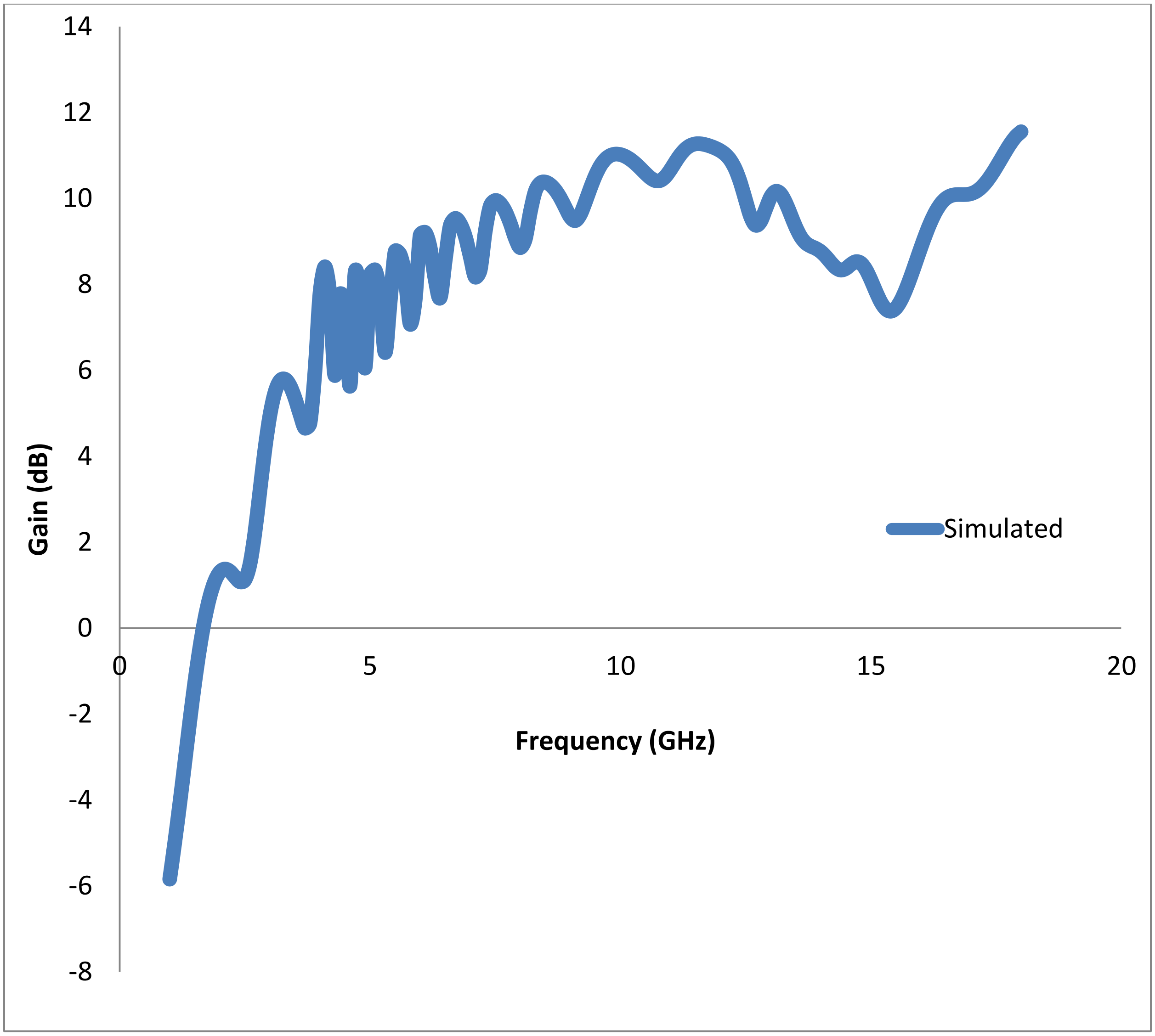

Figure 2.6 Simulated Gains versus Frequency of Corrugated Vivaldi.

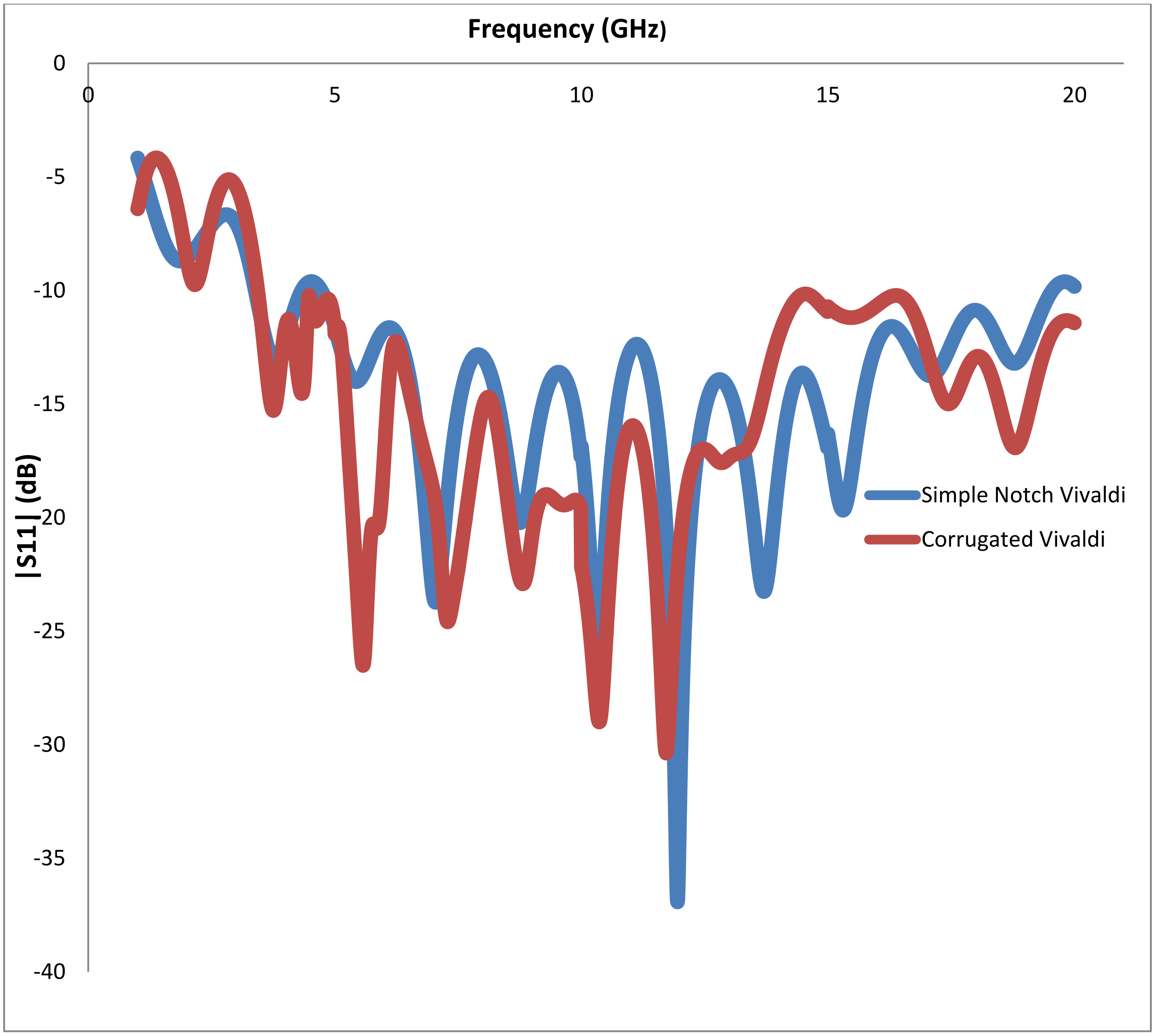

Figure 2.7 Comparison of reflection coefficient for the Simple Notch Vivaldi and Corrugated Vivaldi.

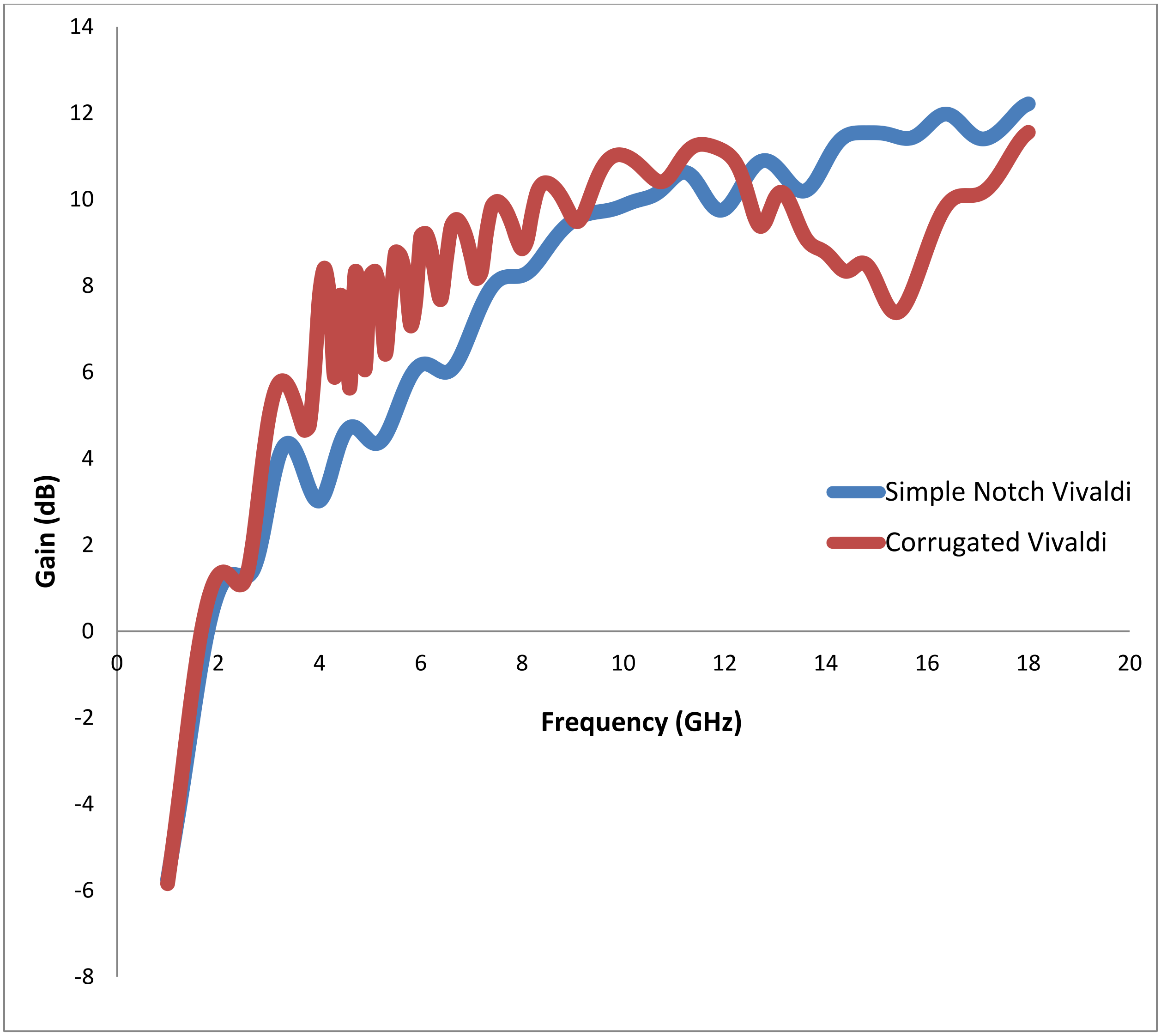

Figure 2.8 Comparison of gain versus frequency for the Simple Notch Vivaldi and Corrugated Vivaldi.

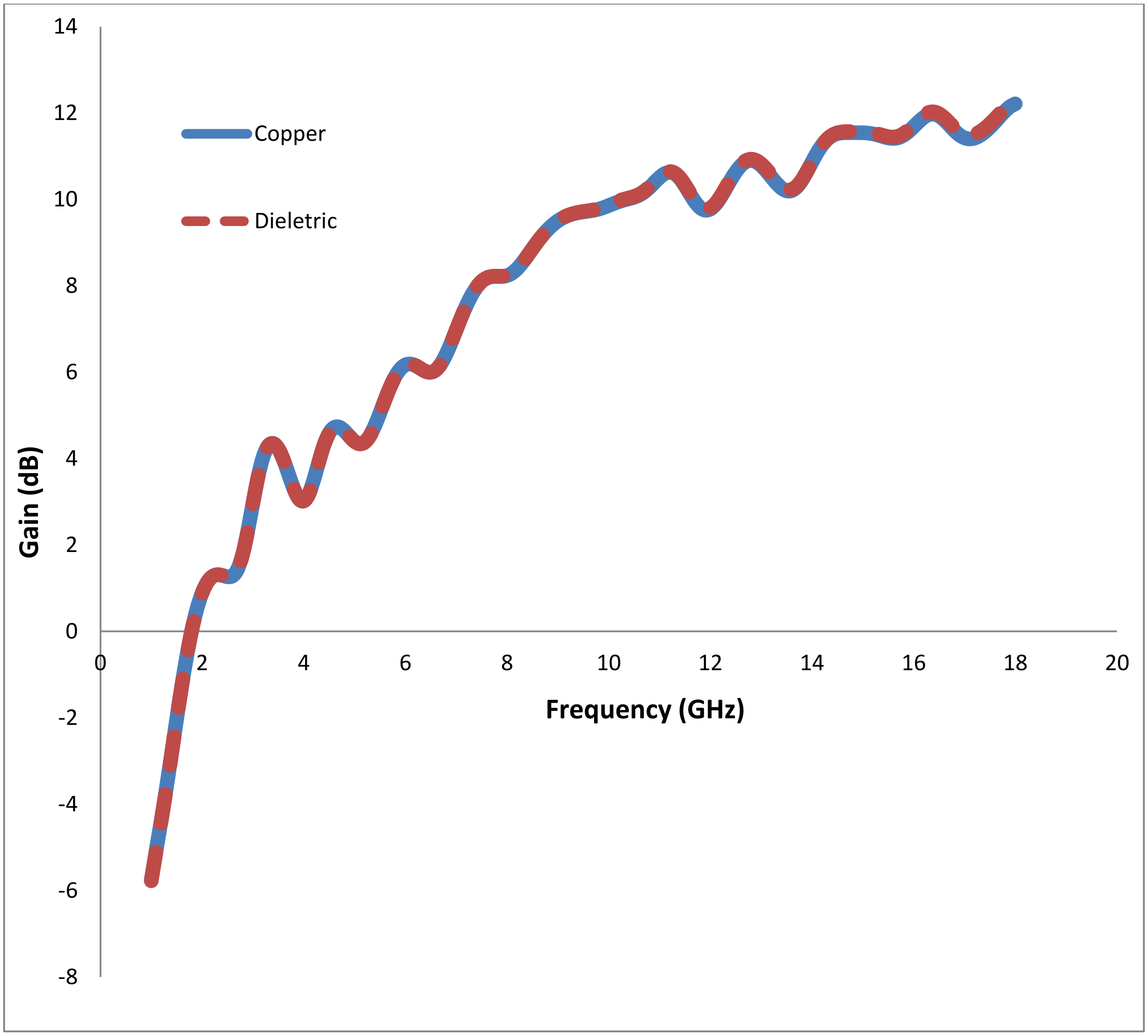

Figure 2.9 Comparison of simulated maximum gain with antenna made entirely with copper and with dielectric covered with a thin copper layer.

2.3 Fabrication and Measurement

After each antenna is designed in HFSS, the 3D model is exported and printed using an Objet Connex350 3D printer. This printer has a 16 μm print resolution, and can be used with a variety of polymer-based materials. In the case of this letter, a VeroWhite plastic-polymer is used to print the antennas. Each antenna is printed in two pieces so that the coaxial cable can be easily inserted. Both sides of the antenna are then fixed together, and the antenna is sputtered with approximately 1μm of copper. Figure 2.10 shows the corrugated Vivaldi antenna before and after the sputtering of thin Cu layer. The reflection coefficient of each antenna is measured with an Agilent N5227A PNA network analyzer. Figure 2.11 and 2.12 shows the reflection coefficient for both the slotline Vivaldi antenna as well as its corrugated counterpart, respectively. The measured reflection coefficients show relatively good agreement with the simulated results. However, there is a slight shift in some of the resonant frequencies of the antennas. This is most likely caused by the sensitivity of the feeding position of the antenna, as well some slight deviation in the printed antenna dimensions. The bandwidth of the antenna is however not disturbed, and as expected the corrugation in the antenna does in fact increase the bandwidth and eliminate any points in the frequency range that were above -10dB. The measured VSWR is also shown in Figure 2.13. A VSWR of less than 2 is shown for both antennas for a very wide range of frequencies. As mentioned above, the VSWR of the initial slotline design does increase above 2 at some intermittent points within the frequency spectrum. The corrugated antenna however has a VSWR that is clearly below 2 from approximately 3.5 GHz to 18 GHz, leaving a bandwidth of 14.5 GHz. Additionally, some select radiation patterns for each antenna are measured. The radiation patterns are measured using a 3D SATIMO antenna measurement system. While each antenna works over a large frequency range, the patterns are measured at 4, 10, and 16 GHz to show the overall behavior at the low, mid, and high frequency ranges. Figure 2.14 shows the radiation patterns of each Vivaldi antenna in both the E (x-y) and H (y-z) planes. Based on the measured results it is obvious that the gain increases with the operational frequency of the antenna as expected. In addition, the beamwidth is decreased as the frequency is increased, which contributes to the increased gain. Comparing between the two antenna designs, it is clear that the corrugated antenna displays an increased gain with respect to the traditional slotline Vivaldi antenna. This is expected considering the VSWR of the antenna is improved between both designs, as well as the covered cavity. The radiation pattern shows a slight deviation of (2 to 4) dB due to several reasons. In the system, the angles which catch the maximum pattern and gain are difficult to obtain based on the placing of the antenna. Secondly, the sensitivity of the connector placement for the coaxial feed can have a large impact of the measured results. The surface roughness of the copper may also have an impact on the results due to the non-uniformity of the sputtering. The miss-match between the measured and simulated results of the antennas becomes more apparent in the higher frequency patterns. Overall, the measured patterns match relatively well with the simulated results, showing the potential of 3D printed antennas for use in UWB antenna applications.

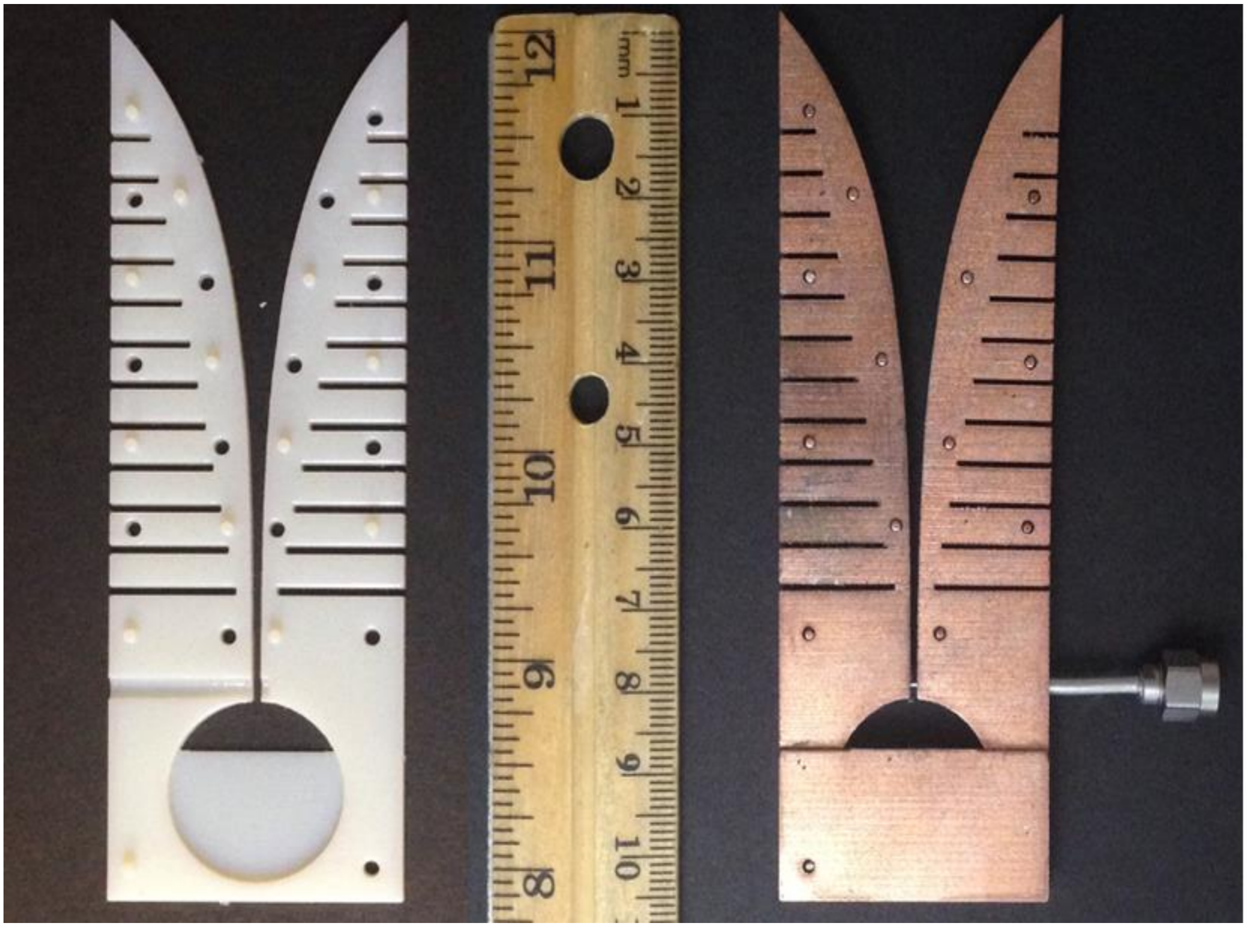

Figure 2.10 3D printed Corrugated Vivaldi before (half piece) and after copper sputtering (completely assembled structure).

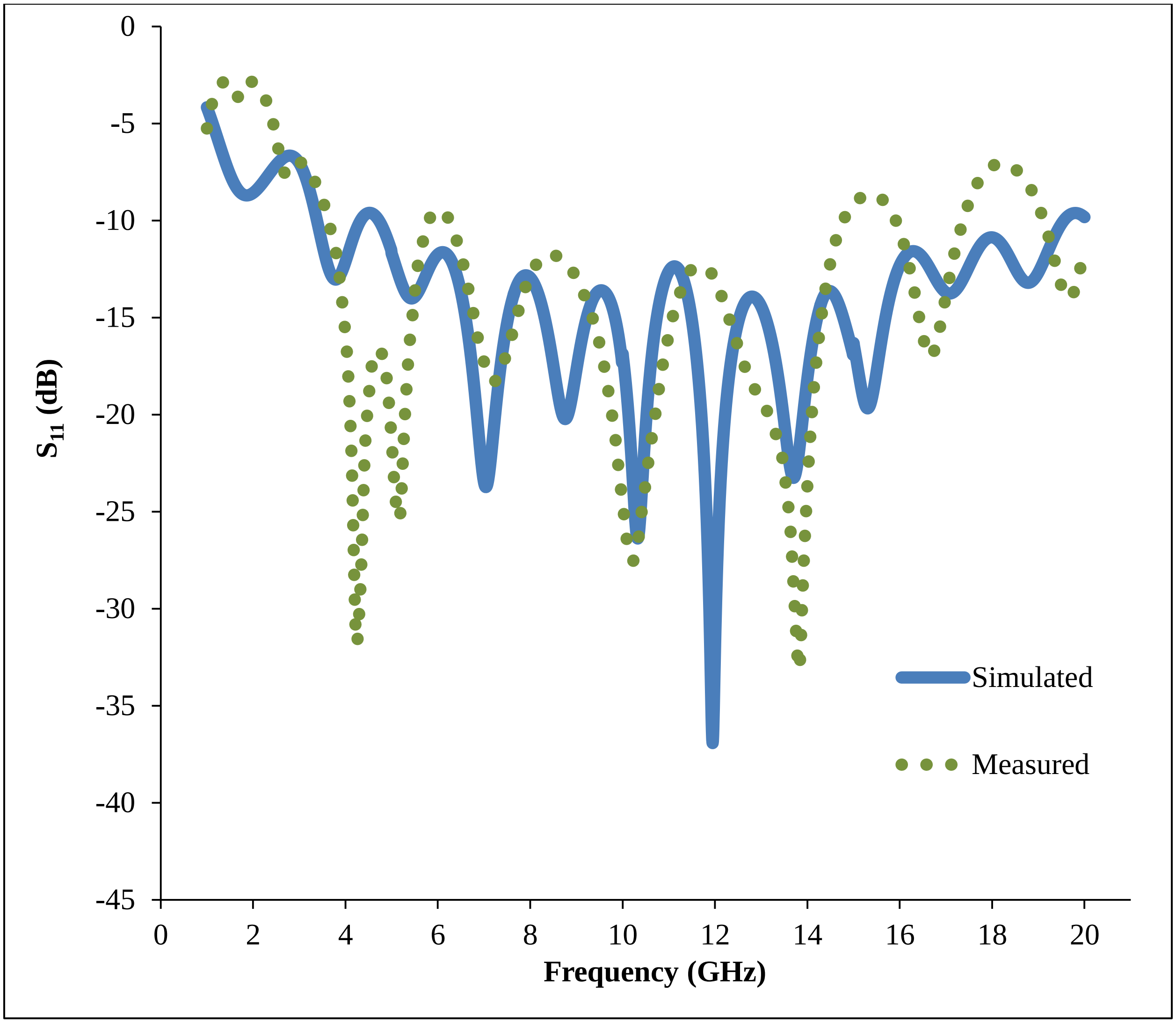

Figure 2.11 Comparison of reflection coefficient between simulated and measured simple notch Vivaldi antenna.

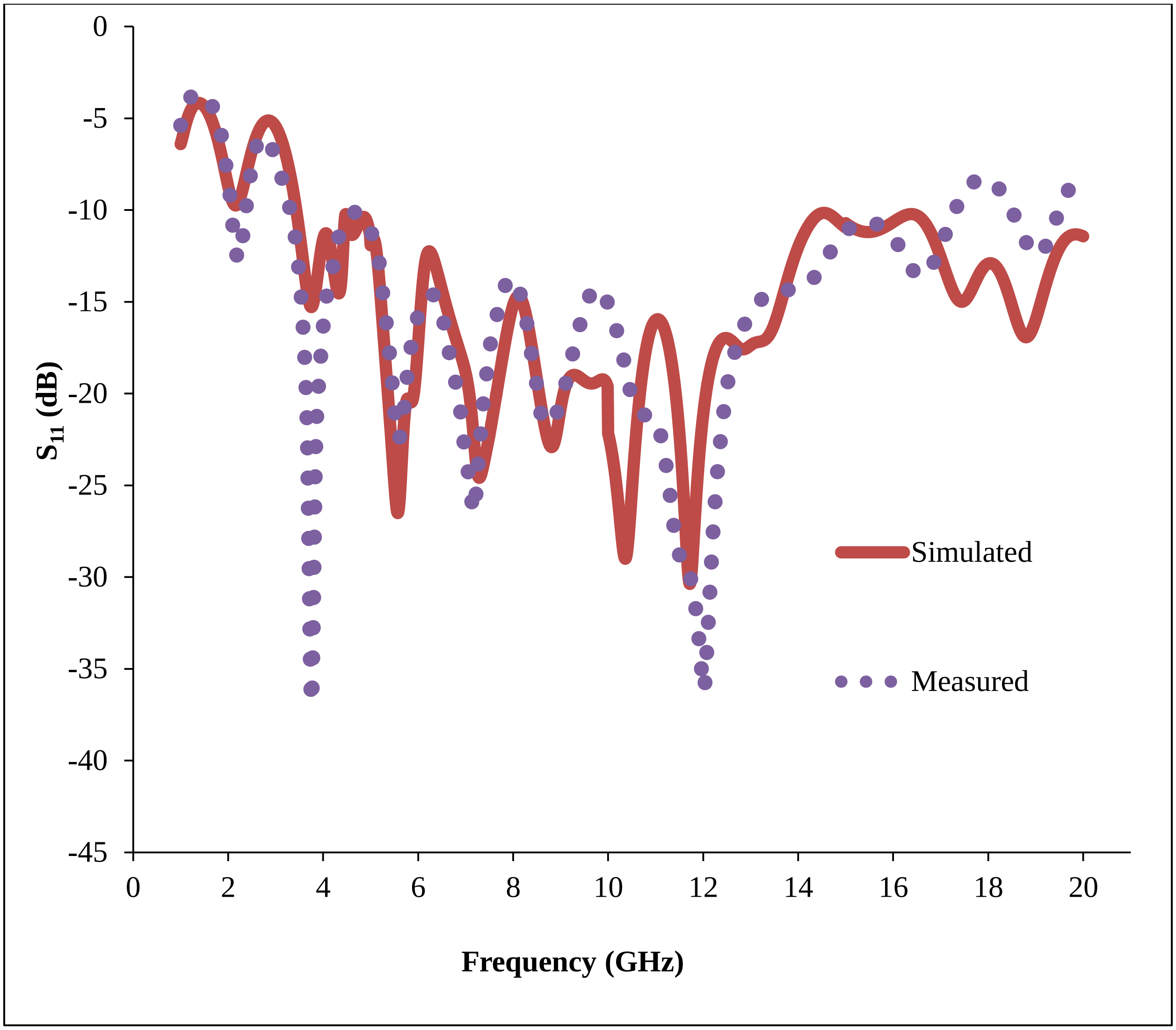

Figure 2.12 Comparison of reflection coefficient between simulated and measured results for Corrugated Vivaldi antenna.

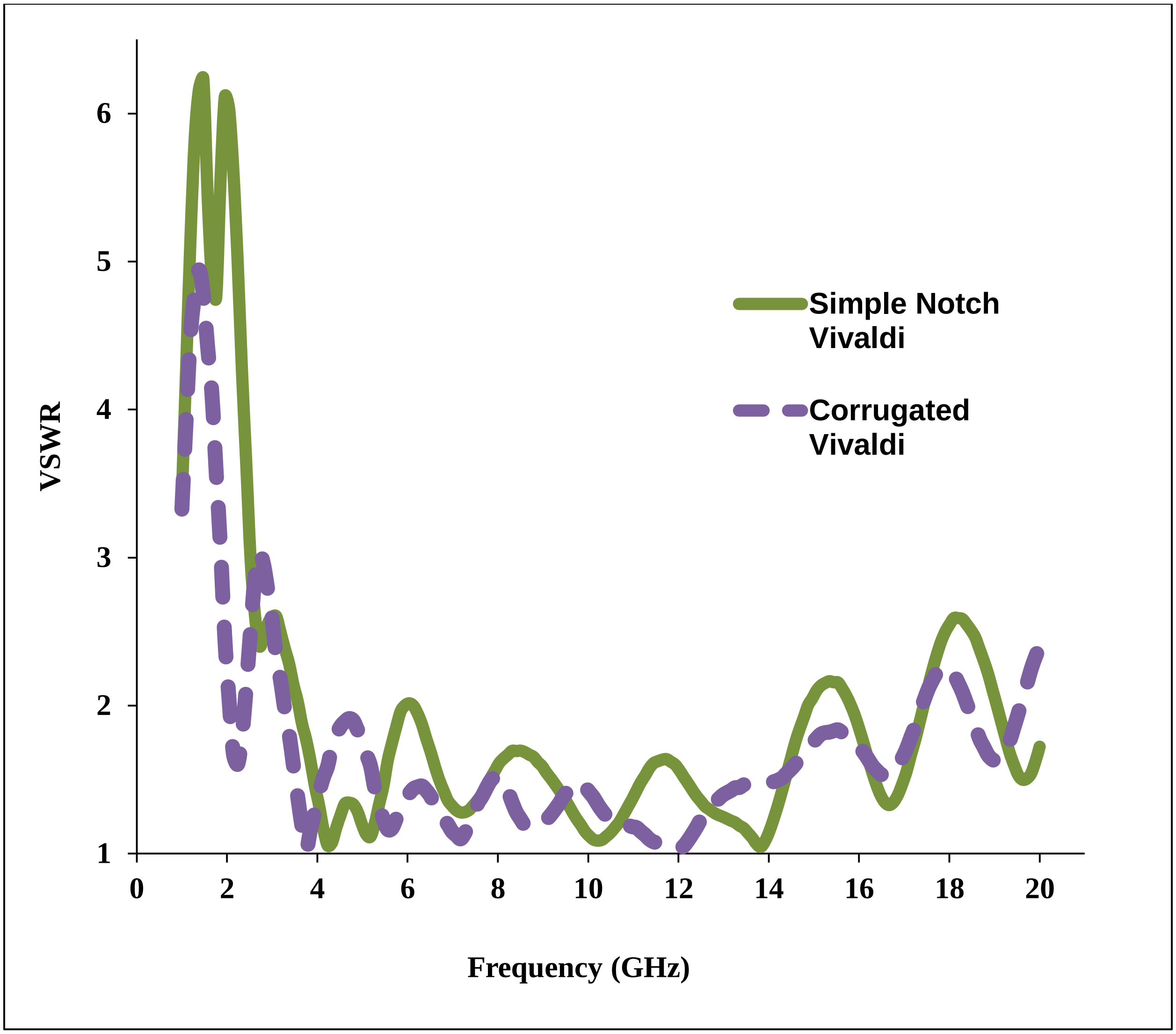

Figure 2.13 Comparison of measured results of simple notch and corrugated Vivaldi.

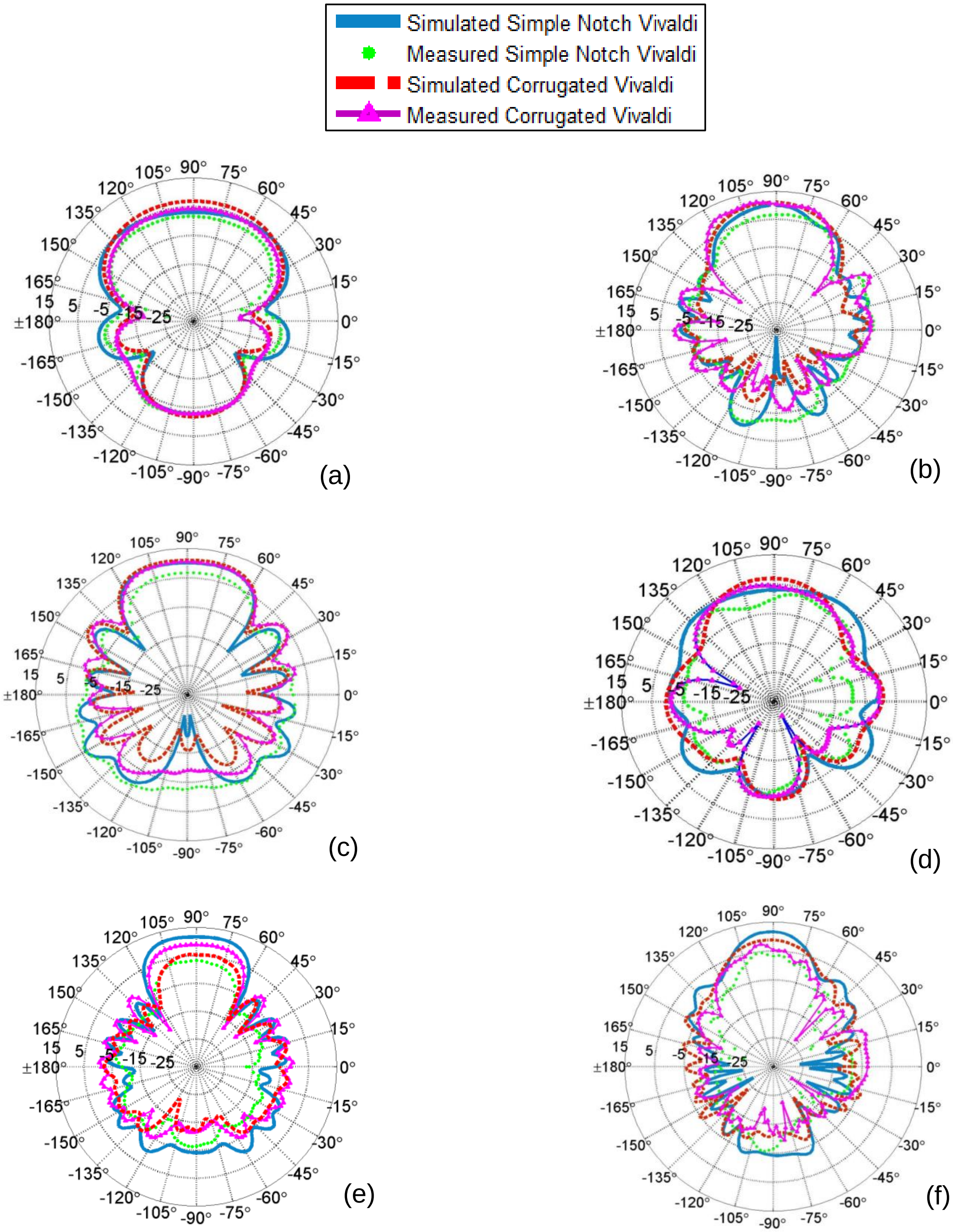

Figure 2.14 Measured radiation patterns of (a)-(b) E and H-planes at 5 GHz, (c)-(d) E and H planes at 10 GHz and (e)-(f) E and H-planes at 15 GHz.

2.4 Conclusion

A new method of producing Vivaldi antennas using metalized 3D printed plastic-polymers is presented. Printing antennas with these materials provides a low-cost, fast, and highly accurate fabrication solution. In addition, both antennas exhibit a large maximum gain of 12 dB as well as an extremely large bandwidth of up to 14.5 GHz. Two types of antennas are fabricated with this method using an ABS plastic covered with a thin sputtered copper layer. The measured and simulated results are shown to match well, displaying the potential of 3D printing in a low-cost UWB antenna design.

CHAPTER 3

Dielectric Loaded Antenna Designs

3.1 Introduction

One of the key advantages of 3D printing is that complex antenna geometries can be designed and printed. It is well known that dielectric loading of antenna elements can be used in focusing of waves. Example includes the use of dielectric lens in horn antennas for enhanced gain. On similar lines, 3D printed structure can be utilized to enhance antenna functionality. Here, two antenna designs are examined using 3D printed parts: i) Dielectric loaded Vivaldi antenna and ii) frequency tuning of monopole antennas. Here, first the base Vivaldi antenna design of the previous chapter is improved and then coupled with dielectric medium to further improves its performance.

.

3.2 Dielectric Loaded Antenna

The greater than ever need to have communication devices that can be used for a number of applications has attracted enormous attention to do research in this area. One of the main components that are required is a proficient design of an antenna. Antenna designs are known to be of a variety of configuration and geometries and are in use in many applications that range from high technology in military or even wireless devices in our daily life. A single antenna such as Vivaldi antenna can be optimized in various ways in the configuration that can improve and modify the antenna parameters which enable it to be used in different types of applications. The challenge of changing the configuration or geometries requires lot of work due to the tedious fabrication process needed to build an antenna such as the Vivaldi. However, 3D printing technology provides an easier alternative to change the configuration or physical design of the antenna. The previous chapter demonstrated the use of 3D printing technology in the design of functional 3D printed Vivaldi antennas. The results showed that 3D printed Vivaldi antenna is suited for several applications because of its broadband operational frequencies, easy to manufacture by using 3D printing, relatively high gain and highly directive radiation pattern. Building on the previous design, several modifications have been made towards the 3D printed Vivaldi antenna by changing the configuration which leads to an improvement in performance of the antenna. Apart from changing the configuration, improving the design, another noteworthy change was made adding a piece of dielectric which is placed in the aperture of the antenna. The concept that will be shown in this chapter will highlight the integration between dielectric materials with Vivaldi antenna that allows the improvement of the antenna parameters.

3.3 Bilateral 3D Printed Vivaldi Antenna

In this section, the modification of the dimension of design of the 3D printed Vivaldi antenna is shown. The same geometries were used based on the previous 3D printed Vivaldi antenna (Simple Notch Vivaldi) but with several modifications that has been made to improve its performance. The first modification was made by adding bilateral pieces that was put in place at the end of the antenna as shown in Figure 3.1. The purpose of the design was done to improve the lower frequency region which leads to an increase in the overall bandwidth. Design of the antenna was carried out using ANSYS HFSS. In the simulations it was assumed that the antenna is built out of solid copper block. In the previous chapter it was shown that by using solid copper give the same result as using a lossy-dielectric material covered with a thin layer of copper.

The first assessment was made by changing the dimension of the bilateral pieces that was place on the simple notch Vivaldi antenna. The simulation was made to determine the effect of the length of the bilateral pieces towards the performance of the Vivaldi antenna. The gain versus frequency was evaluated in Figure 3.2. The variation of the length shows that there is a significant change that occurs by changing the dimension. The best length was determined to be 24.75 mm. This dimension will be used for the bilateral pieces that will be place on the simple notch Vivaldi.

The simulated result of the S-parameters (S11) in Figure 3.3 shows the comparison made between the 3D printed simple notch antenna with 3D printed bilateral Vivaldi antenna. The shift in the bandwidth can be seen clearly seen from the plots. The bandwidth of the simple notch Vivaldi antenna starts to be under -10dB at approximately 4.75GHz while the modified version which is the bilateral Vivaldi antenna start at roughly 1.5GHz. Also, at higher frequencies the bilateral Vivaldi antenna shows better performance with S11 less than -10 dB above 20GHz as compared to the simple notch Vivaldi which stops at approximately19.5GHz. In the structure, the narrower region is used for impedance matching at higher frequencies while the wider section improves the impedance matching at lower frequencies. The S_{11} shows the argument for this statement.

The simulated gain versus frequency for both antennas was determined using HFSS simulations and is shown in Figure 3.4. The frequency that was simulated ranges from 1 to 20 GHz. From the graph it can be seen that there is a significant variation in performance between both the antennas. The bilateral Vivaldi antenna has higher gain than the simple notch antenna over a certain frequency range. At lower than 12.5 GHz, the bilateral antenna has a better gain by as much as 4 dB. This shows that the bilateral section on the Vivaldi helps to improve impedance matching at lower frequencies. Due to the good impedance matching at lower than 12.5 GHz, the gain of this antenna improves significantly. However, at higher than 12.5 GHz, the simple notch Vivaldi performance much better that the bilateral Vivaldi. This can be related back to the Figure S11 which indicates that the S11 at a certain frequency for the bilateral is poorly matched compared to the impedance matching of the simple notch Vivaldi. The gain of the bilateral Vivaldi suffers from the mismatch leading to the gain to reduce. This indicates that the radiation mechanism of the Vivaldi is related to the S-parameters and also shows that the radiation radiates based on the gap position of the Vivaldi. At lower frequencies, the mechanism that helps the radiation is the wider gap of the antenna while the narrower gap helps the radiation at higher frequency.

As noted the Vivaldi antennas have a wide bandwidth, in this case select frequencies are simulated to indicate the radiation pattern for both antennas. 5, 10 and 15 GHz are used to represent the low, middle and high operating frequency for the antennas. The radiation pattern is shown is Figure 3.5. Based on the observation of radiation patterns, antennas show end-fire directivity of both antennas. The beamwidth for bilateral Vivaldi displays a narrower beamwidth compare to simple notch Vivaldi for 5 and 10 GHz. This indicates that the gain is due to the beamwidth of the radiation energy focusing allowing the gain to be higher. However, at 15 GHz the radiation pattern changes for the bilateral Vivaldi with the presence of two side lobes beside the main beam. The splitting of the main beam is the cause in the reduction of the gain. The energy is lost to the side lobes. The side lobes may be due to the radiation coming out of the bilateral pieces. Nevertheless, in this case the beam of the simple notch Vivaldi still maintains the main beam and allowing the gain to increase.

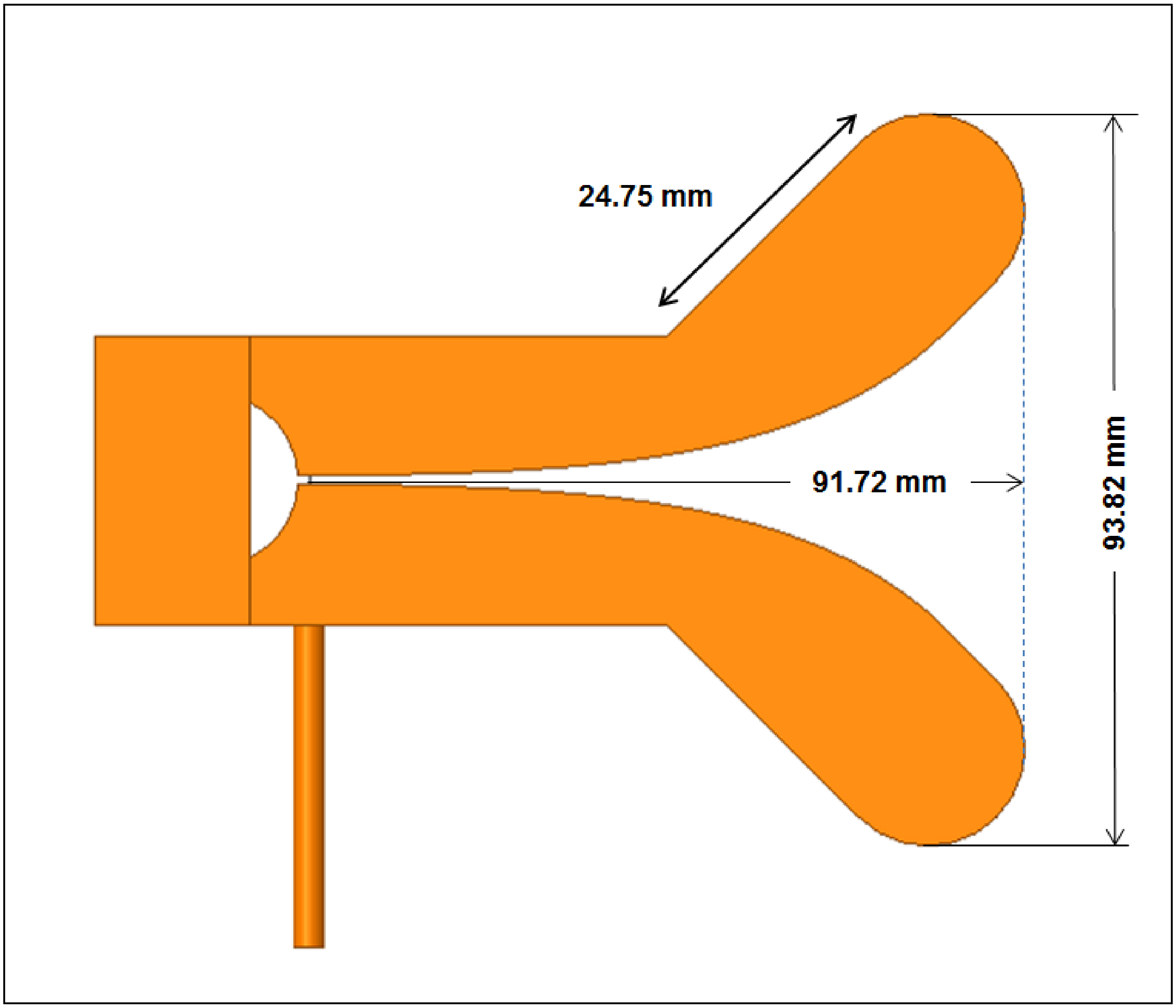

Figure 3.1 Design parameters of the bilateral antenna.

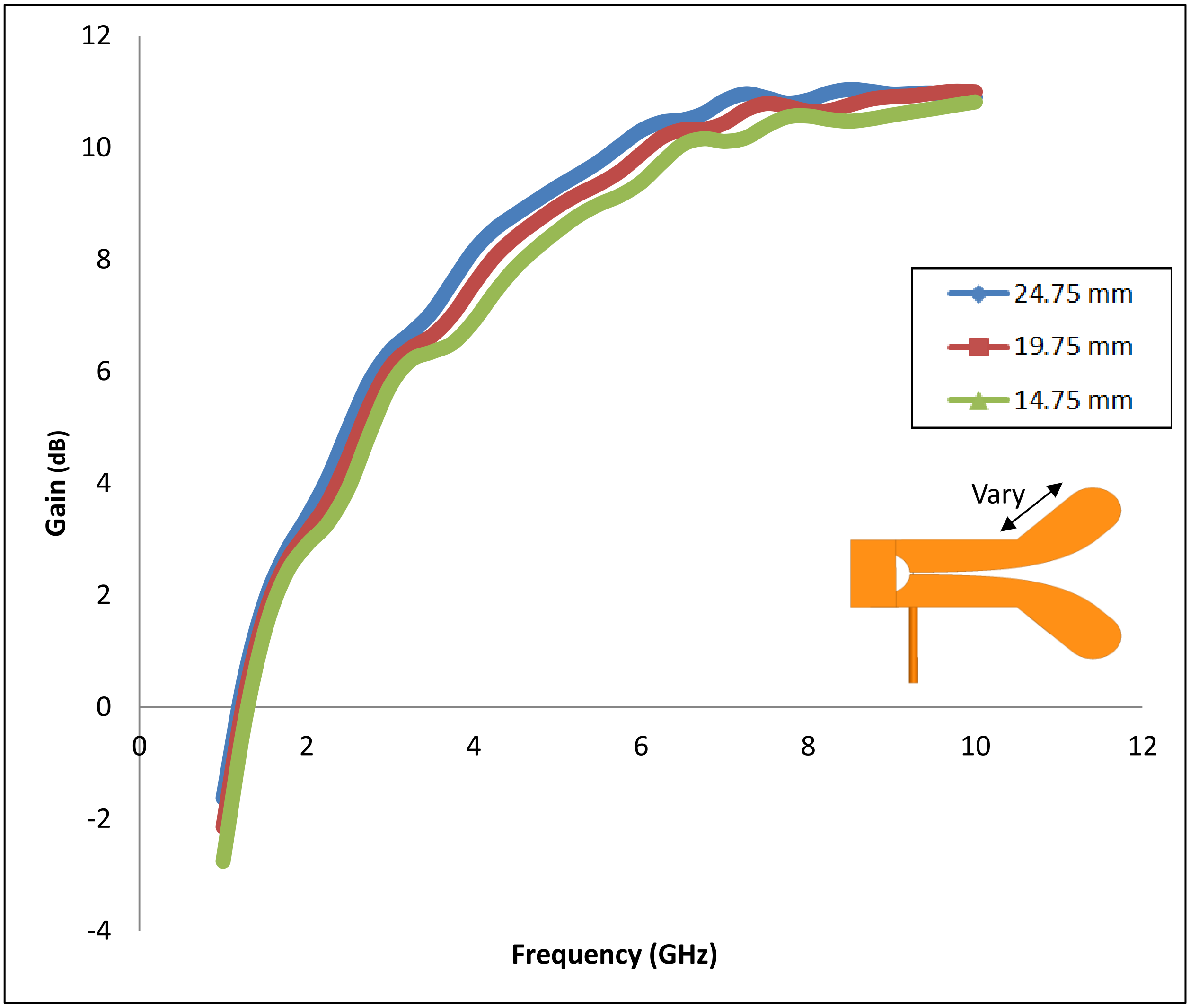

Figure 3.2 Gain versus frequency based on the variation of length of the bilateral Vivaldi.

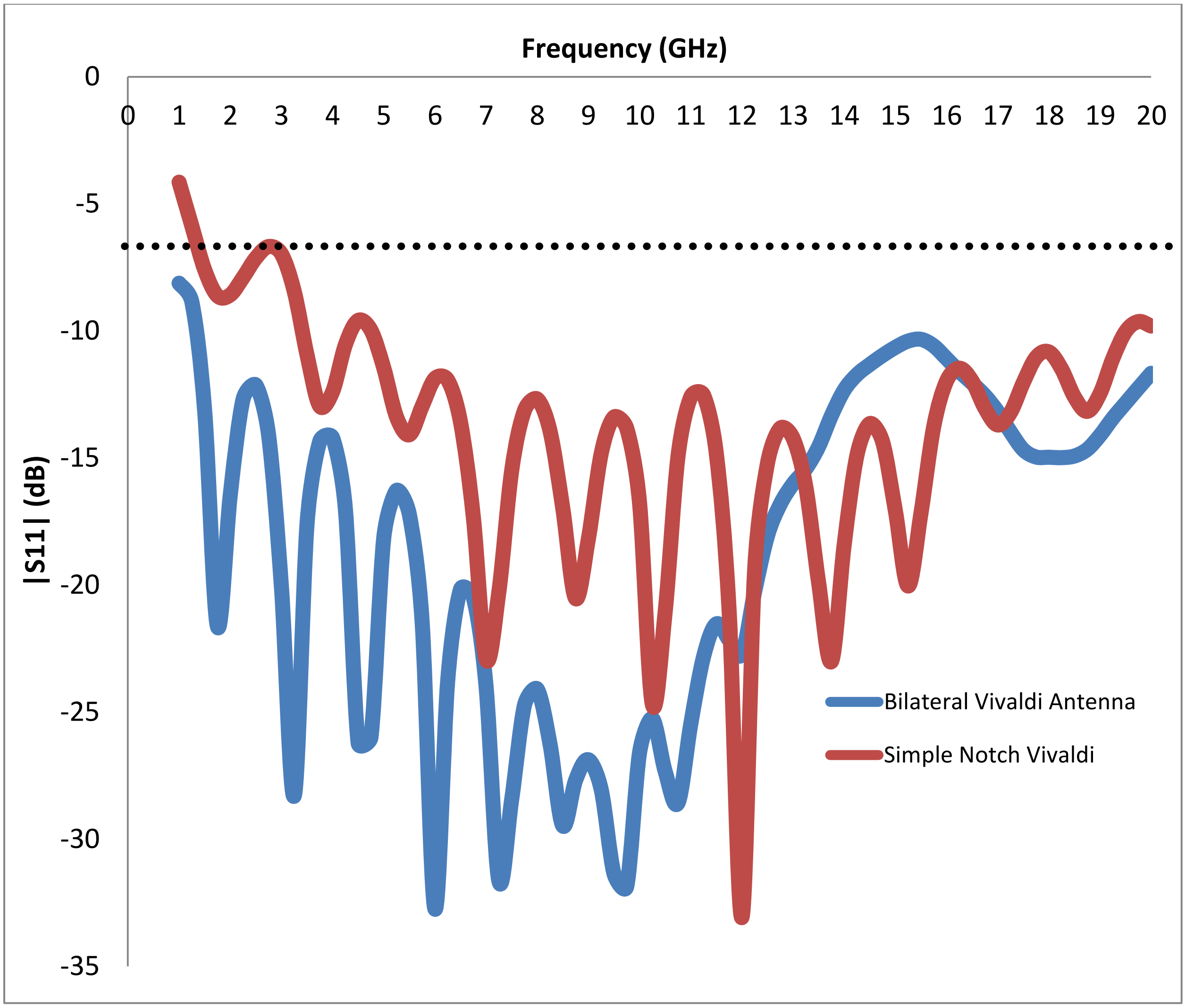

Figure 3.3 Simulated reflection coefficients of Simple Notch Vivaldi and Bilateral Vivaldi Antenna.

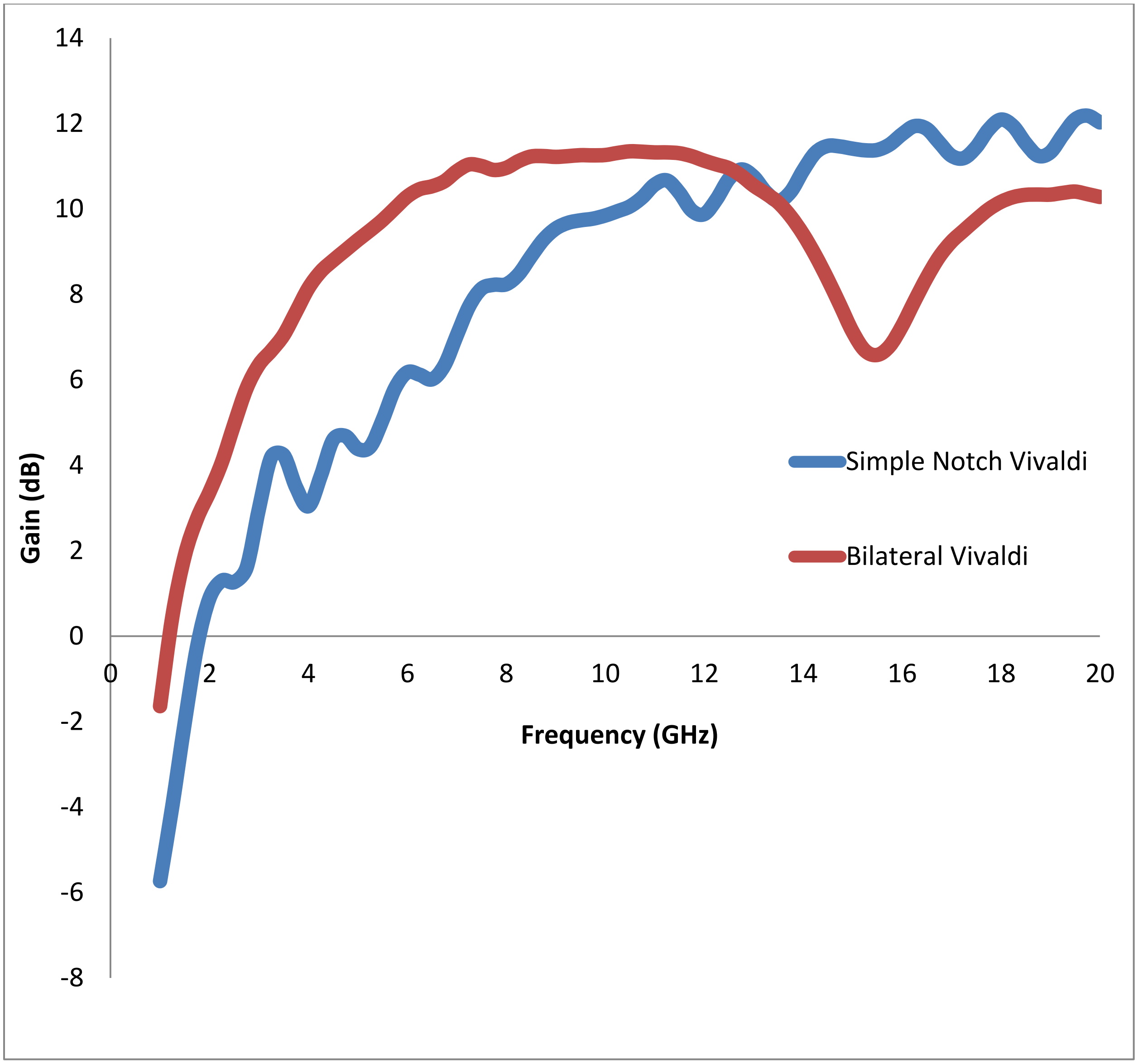

Figure 3.4 Comparison of simulated gain versus frequency of Simple Notch Vivaldi and Bilateral Vivaldi.

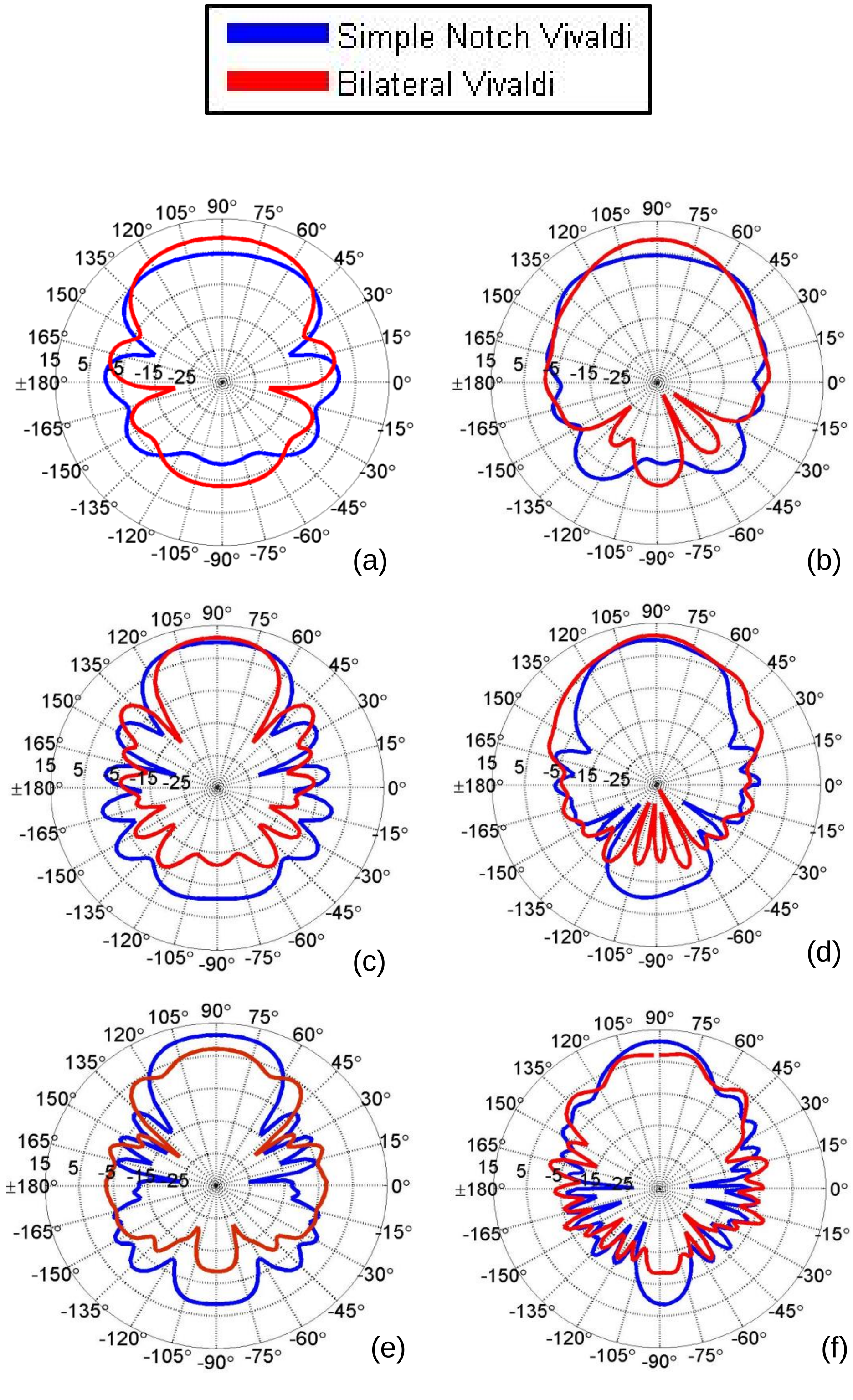

Figure 3.5 Simulated radiation patterns of (a)-(b) E and H-planes at 5 GHz, (c)-(d) E and H planes at 10 GHz and (e)-(f) E and H-planes at 15 GHz

3.4 Bilateral 3D Printed Vivaldi Antenna with 3D dielectric component

In the previous section it was shown that the bilateral section improves the performance in the Vivaldi antenna over a select frequency region. However, the gain decreases at higher frequencies due to mismatch of the antenna to the coax feed. In order to improve the overall performance, a dielectric piece is placed in the aperture of the bilateral Vivaldi antenna. The dielectric piece acts as a focusing material to guide the radiation energy in the material so that the radiation is enhanced in the end fire direction. Also, this allows the radiation beamwidth to be much narrower due to focusing by the dielectric region. In this section, several dielectric shape is designed in determining whether the configuration of plays a role in the performance of the antenna. The dielectric is made out of the same material uses to fabricate the antenna which is acrylic based polymer called Acrylonitrile butadiene styrene (ABS). The configuration that was designs for the dielectric is as following: rod, rectangular, corrugated and circular shape dielectric that can be seen in Figure 3.6. In the simulation the permittivity of the dielectric was 3.0.

Several simulation results were analyzed to further verify the improvement made by the dielectric. The first simulation result shows the S-parameters (S11) of each of the bilateral Vivaldi inserted with dielectric is shown in Figure 3.7. The S11 for the rectangular, circular and corrugated antenna has a similar starting frequency at 2.25 GHz while the rod has slightly higher starting point. The rectangular dielectric suffers from mismatching at the range of 8 to 10 GHz which causing a discontinuity for the bandwidth. The circular and corrugated dielectric shows a similar pattern with slight deviation which gives the best bandwidth for the bilateral Vivaldi.

Correspondingly the pattern of E-field was simulated to observe the wave propagating in the dielectric pieces. Each antenna E-field was presented in Figure 3.8-3.11. Different shapes of the dielectric show an interesting wave pattern. The rod dielectric displays that the wave does not propagate until the end of the rod. It might be because of the energy of the propagation is insufficient to force the wave to the end. The rectangular E-field shows that the wave propagates until the end. Conversely, the wave shows that the wave is disperse and not focus at the end. Both corrugated and circular dielectric shows that the wave is converging when it reached the end. The may lead to a higher gain due to the focusing element of the dielectric structure.

By using the circular and corrugated dielectric will be further evaluated in determining the performance of the dielectric by having the simulation result for the gain versus frequency that is represented in Figure 3.12. The gain of both antenna shows almost similar result in the gain. Nevertheless at a certain frequency each of the antennas shows higher again than the other one. The overall gain over the range of frequency shows that circular dielectric has an extra edge over the corrugated dielectric.

Based on the performance of the dielectric pieces that was inserted in the aperture of the bilateral Vivaldi, the comparison will be made to evaluate the performance compare to the bilateral Vivaldi without the dielectric. The assessment will be made by comparing the S-parameters, the gain, radiation pattern and also the beamwidth of the antenna.

The first comparison was made for the S-parameters of both antennas which the bilateral Vivaldi with dielectric and with non-dielectric (air) is shown in Figure 3.13. In the results shows that the dielectric causes the frequency to shift to a higher frequency meaning it is not impedance match as good in the lower frequencies. The bilateral dielectric Vivaldi antenna also suffers from the poor impedance matching at higher frequencies. The dielectric integrated with the antenna might not be fully optimized. A poor S11 does not mean that the overall performance of the antenna is worse. Further evaluation will be made in showing other antenna parameters.

The second assessment was made by comparing the gain versus frequency for both antennas which are presented in Fig 3.14. At the lower half of the frequency range that was measured (under 12.5 GHz) shows that the gains of both antennas are more or less. However as the frequency increases the gain of the antenna for the bilateral Vivaldi with dielectric maintain the gain and sometimes increases while the bilateral Vivaldi without the dielectric decreases in the gain. These shows an indication that the dielectric insertion on to the bilateral Vivaldi helps improve the gain.

Advance valuation was made to see any sign that shows the gain improvement is due to the dielectric. The radiation pattern for both antennas is studied and the result is shown in Figure 3.15. As expected the radiation pattern of both shows consistent pattern as expected for a Vivaldi antenna. However, an interesting pattern emerges at higher frequency. The beamwidth of the bilateral Vivaldi with the dielectric shows a narrower radiation pattern compare to the bilateral Vivaldi without the dielectric. This can indicate that the dielectric component in the Vivaldi help focuses the beam and allows the directivity of the antenna to be more shaper. As the beam narrows the energy of the radiation concentrate to an end fire direction making the gain increase at that frequency. This proves that dielectric help improving the gain of the antenna.

For convenience a comparison between the simple notch Vivaldi antenna and the bilateral Vivaldi with dielectric (circular shape) is made to show improvement in the gain performance. The gain versus frequency is shown in Figure 3.16, the dielectric region help improves the gain. The combination of the dielectric plus the bilateral Vivaldi gives two advantages. The first advantage is that the performance improves in the lower frequency is improved by having a higher gain while the second advantage is maintaining the gain at higher frequency.

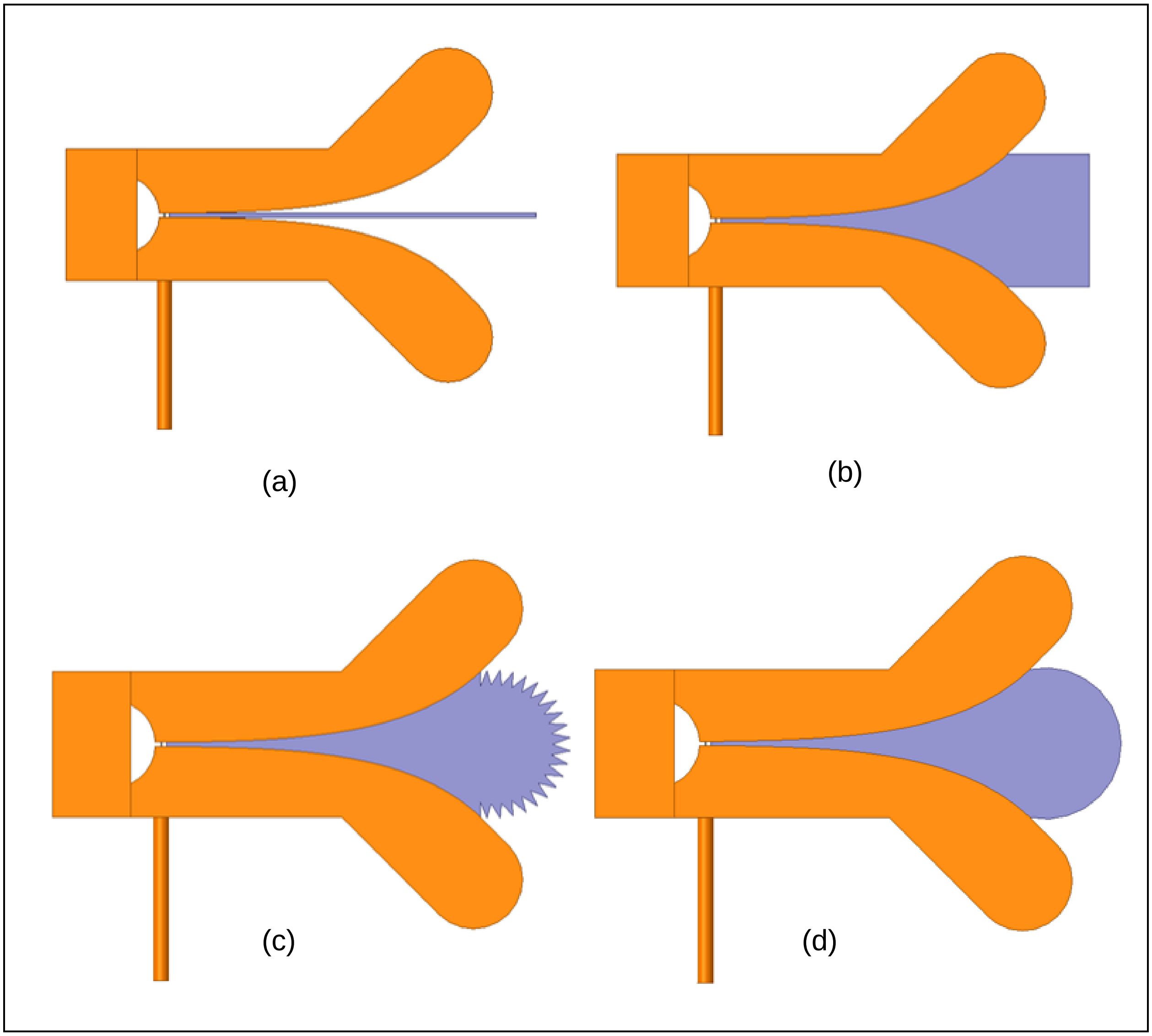

Figure 3.6 Designs parameters of (a) Rod (b) Rectangular (c) Corrugated (d) Circular shapes dielectric inserted into the aperture of the Bilateral Vivaldi.

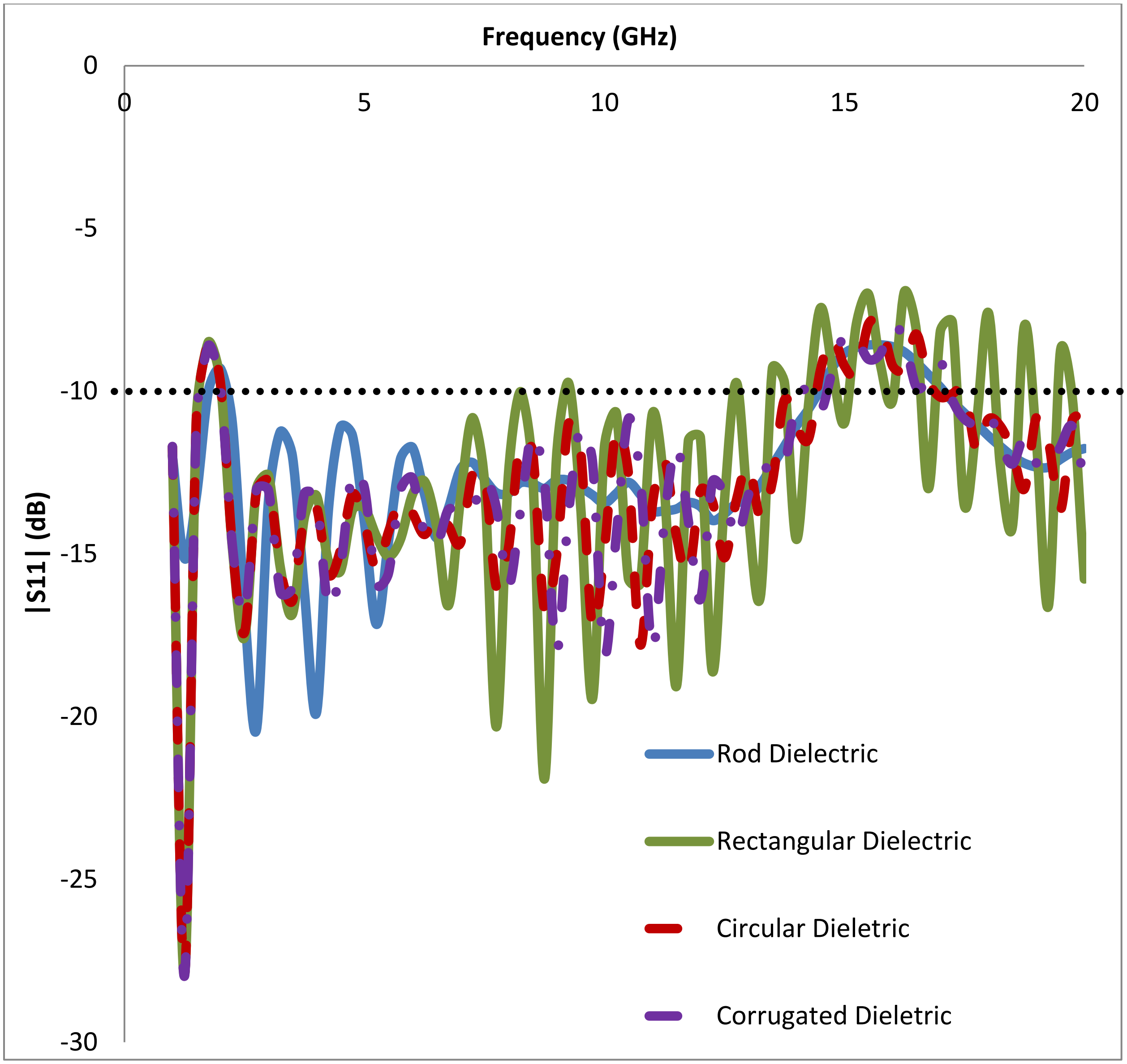

Figure 3.7 Simulated reflection coefficients of various shapes of dielectric inserted in the aperture of the Bilateral Vivaldi.

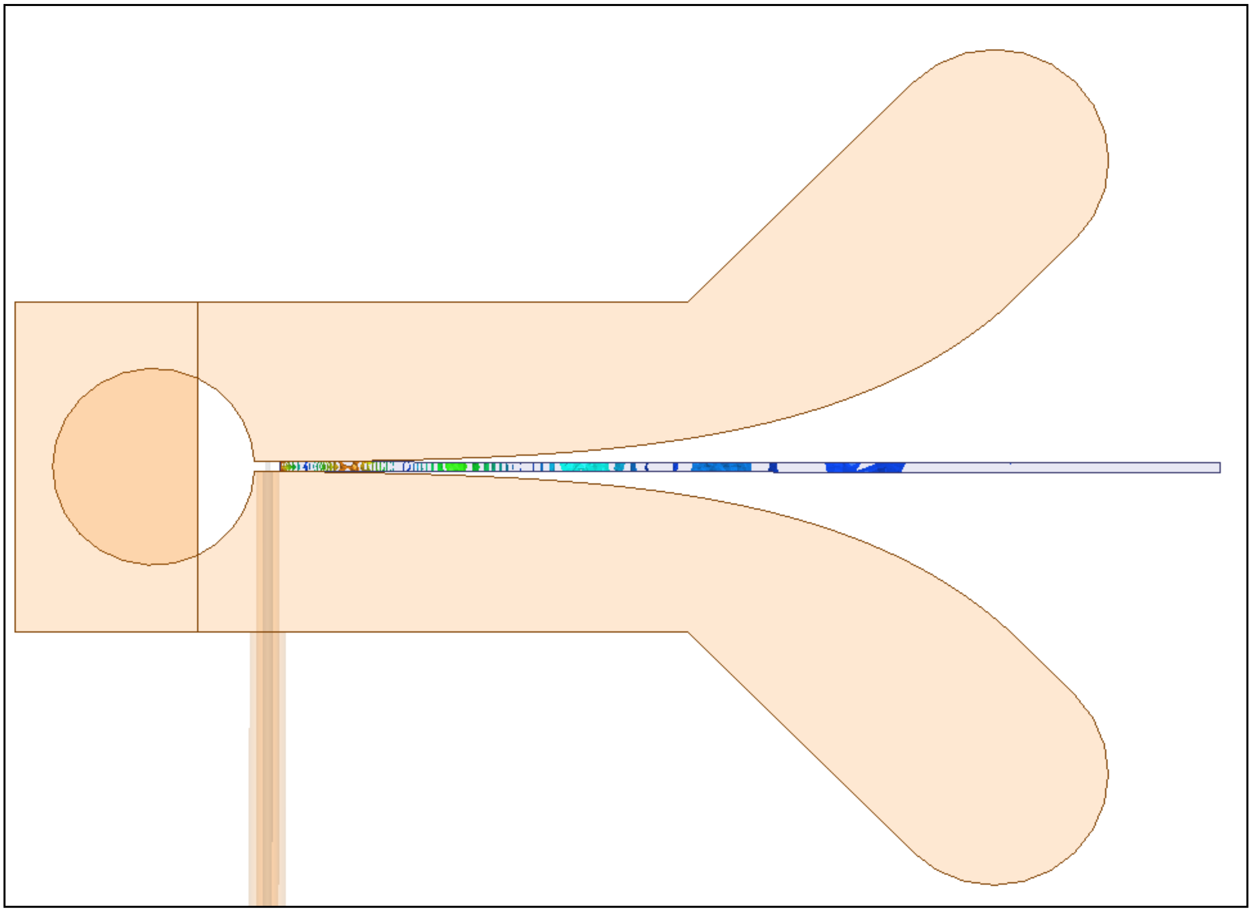

Figure 3.8 The E-field of bilateral Vivaldi with a rod shape dielectric.

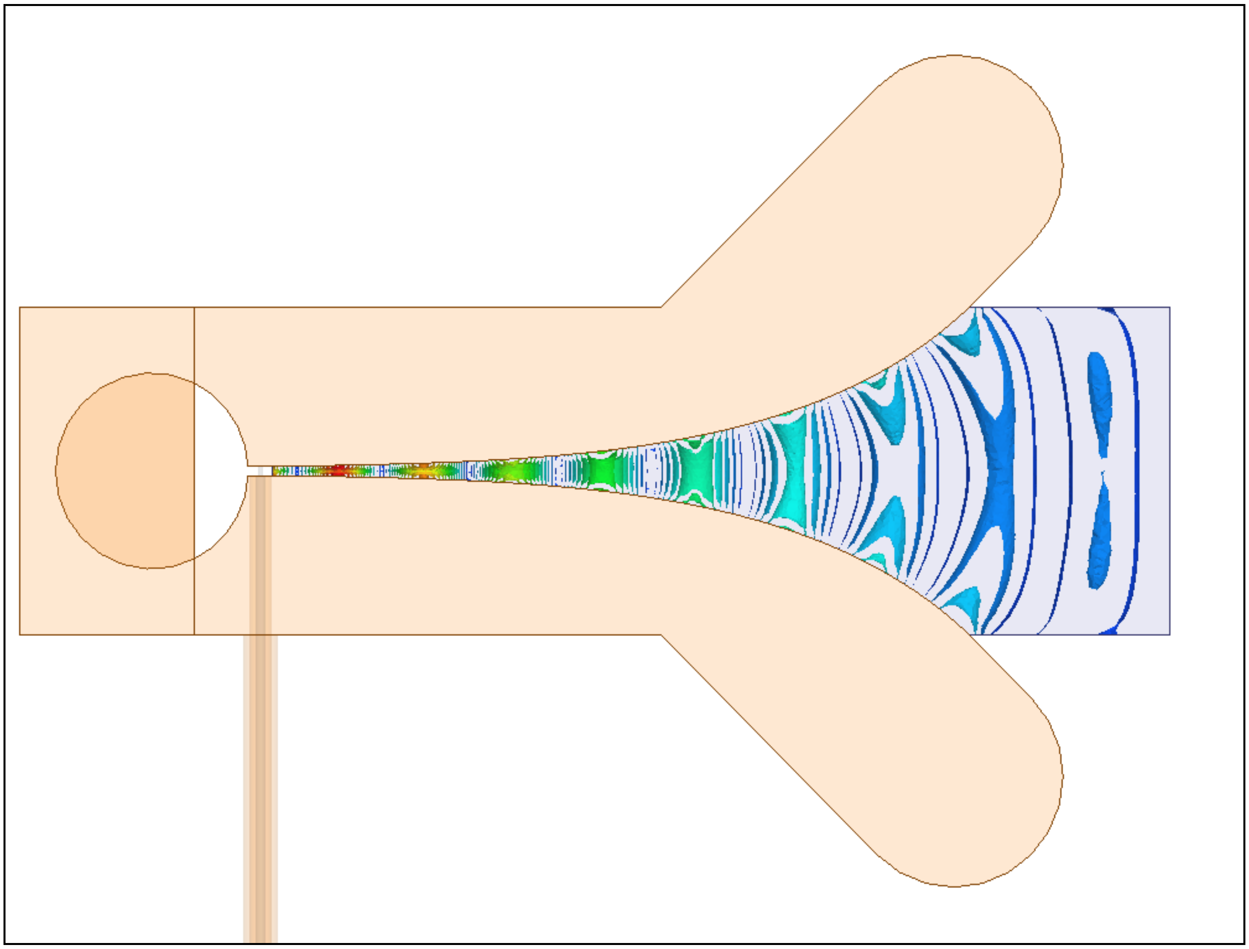

Figure 3.9 The E-field of bilateral Vivaldi with a rectangular shape dielectric.

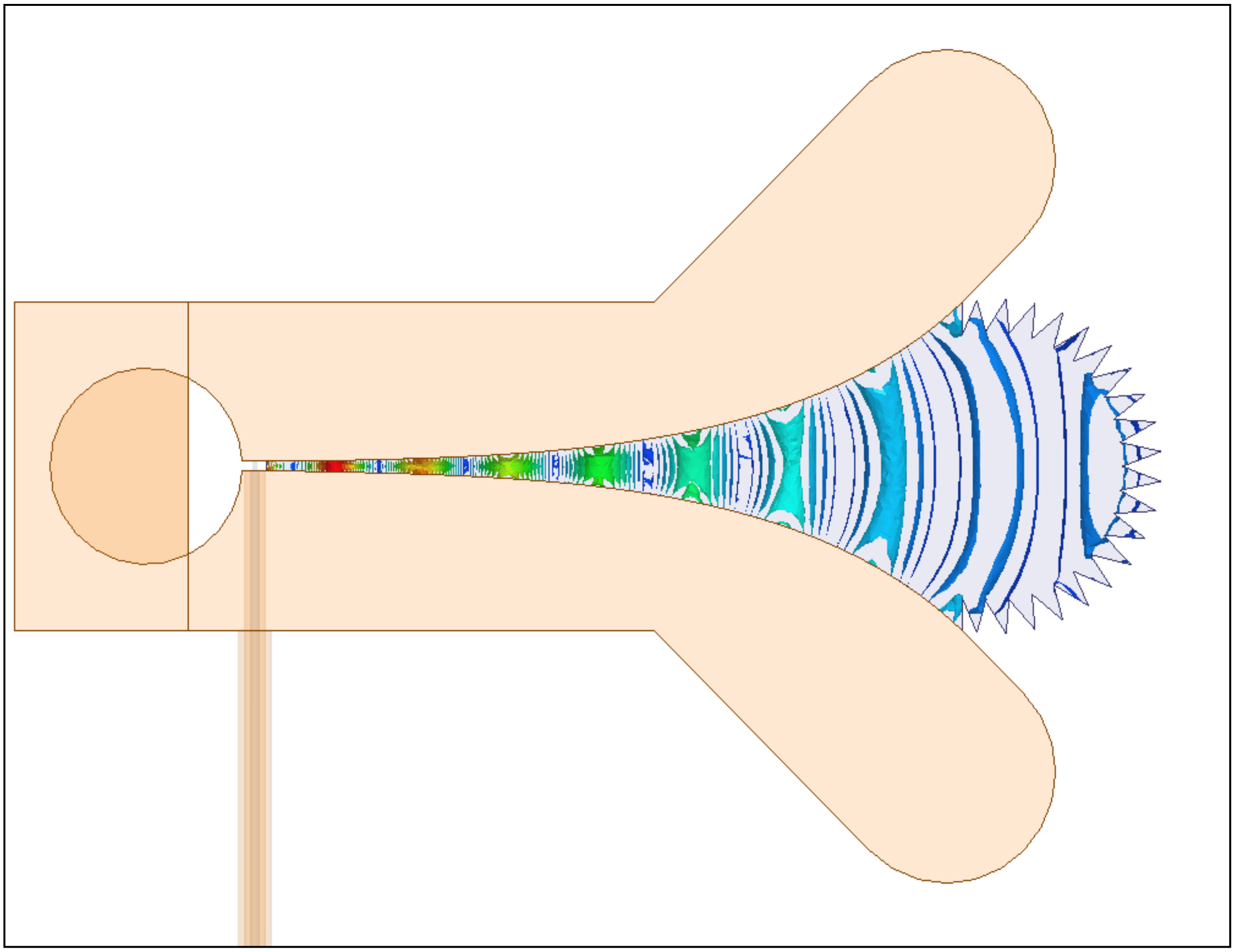

Figure 3.10 The E-field of bilateral Vivaldi with a corrugated shape dielectric

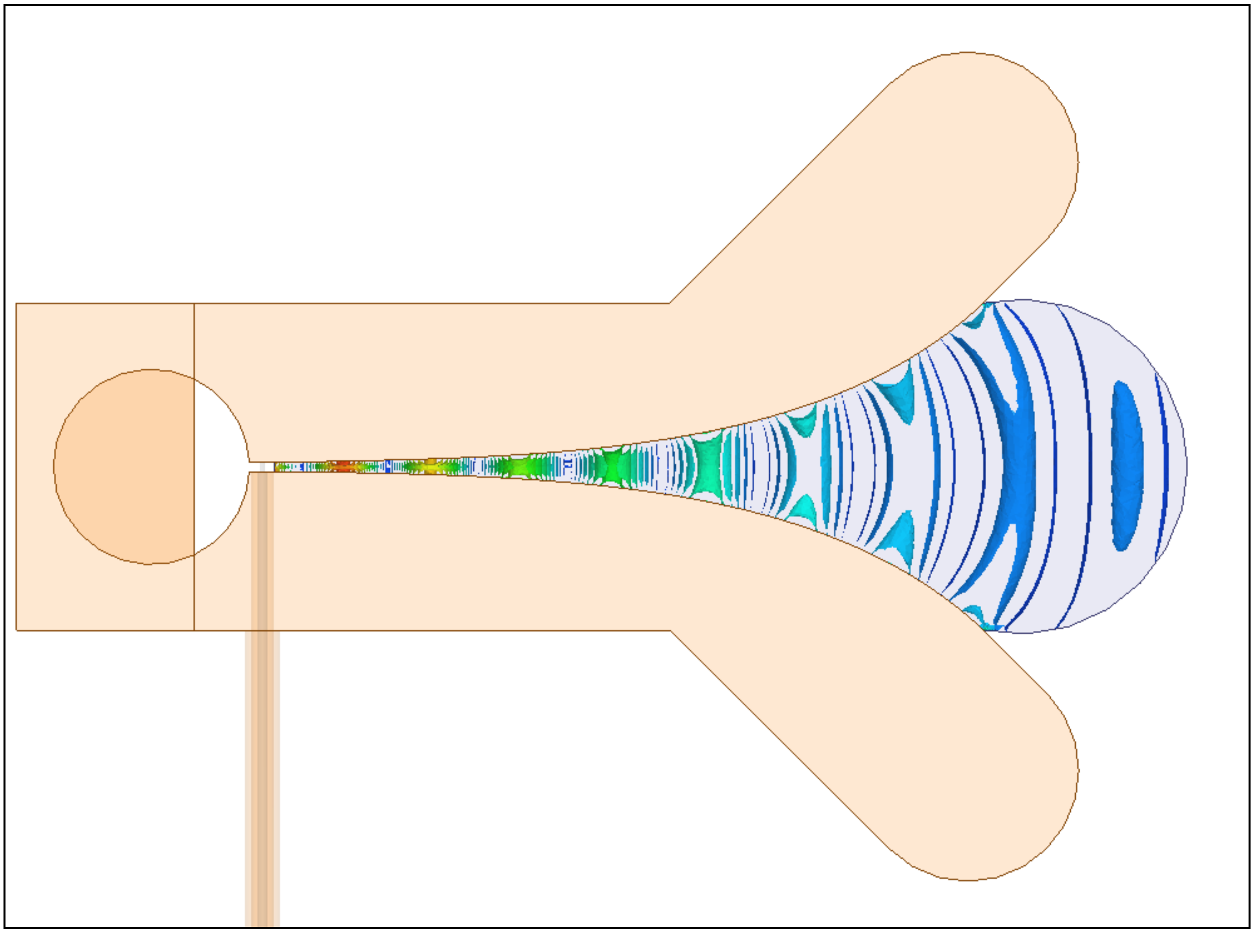

Figure 3.11 The E-field of bilateral Vivaldi with a circular shape dielectric.

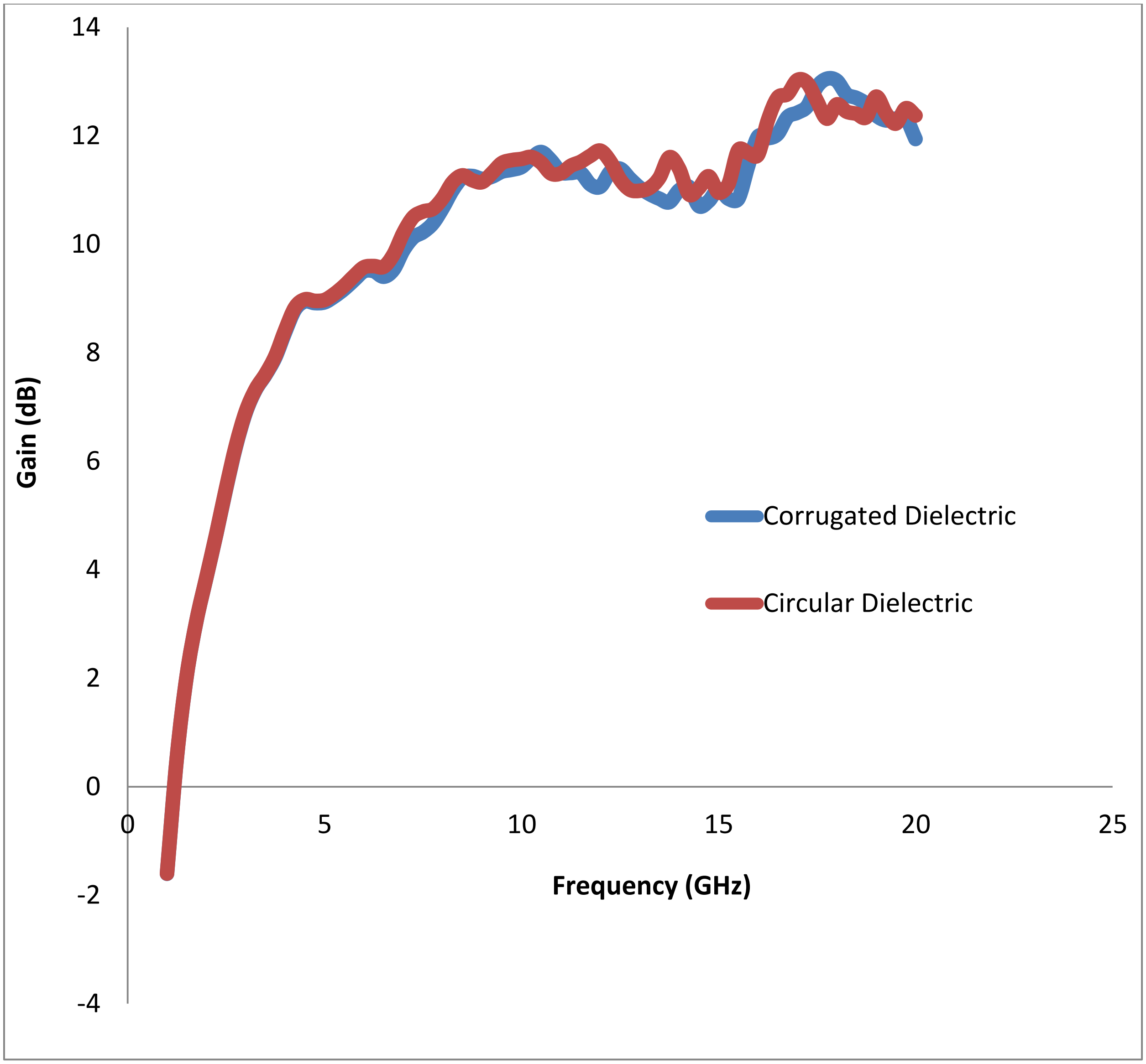

Figure 3.12 Simulated results of gain versus frequency of Corrugated and Circular Dielectric shape.

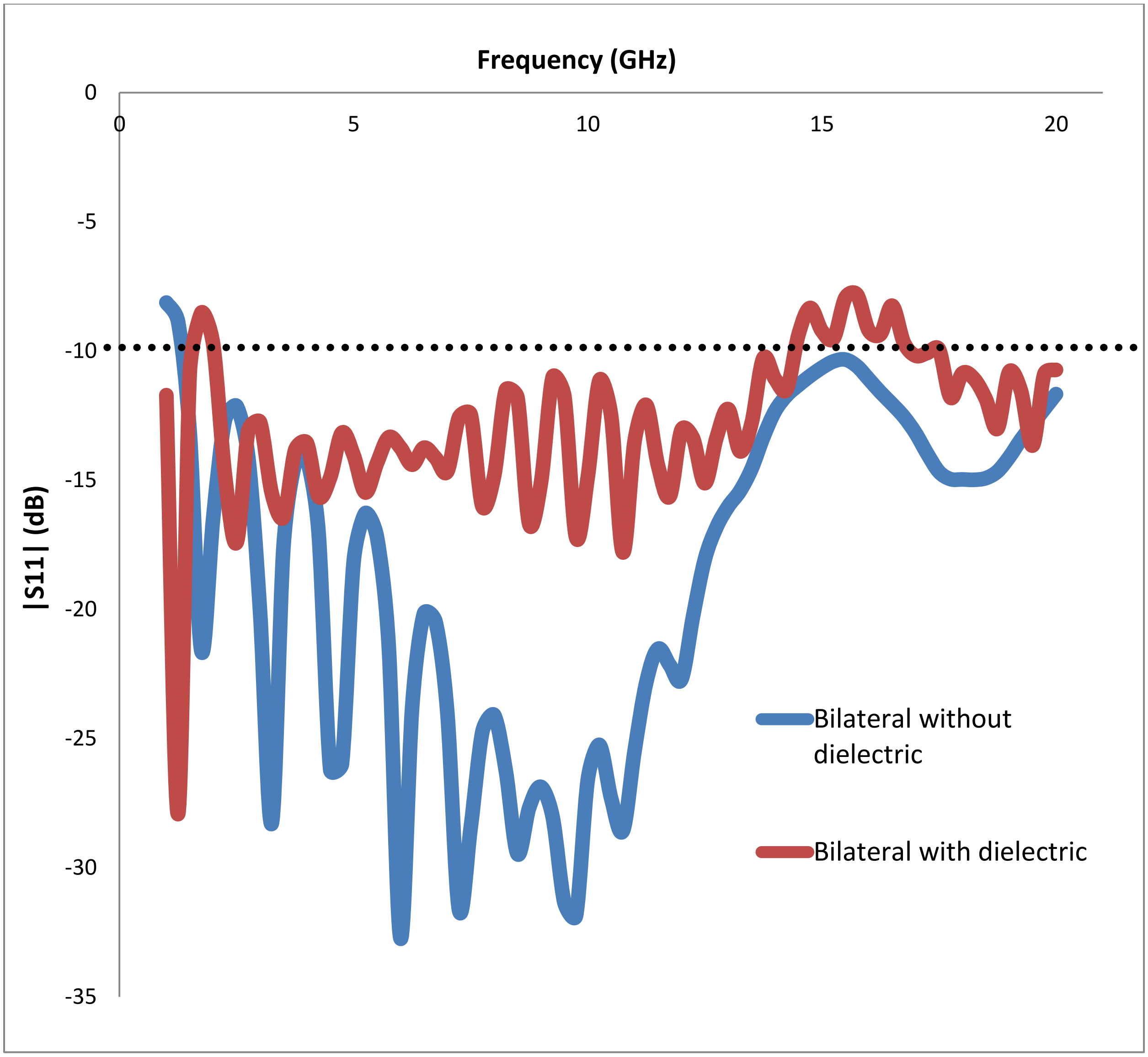

Figure 3.13 Simulated reflection coefficients of bilateral without dielectric and Bilateral with dielectric Vivaldi.

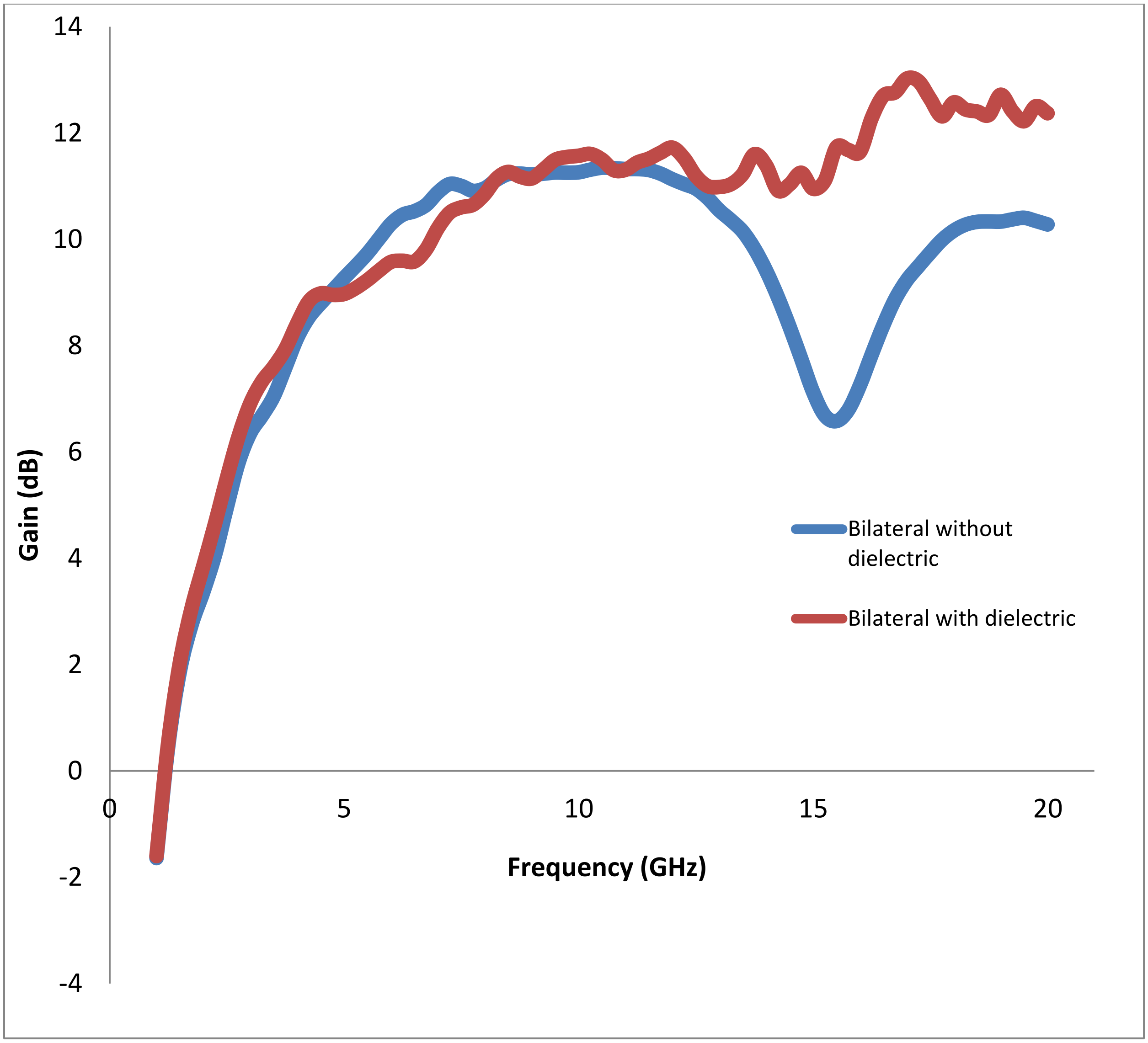

Figure 3.14 Simulated results of gain versus frequency of Bilateral without and with dielectric Vivaldi.

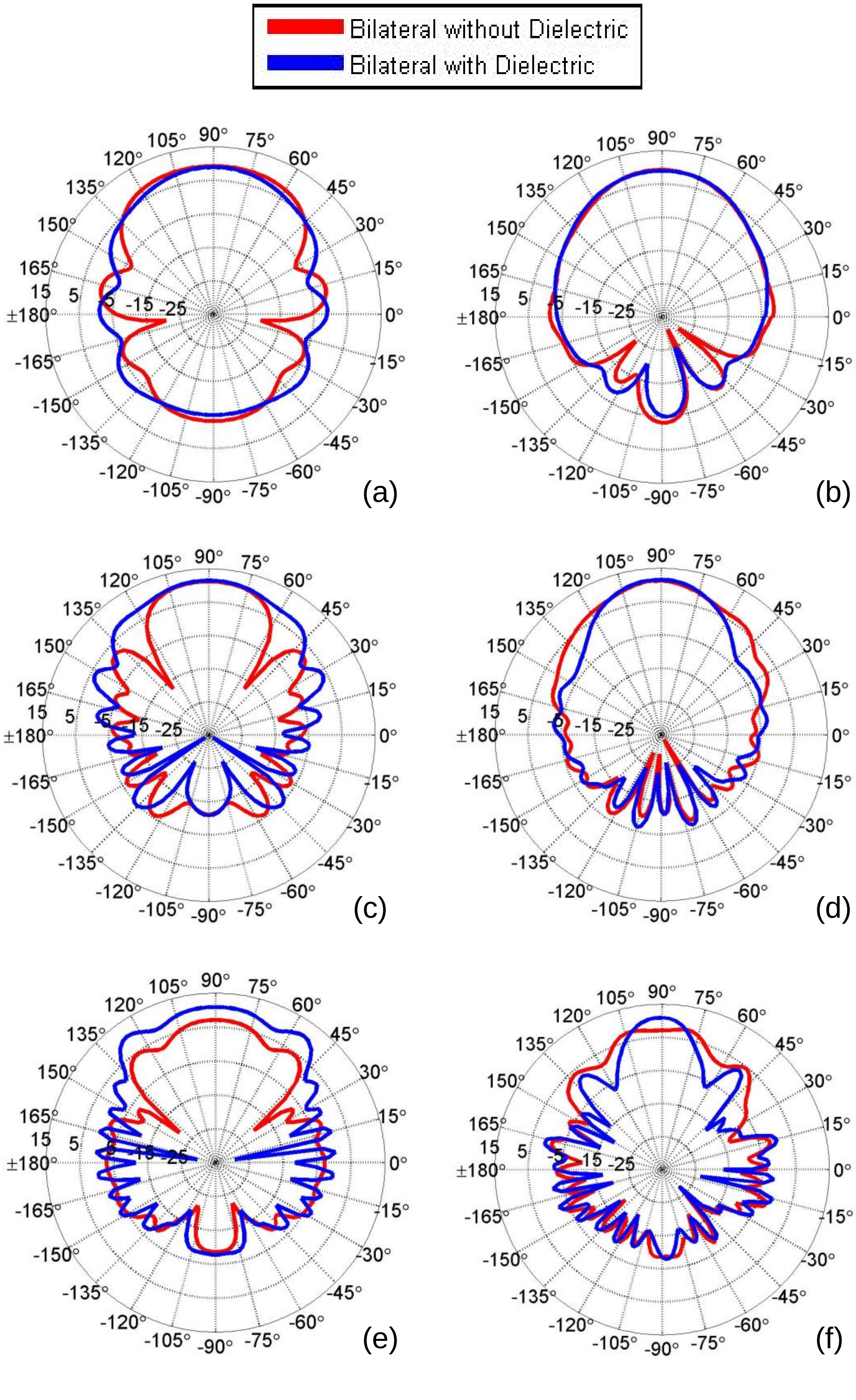

Figure 3.15 Simulated radiation patterns of (a)-(b) E and H-planes at 5 GHz, (c)-(d) E and H planes at 10 GHz and (e)-(f) E and H-planes at 15 GHz.

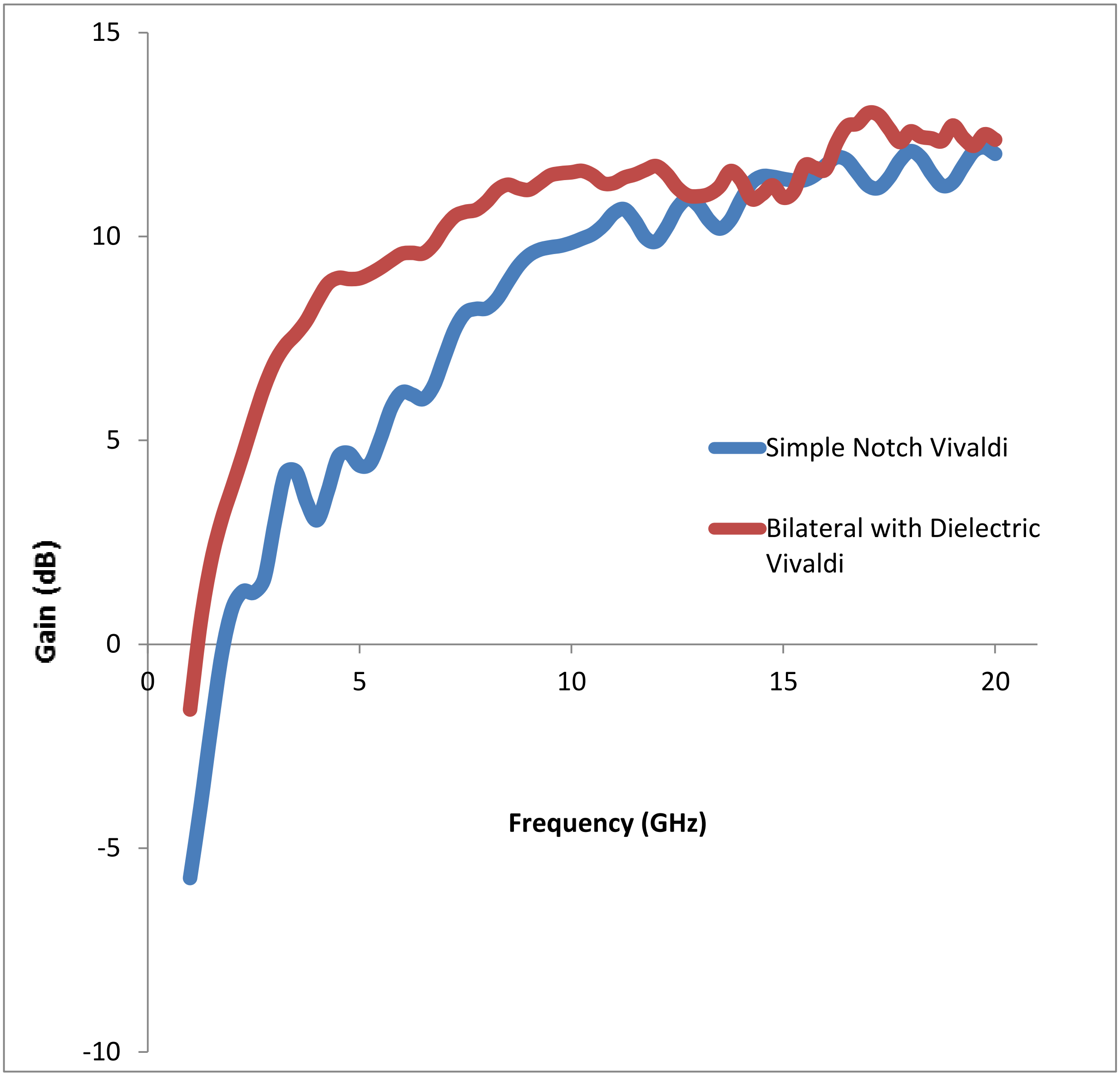

Figure 3.16 Simulated results of gain versus frequency of Simple Notch and Bilateral with Dielectric Vivaldi.

3.5 Fabrication of Bilateral 3D Printed Vivaldi with and without Dielectric Loading

In the previous section different Vivaldi antenna designs were simulated. Some of the designs show significant improvement in the overall performances. The design chosen for fabrication was the bilateral section of 24.75mm loaded with a circular shape dielectric. As in the previous chapter, the fabrication was carried out using 3D printed machine (Objet Connex350). The polymer material chose for fabrication is Acrylonitrile butadiene styrene (ABS) which was found to have the lowest loss among the materials available for fabrication. The printed bilateral antenna was coated with a thin copper using a sputtering machine (1µm). Prior to Cu deposition, a thin layer of titanium (150Å) was deposited to enhance adhesion between ABS layer and the copper layer. In order to integrate coax cable into the structure, the antenna was printed in two half pieces. Alignment pins were printed on the half structures to ensure good alignment between the two pieces.

Figure 3.17 shows the 3D printed bilateral Vivaldi antenna prior to the deposition of the copper conductive layer. Figure 3.18 shows the same structures after Cu blanket deposition. Figure 3.19 shows a completely assembled Vivaldi antenna structure. A coax cable was inserted between the two half pieces to form a connected. The center wire of the coax cable was extended through the central gap forming a coupler. The other end was aligned using a small hole that was printed into the structure during the 3D fabrication. The dielectric (non Cu coated structure) was inserted in the slot region.

This structure is also built from ABS polymer material. This structure could be easily inserted and removed during the measurements.

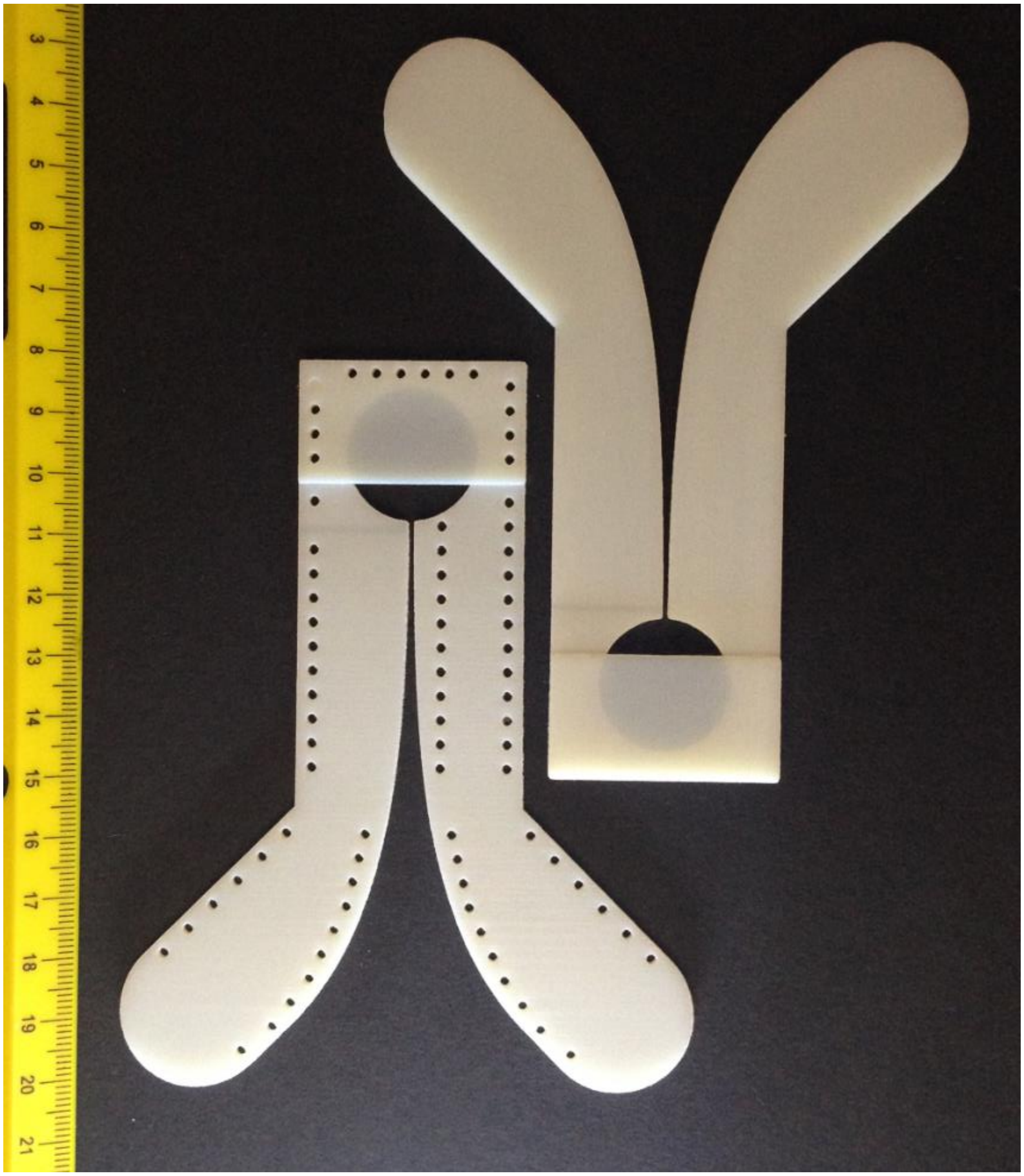

Figure 3.17 As fabricated bilateral Vivaldi prior to deposition of Cu layer and assembly.

Figure 3.18 Fabricated Bilateral Vivaldi after blanket copper coating on both sides of the structures.

Figure 3.19 Fabricated Bilateral Vivaldi coated with copper plus the circular dielectric with the coaxial cable place in the antenna.

3.6 Measurement of Antenna Reflection Coefficient

The reflection coefficient of the antennas was measured using a vector analyzer, Agilent N5227A, over a frequency range of 1 GHz to 20 GHz. The measured reflection coefficient of each antenna as well as the simulated results is presented in Figure 3.20 for the 3D printed bilateral Vivaldi without the dielectric component and Figure 3.21 for the 3D printed bilateral Vivaldi with dielectric inserted in the aperture of the antenna.

The measured and simulated results have a similar trend with the exception of extra strong resonances in the measured results. This is largely attributed to the feed point. The impedance matching was determined to be sensitive to the feed location in the slot region. In the simulations the feeding point was optimize to give the best reflection coefficient possible; however, during fabrication it is difficult to attain a good match as the coax is mounted manually. Another factor that can effect is the fabrication resolution, especially the dimension of the slot region.

In the 3D printed bilateral Vivaldi with dielectric insert, Figure 3.21, extra resonances in the measured S11 are noticeable. In this design, the dielectric is inserted in the metalized section. In this structure, there is an air gap presented between these structures. This air gap affects the impedance matching, especially at lower frequencies.

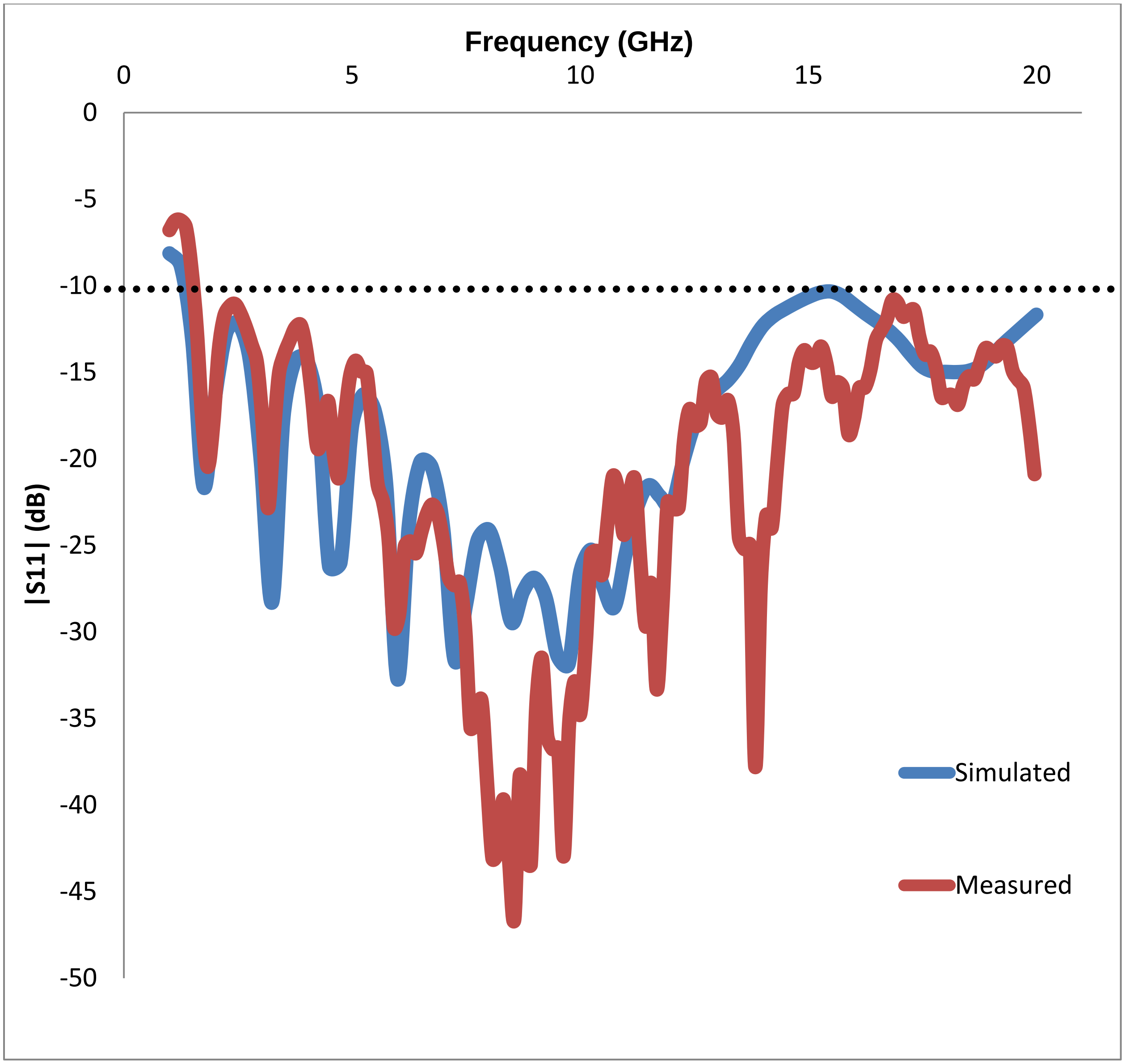

Figure 3.20 Simulated and Measured of 3D printed Bilateral Vivaldi without dielectric component.

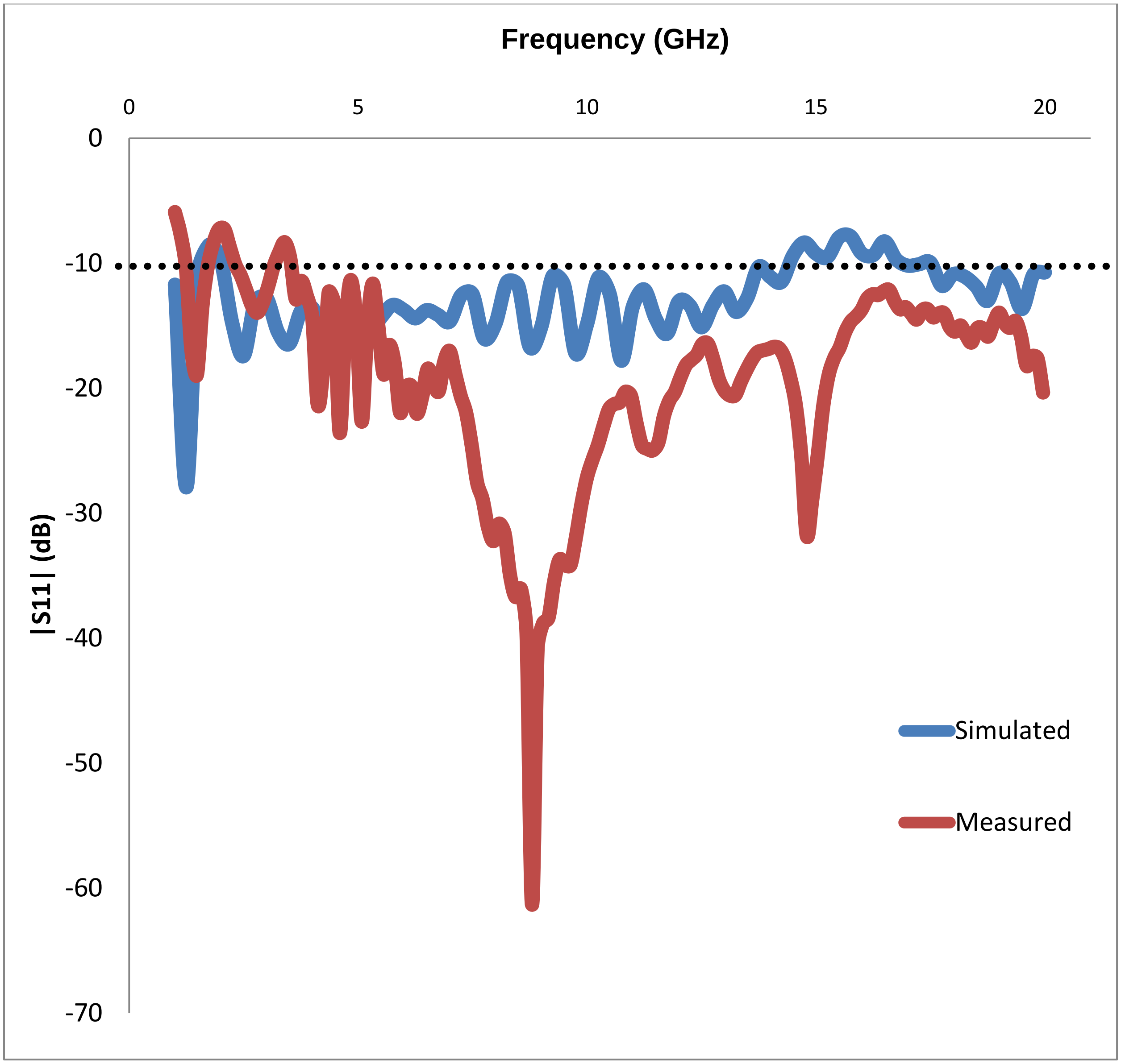

Figure 3.21 Simulated and Measured of 3D printed Bilateral Vivaldi with dielectric component.

3.7 Measurement of Antenna Radiation Characteristics

The radiation characteristic of the antennas was measured using a SATIMO near-field measurement system. The measured gain as a function of frequency is shown in Figures 3.22 and 3.23 without and with dielectric component, respectively. These figures also show the simulated results.

Figure 3.22 shows discrepancy in the gain versus frequency. The increase shows similar pattern of increase of decrease of the gain. However several disagreements were shown around 2 to 4 dB of differences due to several factors. The first reason might be because of the dimension of the design was a bit off compare to the design in simulation. The resolution of the printer might cause some difference in the dimension and also some residue of the material might still be intact on the antenna. Secondly, due the sensitiveness of the coaxial position will cause the loss in the gain. Loss in the coaxial and the system cables may give to the fact that the gain reduces significantly. One of the other factors that give reduction in gain is the surface roughness of the antenna. The uneven layer of copper during the sputtering process can cause discrepancies towards the wave to propagate can cause the gain to decrease.

On the other hand, in Figure 3.23 shows a much more reduction in the gain. The same cause can be said as the above statement. In addition, several factors due the dielectric also play a role in the inconsistency in the simulation and measured. In the simulation the dielectric that was used without any loss considered. However, when the fabrication was done, it is found that the dielectric properties have the loss tangent of 0.02. That loss tangent also causes the gain to decrease. Adding to the loss, there is gap that was found in between the dielectric and the inside of the aperture of the antenna. Due to the gap, the radiation might leak away causing lessen in gain.

A second simulation was done to verify the effect of the loss in the dielectric was included in Figure 3.23 as well. It shows that the measure and the simulated have a similar pattern but a discrepancy in the gain. This shows that the loss tangent plays a role in the reduction of the gain. However that simulation does not take account of the other losses which was due to the position of the feeding point, differences in the dimension simulated and fabricated, and the surface roughness.

Further analysis was done in order to see the radiation pattern of Bilateral Vivaldi with and without the dielectric. Figure 3.24 shows the radiation pattern that was measured using a 3D SATIMO antenna measurement system. The measurement was done at a specific frequency as a representative of low, mid and high frequency for 5, 10 and 15 GHz. It shows that the radiation pattern of the Bilateral Vivaldi with the dielectric shows the gain to less that the bilateral Vivaldi without the dielectric. This is due to the loss of the dielectric properties. However an interesting indication shows that the dielectric has a lesser beamwidth compared to the antenna without the dielectric. It shows that the dielectric helps focusing the beam but due to the loss tangent of the dielectric causing the gain to decrease. The ABS was used as the dielectric because it was the lowest loss dielectric material available for 3D printing. Based on the concept shown the used of lesser lossy material allows the dielectric to function as predicted in the simulation. As for future research a low loss material will be used.

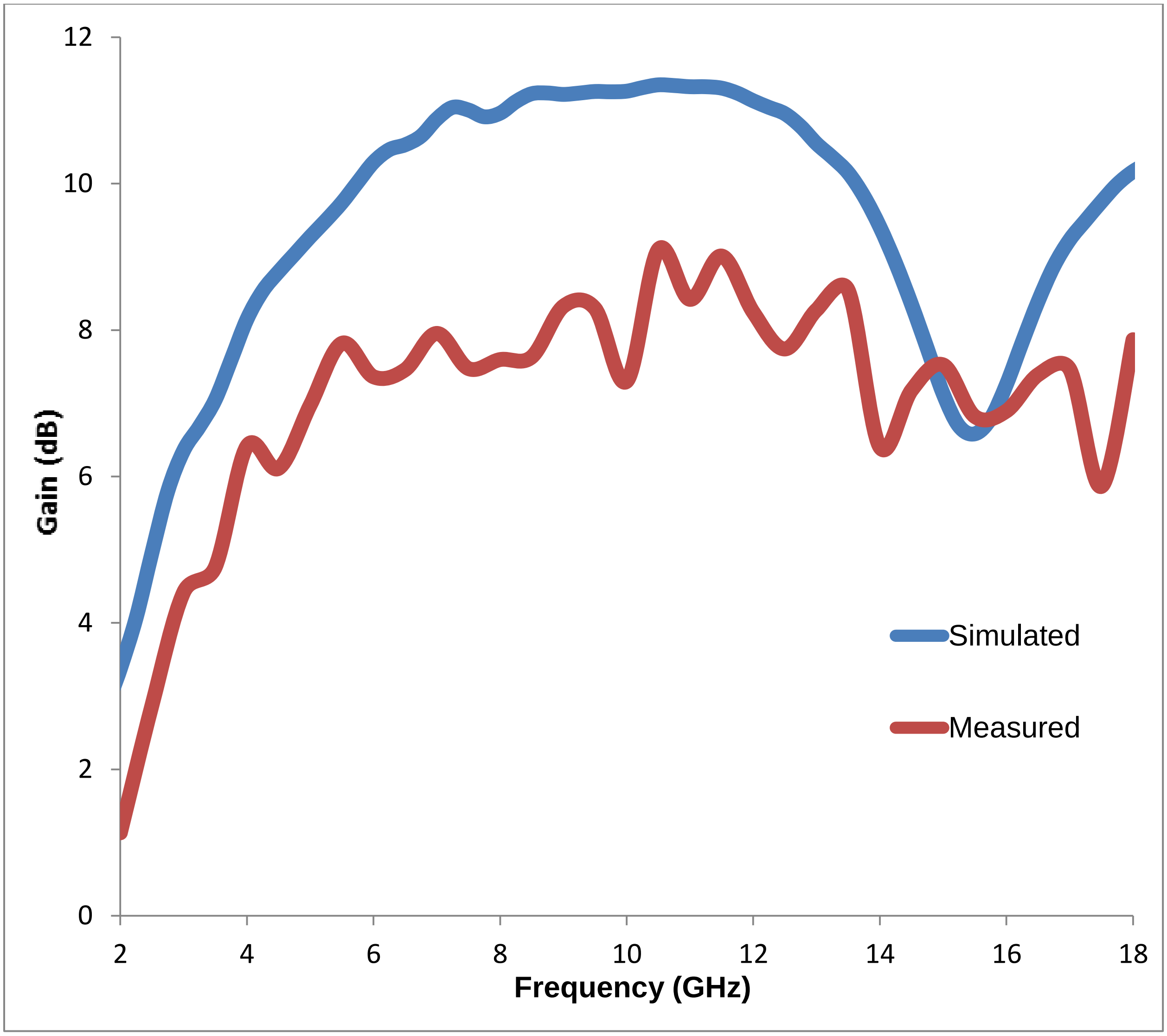

Figure 3.22 Simulated and Measured gain of 3D printed Bilateral Vivaldi without dielectric component.

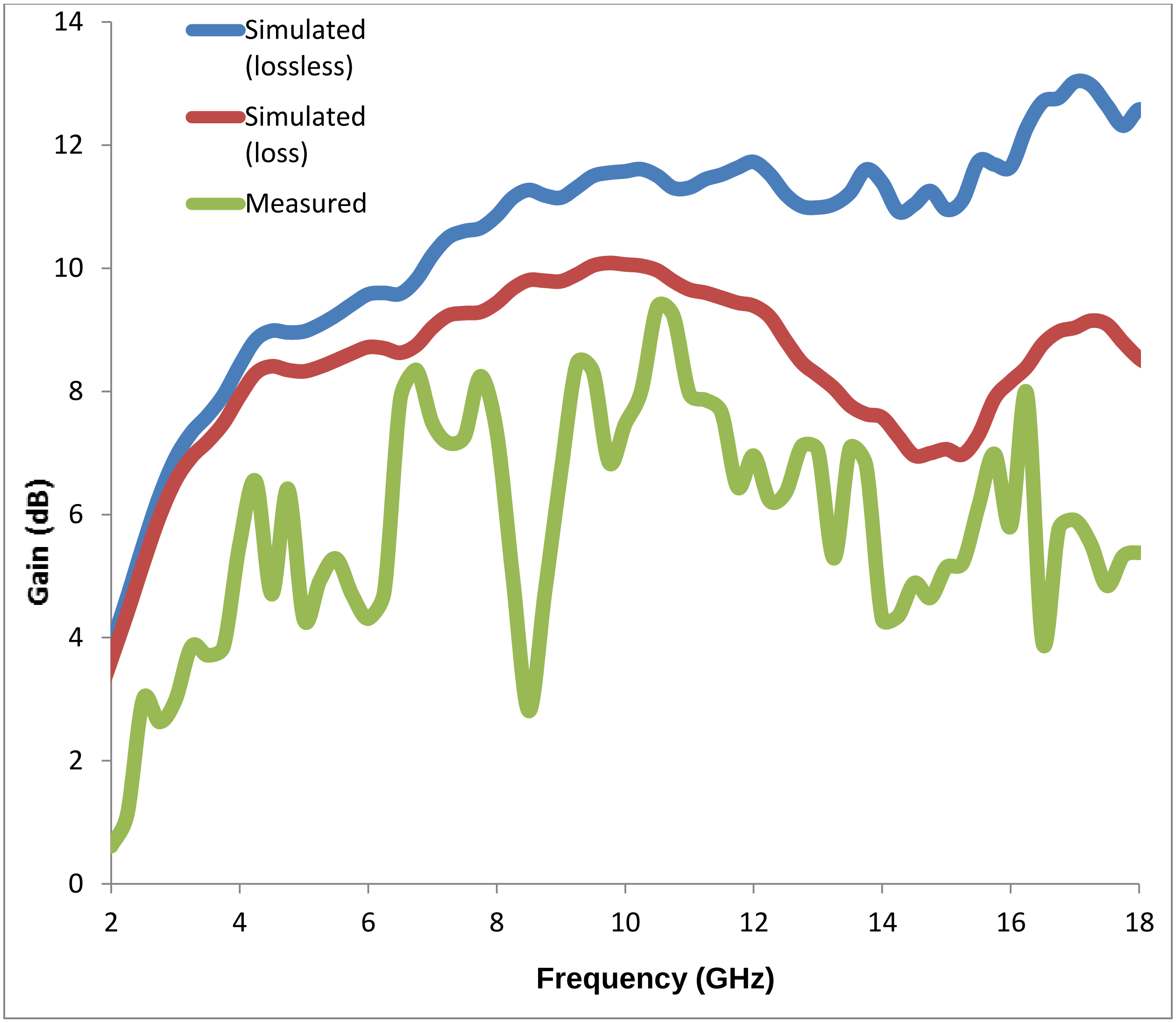

Figure 3.23 Simulated and Measured gain of 3D printed Bilateral Vivaldi with dielectric component. Simulations are carried out for dielectric component with and without loss tangent.

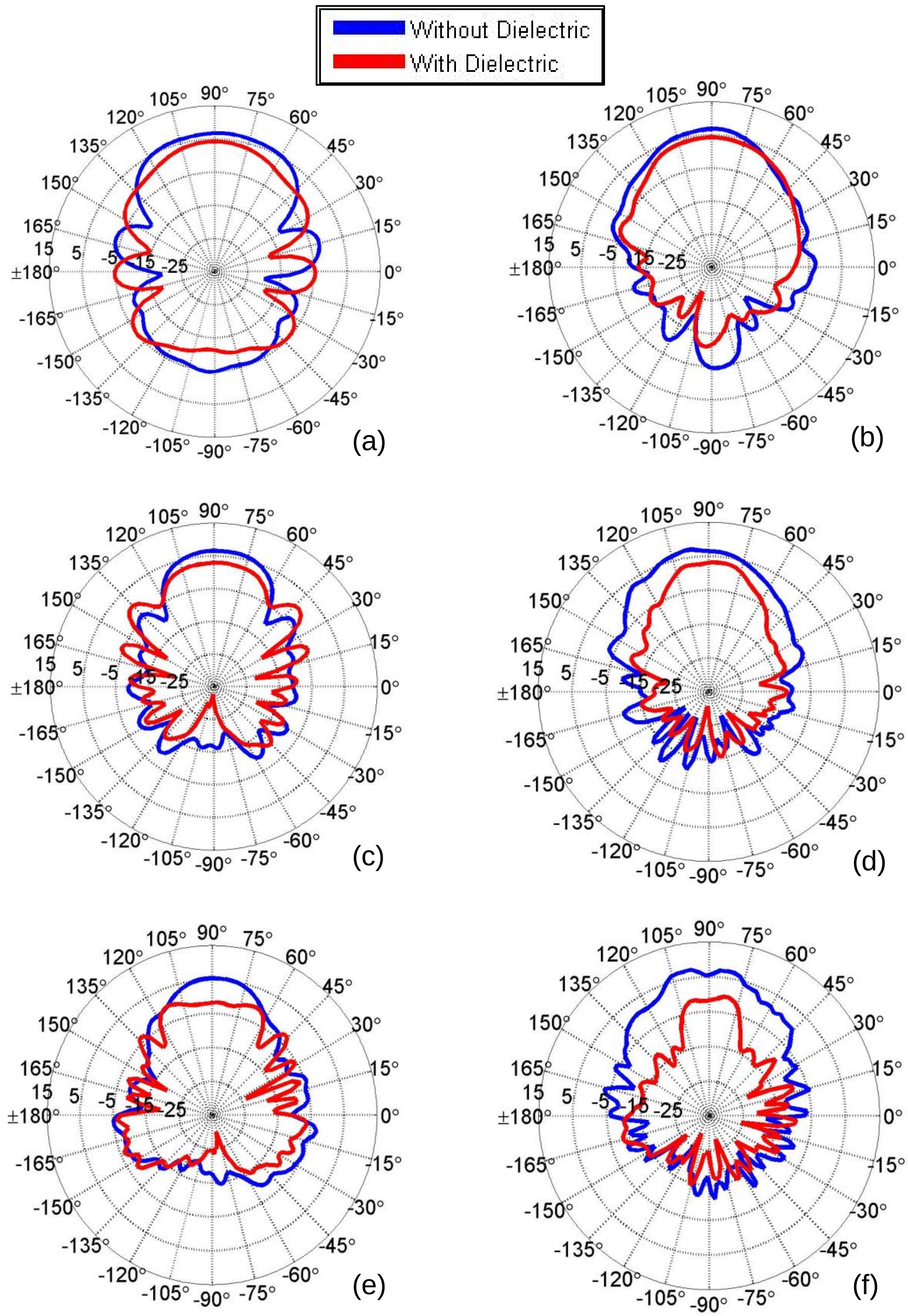

Figure 3.24 Measured radiation patterns of (a)-(b) E and H-planes at 5 GHz, (c)-(d) E and H planes at 10 GHz and (e)-(f) E and H-planes at 15 GHz.

3.8 Different of Dielectric Structure for Antenna

In the modern age, the communication has become easier with the development of wireless communication system technology. Different wireless systems have diverse operating frequency bands. One of the easiest solutions in having multi operation antenna is by adding more antennas in the system. This will lead the increase of the device's dimensions and as well as having trouble due to the coupling of each antenna that was mounted. Based on these problems the need of having an antenna that can operate in different range has developed interest in the design of a tunable antenna. The research on tunable antennas has been studied before [85]-[86]. Several methods have been successfully demonstrated that show the capability of tuning the resonant frequency of antenna elements. One of the ways is by using electronic tuning. The antenna was tune by using switchable capacitive load circuit which allows the antenna to have a wider operating bandwidth [87].

In this section, an alternative way in tuning the operating frequency was shown. Building on the advantages of 3D printed technology, more complex structure can be made. In this section the design of different shapes of dielectric using 3D printed which enable the tunability of antennas. As a proof of concept, a monopole antenna was used to show the effectiveness of dielectric loaded element to tune the frequency of the antenna. Monopole antenna was chosen because it is considered as one of the basic antennas that have been used for communications purposes. This is due to the fact that a monopole antenna is a simple design and the cost of fabrication is also low. A wire monopole antenna has a specific characteristic which is it has a narrow bandwidth. Taking advantage of this characteristic, the concept of 3D printed dielectric loaded shows the capability to tune the operating frequency.

3.9 Dielectric Loaded Monopole Antennas

The operating frequency of the monopole antenna can be tuned by changing the dielectric properties of the surrounding medium. 3D printed dielectric structures can be utilized to surround the monopole antenna. In the 3D printing, the dielectric constant of the medium is fixed. Thus, instead of changing the dielectric constant of the surrounding medium the shape of the structure was utilized to achieve frequency tuning. As a proof of concept, several cylindrical pieces were fabricated to be used in dielectric loading the antenna elements. The dielectric loading elements were fabricated using the same technique described in the previous chapter. Several pieces with diameter of 5mm, 9mm and 13 mm were fabricated and photos of these structures are shown in Figure 3.5. These rings were used individually or by stacking several of these pieces. Figure 3.26 shows a monopole antenna surrounded by dielectric ring.

The characterization of the antenna was done by measuring the reflection coefficients using a network analyzer, Agilent N5722A. The first measurement was done by just using one piece of the cylindrical dielectric loaded pieces place wrapping the wire monopole of each dimension. The S-parameters (S11) is then shown in Figure 3.27 to see the change of frequency. The main reference is the monopole without any dielectric loaded was also measured at 9.75 GHz. Any shifting in frequency will indicate that the dielectric elements act as a loading material. A clear shift in frequency can be seen when the dielectric was placed on the wire monopole. As the dimension of the dielectric increases the operated frequency shifted to the right. This shows that the permittivity of the dielectric was present allowing the shift in frequency.

Following dielectric extra pieces with the same dimension was placed on top of each other to see the effect of any shifting in frequency can be seen in Figure 3.28. The appearance of two resonance peaks can be seen. The first resonance peaks show that it was shifted to the left side while the second resonance shows the frequency shifted to the right. The shifting is due to the diameter and height of the dielectric loaded.

This proves that the 3D printed structures can be used for dielectric loading that enables the antenna resonant frequency shift. Further investigation will be done in the future. One aspect that will be investigated is by using 3D printed granules. The 3D printed granules configuration will look like a Lego shape. In this case the monopole structure will be surrounded by the 3D granules to form a geometrical shape that allows the operation frequency to be shifted according to the desired frequency.

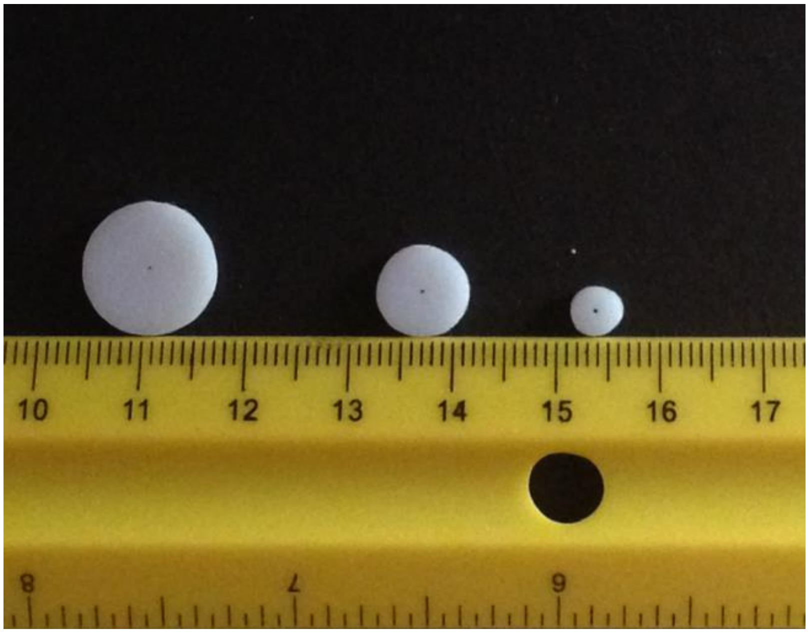

Figure 3.25 Fabricated 3D cylindrical dielectric components.

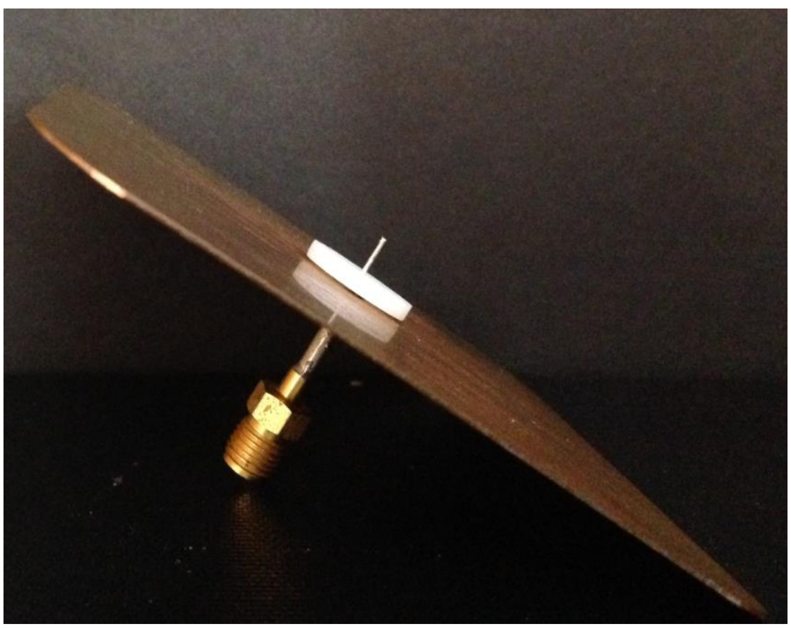

Figure 3.26 Dielectric structure used in loading the antenna element.

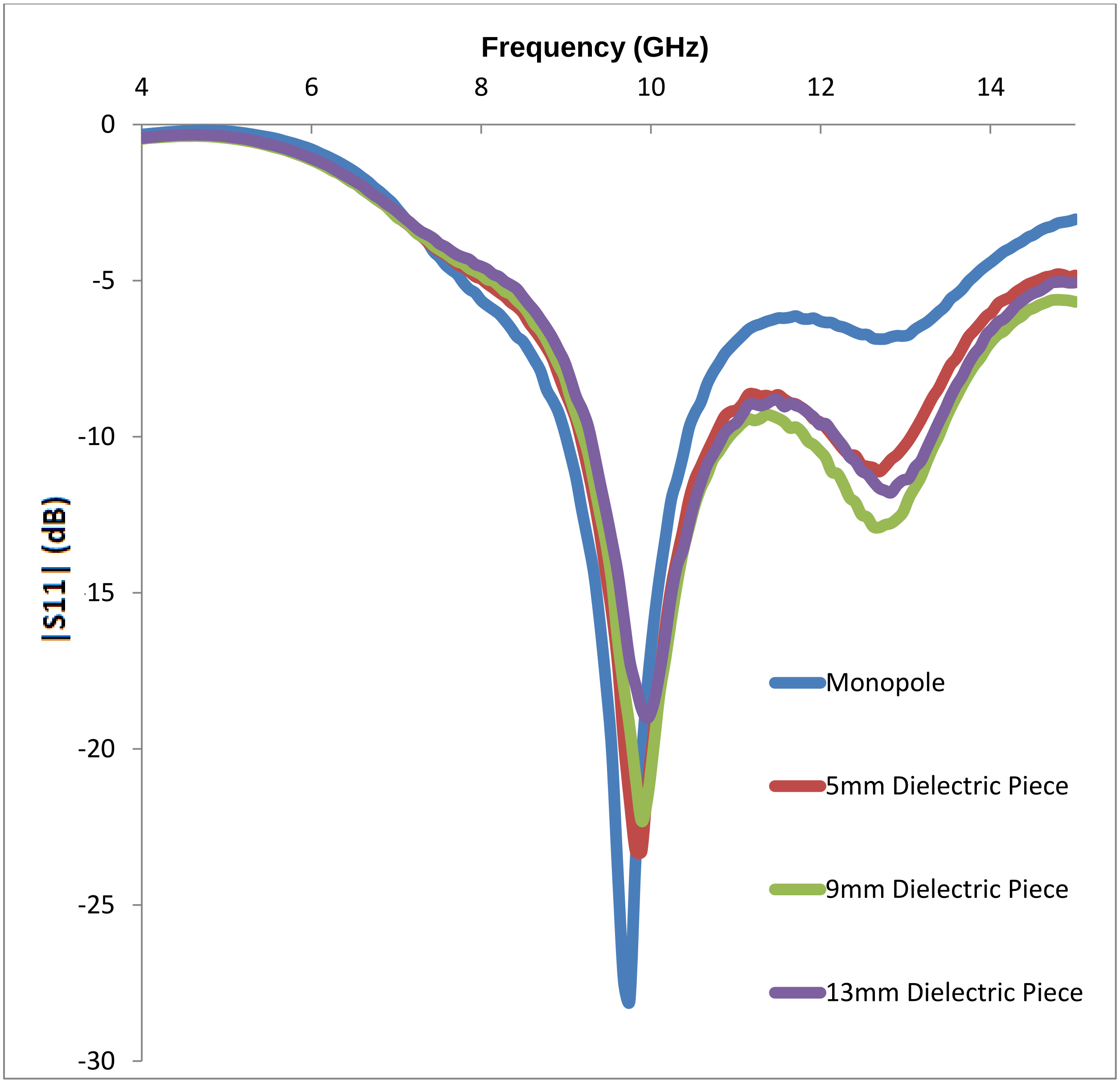

Figure 3.27 Measured reflection coefficients of a monopole loaded with different diameter dielectric rings (5mm, 9mm and 13mm) dielectric pieces.

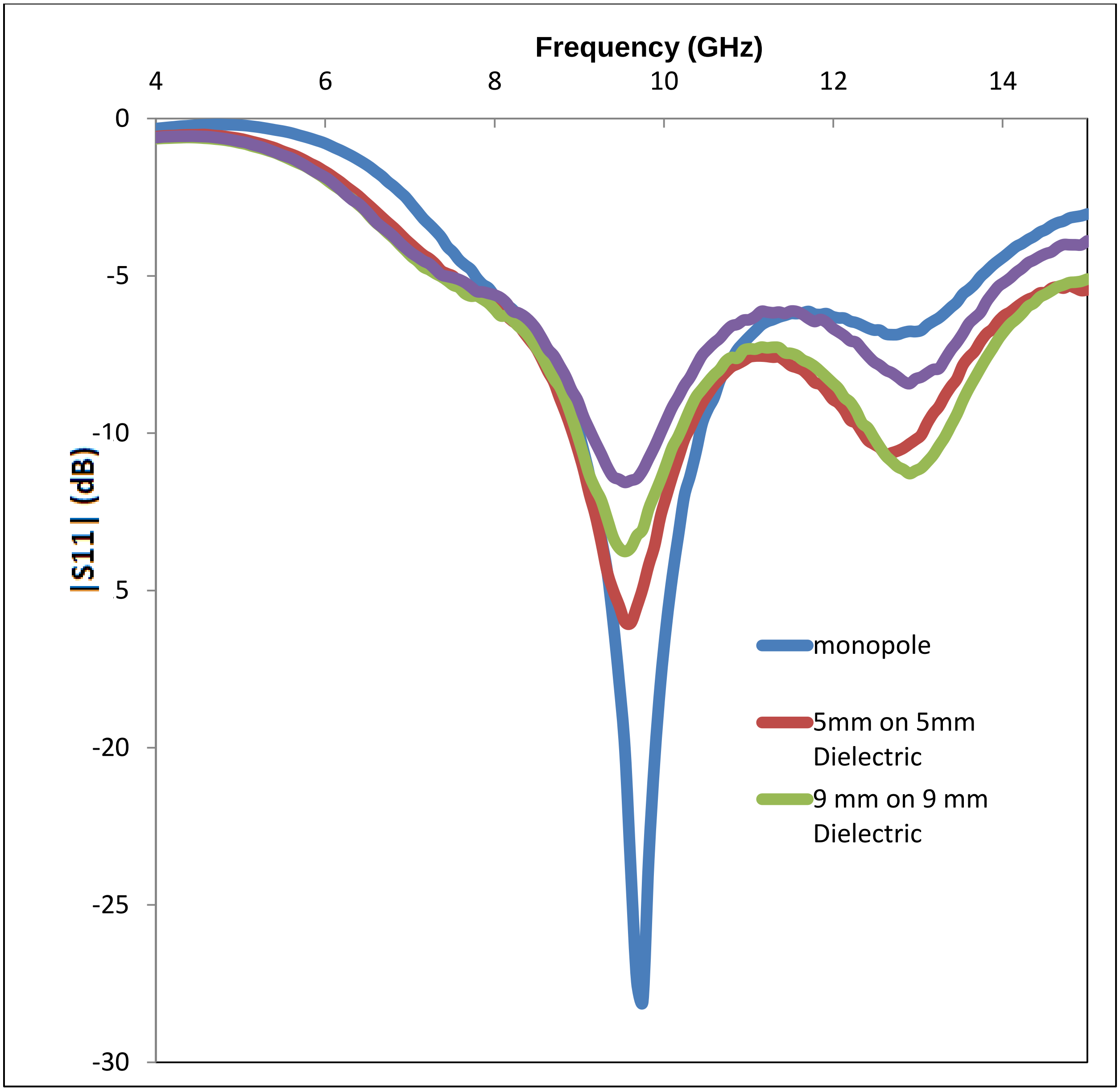

Figure 3.28 Measured reflection coefficients of a monopole loaded with bi-layer dielectric rings for different diameters (5mm, 9mm and 13mm) dielectric pieces.

3.10 Simulated Design of Granule Antenna aka Lego Antenna

From the above measurements it is clear that dielectric loading can be used in the design of novel antennas with improved performance. Here, a new type of antenna structure is demonstrated that can be physically reconfigured called granule antenna. Antennas have become an integral part of day-to-day electronics, ranging from hand-held electronics to environment sensors. There is significant interest in reconfigurable and tunable antenna elements so that they can adapt to their environment. Frequency of operation of an antenna element can be tuned by loading with electronic tuning elements (e.g., varactor diodes) or by physically changing the structure of the antenna.

Here a novel reconfigurable antenna design is introduced based on rearrangement of physical layout of the antenna structure. The physical structure of an antenna can be subdivided into small 3D granules and these granules can be rearranged to form any geometry (interchangeable antenna). The idea of interchangeable antenna comes from the idea of using Lego shape material as a building block in the assemblymen of an antenna. Lego blocks can be stacked to create different 3D shape objects. Similarly, small 3D printed blocks (granules) conducting blocks can be used to form any complex 3D antenna elements to achieve desired performance (operating frequency and radiation pattern). For example, a simple monopole antenna can be transformed to a folded antenna just by rearranging the granules. Thus, a new design is obtained in a short time while avoiding remanufacturing of new designs. Multiple structures can be made by using different shape of Lego like granules to create a new antenna design.

As a proof of concept, several designs of 3D folded antenna with the addition of 3D printed blocks were simulated. Figure 3.29 to Figure 3.32 shows the design of the antenna. In the simulation, the 3D block structures were made from ABS and also copper. Simulated result is presented in Figure 3.33 shows the reflection coefficient of the reference, first, second and third design of 3D folded antenna including the 3D block structures. The reason for doing this is to see the interchangeable combination needed to change the frequency of the antenna. The reference structure of the 3D folded antenna shows the operational frequency of 2.81 GHz. By adding the 3D block structures, the frequency is shifted and the new operating frequencies are 1.84 GHz, 1.71 GHz and 1.61 GHz, respectively. This shows the ability to tune the resonance frequency by using different combinations of the 3D blocks structures. Furthermore, this approach also allows in the minituarization of the antenna element. The fabrication was done in order to verify the simulated results. However, due to the limitations of the 3D printed machine and also the sputtering machine the elements were difficult to fabricate. In the future, further steps will be implemented in order to prove the concept of this 3D printed granule based antenna.

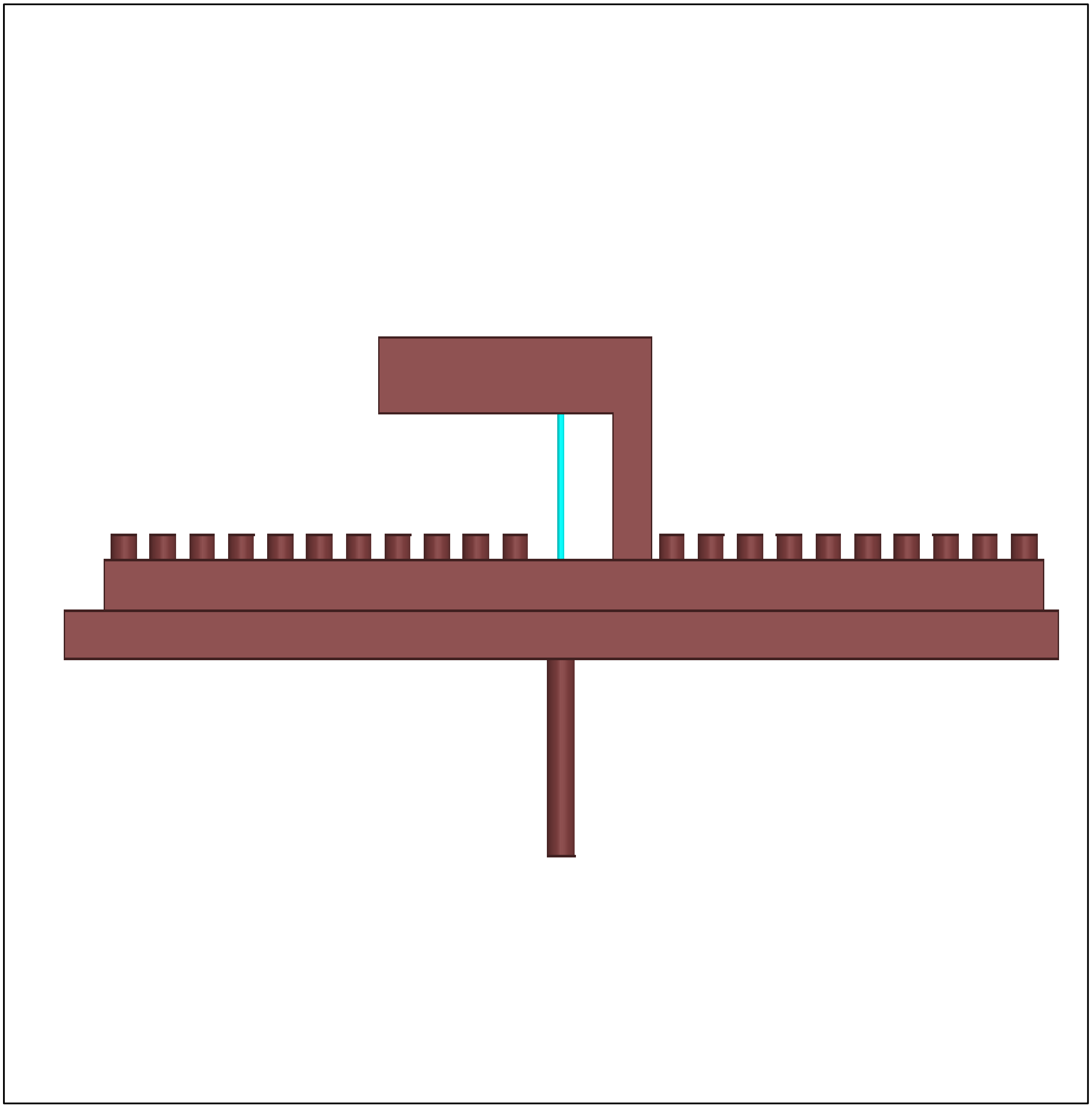

Figure 3.29 Reference structure for a 3D folded antenna.

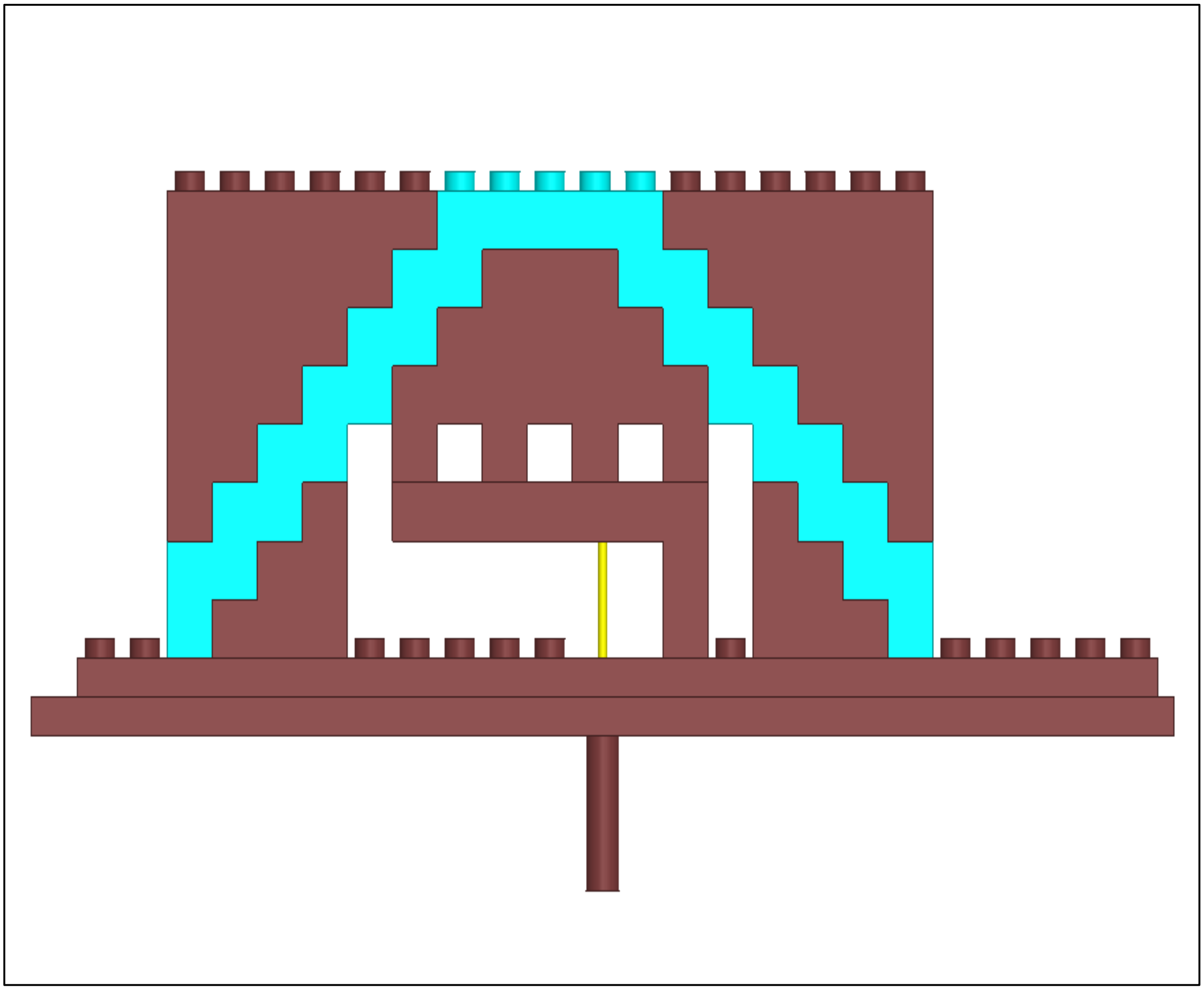

Figure 3.30 First Configuration of 3D folded antenna with additional of 3D printed blocks.

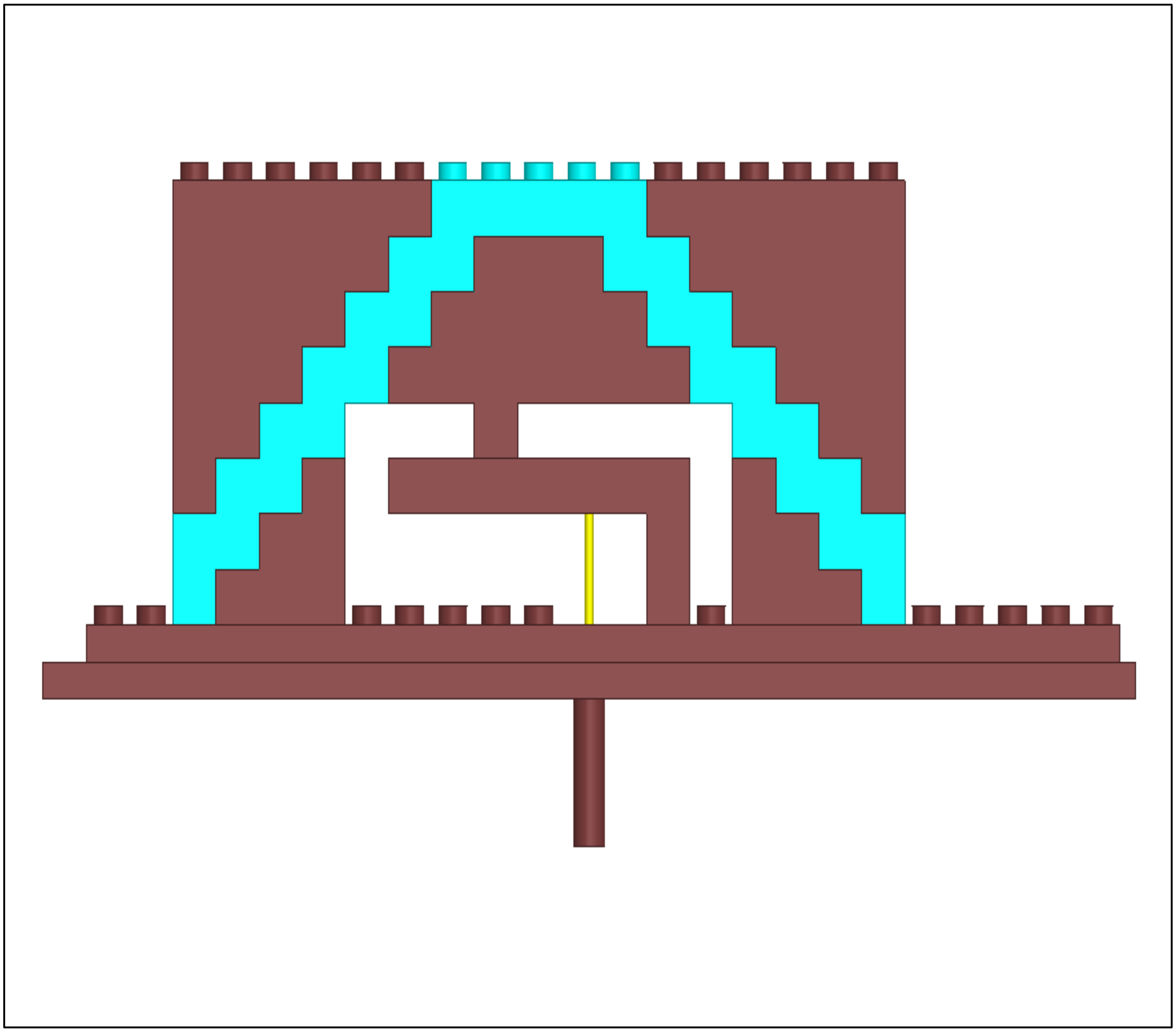

Figure 3.31 Second Configuration of 3D folded antenna with additional of 3D printed blocks.

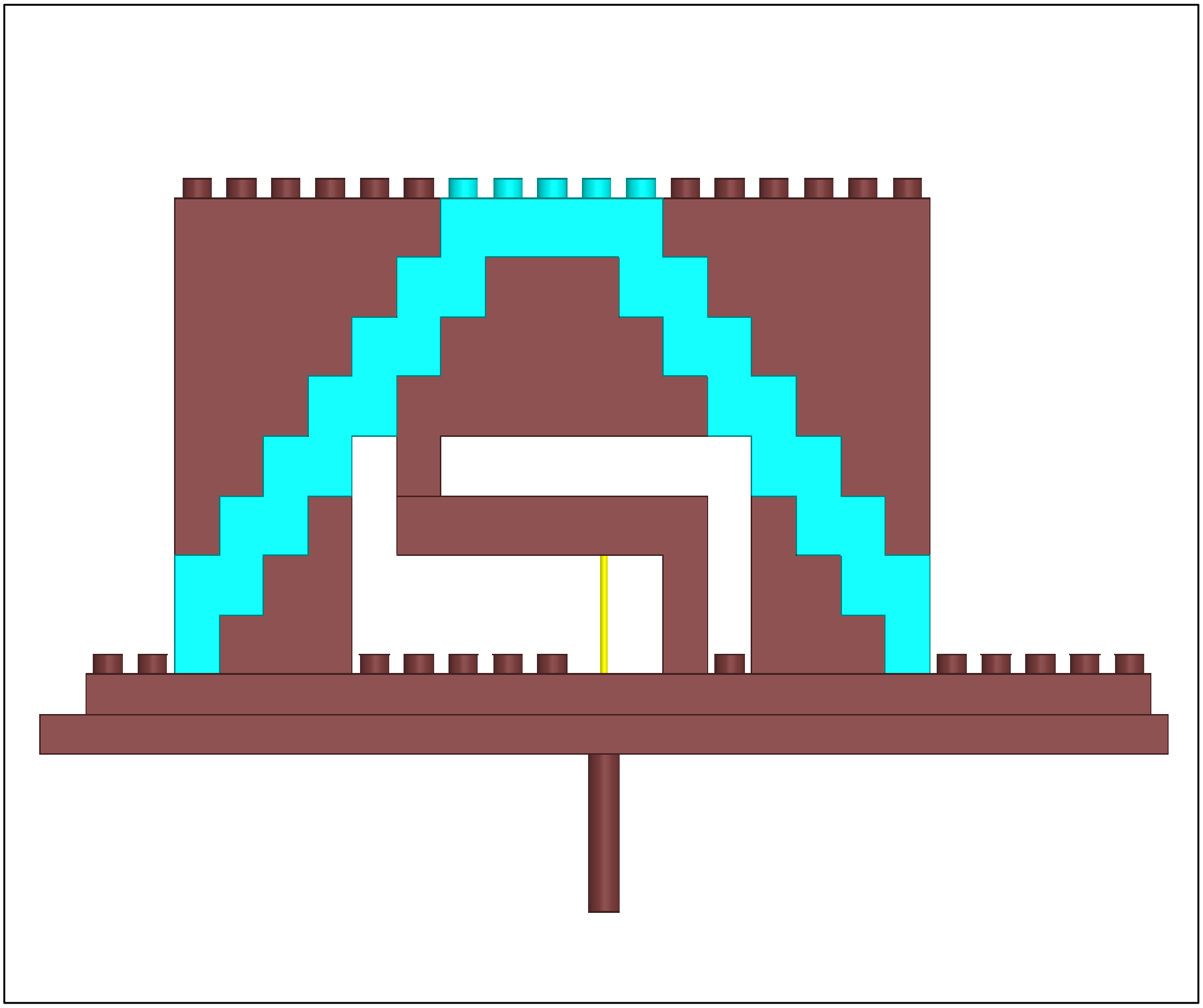

Figure 3.32 Third Configuration of 3D folded antenna with additional of 3D printed blocks.

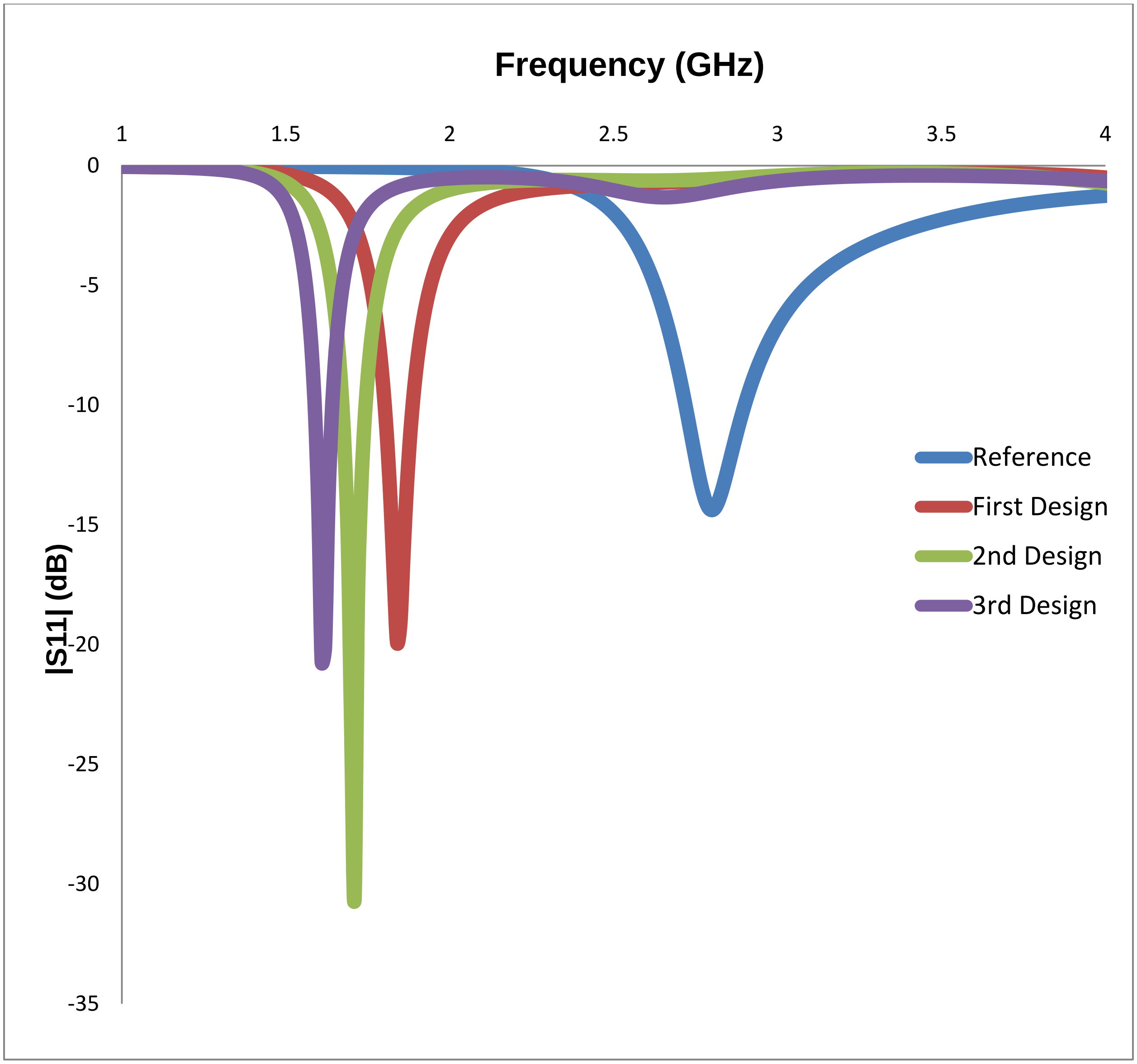

Figure 3.33 Simulated reflection coefficients of 3D folded antennas.

3.11 Simulation and Measurement of 3D Printed Patch Antenna

Patch (Microstrip) antenna is one of the widely used antennas due to its simplicity, lightweight, inexpensive and compatibility. The basic structure of patch antenna consists of a dielectric substrate in the middle of the metalized ground plane located on the bottom side while metalized radiating patch at the top shown in Figure 3.29. A 3D patch antenna was designed and simulated using HFSS. The dimension of the design was given as well in Figure 3.29. In the simulation show that the patch antenna operates at 5.26 GHz. Based on the simulated design, a 3D printed patch antenna was fabricated using 3D printing technology as use in previous fabrication. The substrate use is the same material that has been used in the past to fabricate the Vivaldi antenna which is ABS. The patch was metalized by using a sputtering machine where a copper layer was placed. The fabricated 3D printed patch antenna is shown in Figure 3.30. The reflection coefficient is measured using a vector analyzer device called Agilent N5227A network analyzer. The comparison was made between the fabricated 3D printed patch antenna and the simulated 3D patch antenna is shown in Figure 3.31. The operational frequency for the measured 3D printed patch antenna was 3.48 GHz. The results show very good agreement between the simulation and the measured data. The slight difference is most likely due to the air gap located between the ground plane and the substrate. Collectively, the result shows that a simple patch antenna can be fabricated using 3D printing technology.

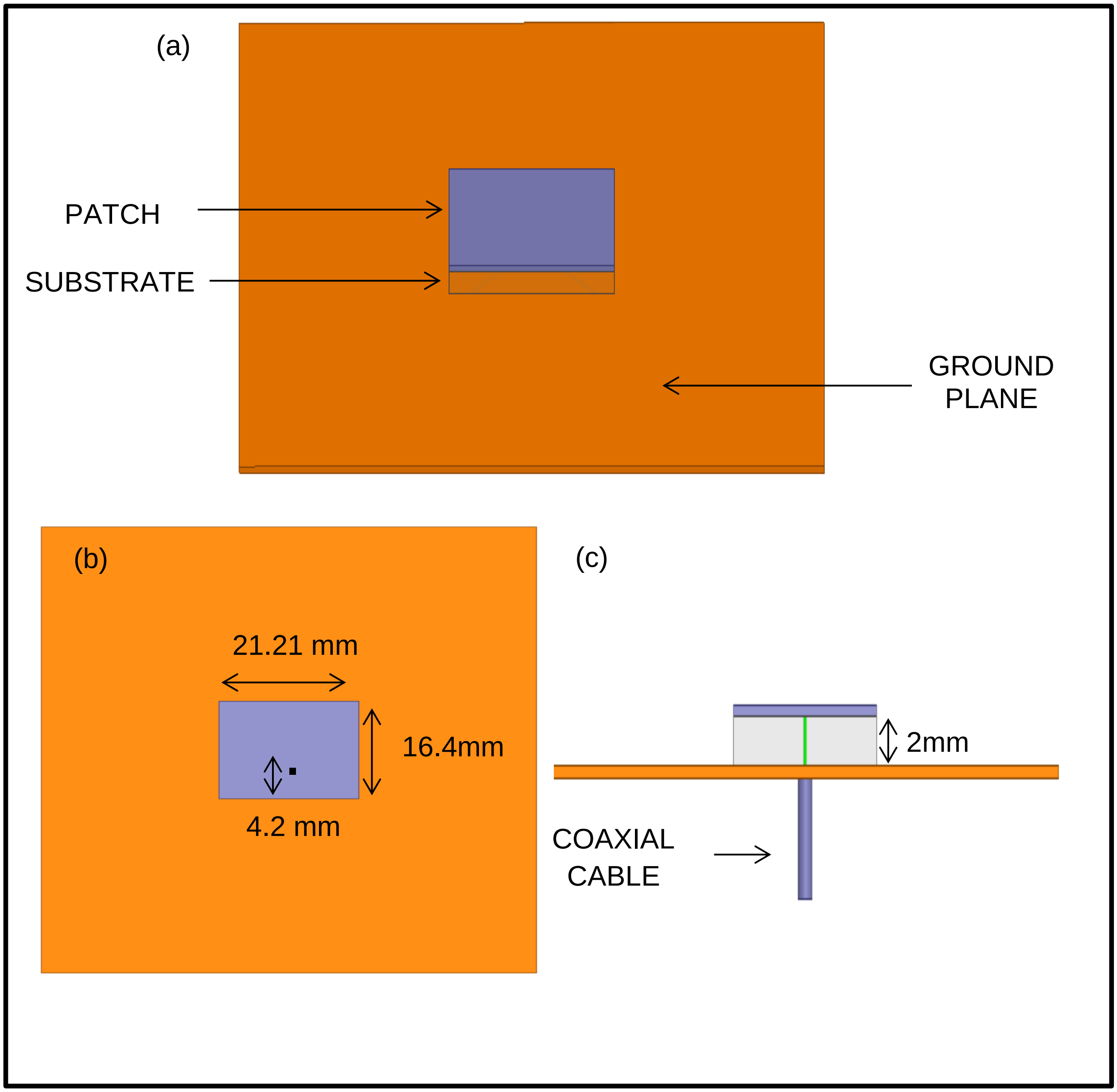

Figure 3.34 3D patch antenna design (a) 3D view (b) Top view and (c) Side view.

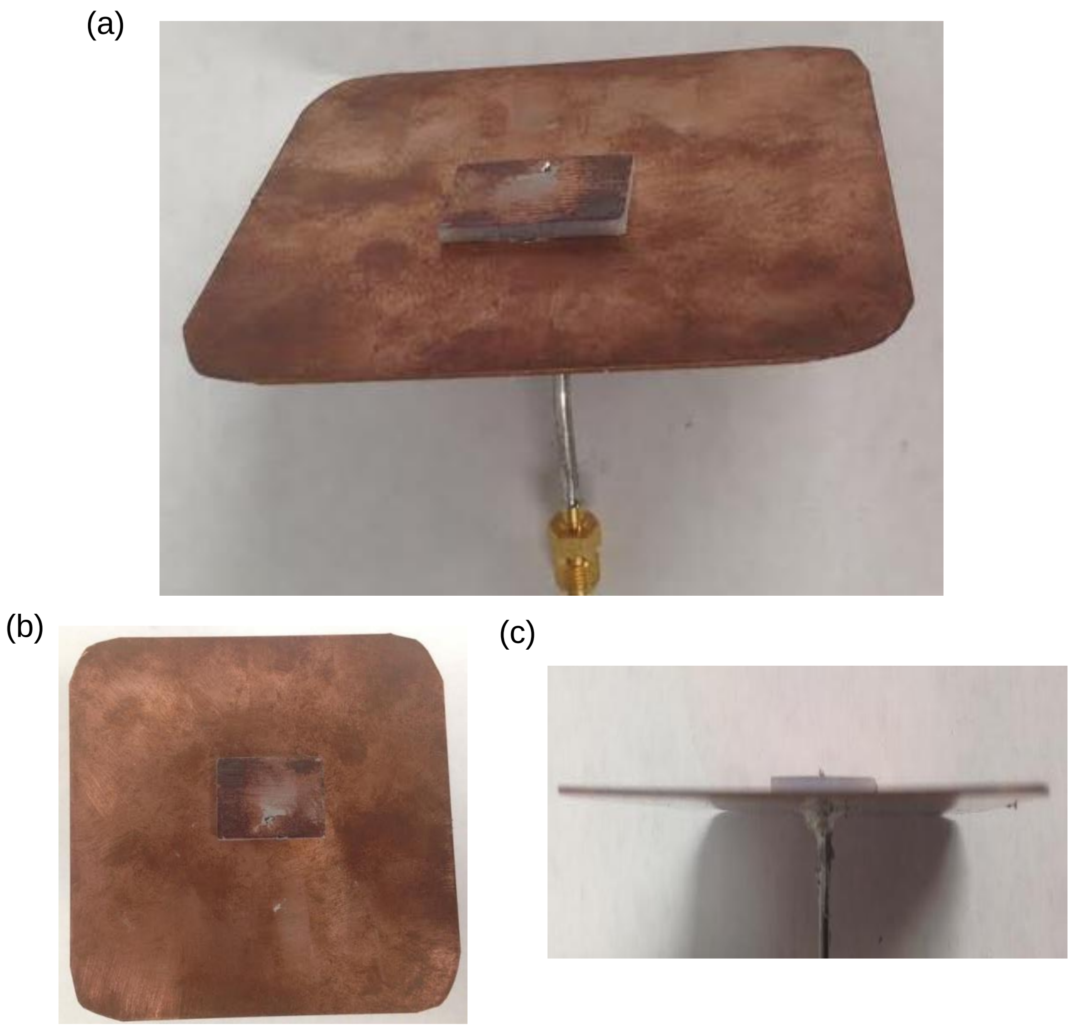

Figure 3.35 Fabricated 3D patch antenna design (a) 3D view (b) Top view and (c) Side view.

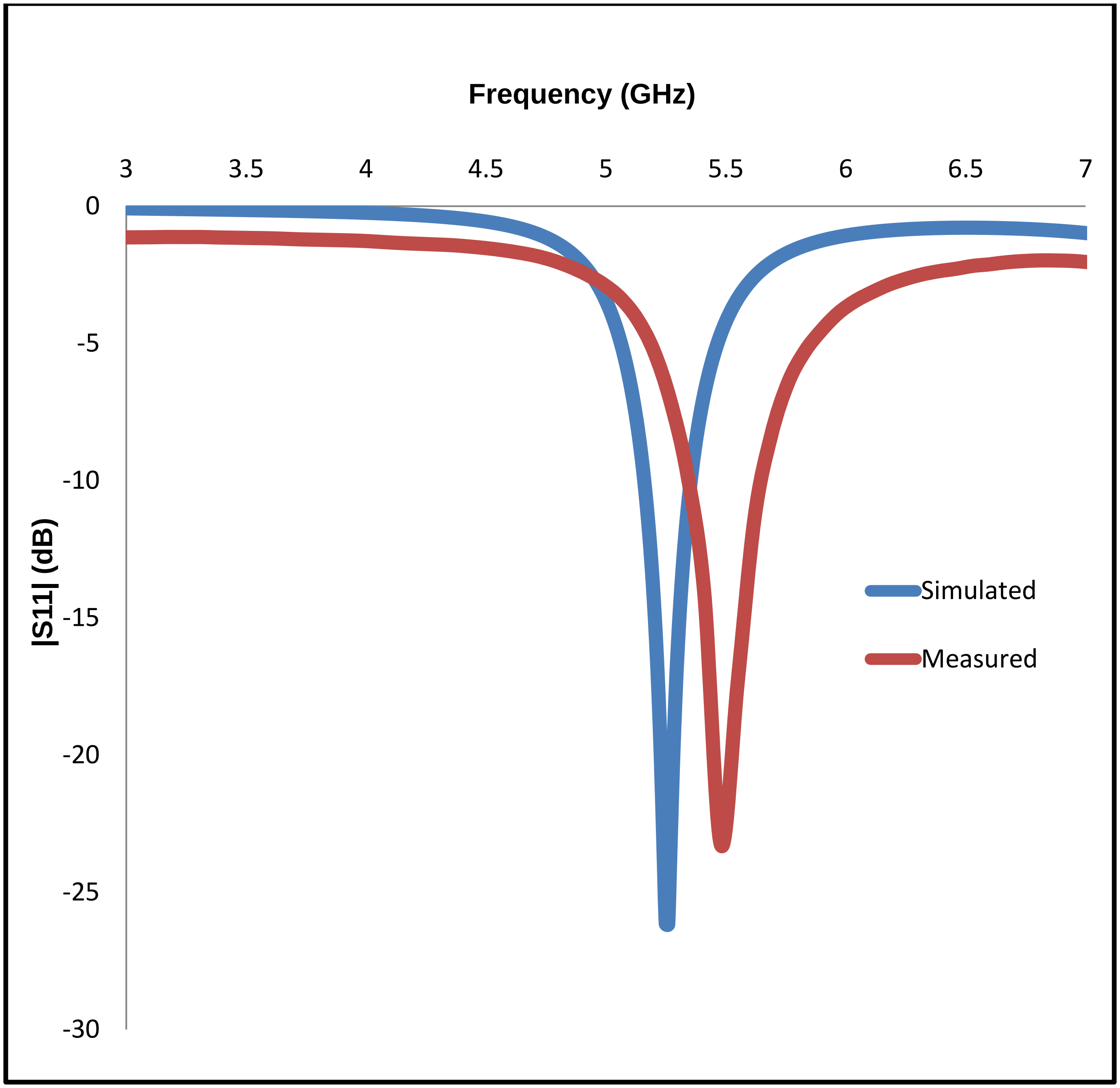

Figure 3.36 Simulated and Measured of 3D printed patch antenna for reflection coefficient.

3.12 Conclusion

The main focus of this chapter was to design 3D printed antenna that was able to integrate 3D printed dielectric as well. The first design of the 3D printed Vivaldi antenna was an improvement made from the previous chapter. The addition of bilateral pieces at the end of the Vivaldi helps improve the bandwidth and the gain of the antenna. Further modification of the antenna by placing 3D printed dielectric component into the antenna. The dielectric component was used as a focusing element which guided the wave and enables the beamwidth to be narrower. However, the fabricated 3D printed dielectric has high loss (dielectric loss tangent). This resulted in a much lesser gain and bandwidth as compared to simulation results.

Taking advantage of the 3D printing capability, 3D printed cylindrical dielectric was developed to load the monopole antennas. The cylindrical dielectric was placed onto a monopole that allows the monopole operational frequency to be shifted. The dielectric component that was used act as a loading element that allows the tunability of the monopole antenna. Using the same concept, a 3D granule structure was designed to act as an interchangeable structure which is used to load a folded antenna. The interchangeable structure allows the tunability of the folded antenna as well as in its minituarization.

A 3D patch antenna was simulated and measured to show that the substrate dielectric can be 3D printed. Overall the patch antenna shows reasonable similarity in the operational frequency. The discrepancies are due to the air gap located between the substrate and the ground plane (copper plate). The air gap effectively reduced the dielectric constant of the substrate and thus the frequency shifts to higher values as seen in the measured results.

Chapter 4

Conclusions

In this thesis, 3D printing technology has been used as a fabrication technique to produce a range of antenna designs. 3D printing technology has shown its practical application to fabricate limitless shape and structure that is suited for various applications and novel antenna designs.

In Chapter 2, the fabrication of two Vivaldi antenna designs using metalized 3D printed plastic-polymers is presented. The printed antennas with these materials provide a low cost, light weight and an accurate fabrication solution. In addition, both antennas exhibit a high maximum gain of around 12 dB as well as providing a wide bandwidth, approximately 14.5 GHz. The antennas were fabricated using an ABS polymer material and covered with a thin layer of sputtered copper. The measured and simulated results are shown to match well, displaying the potential of 3D printing wideband antennas. This antenna design using 3D printing is demonstrated for the first time under this research work.

Chapter 3 shows approaches to improve the Vivaldi antenna design that can readily be fabricated using 3D printing. A bilateral piece was added in order to improve the impedance matching of the antenna and to further improve the bandwidth. Further improvement in performance is achieved by incorporating a dielectric component in the aperture region of the antenna. The dielectric was used as a focusing element to guide the radiation energy. The simulated results showed improved bandwidth and higher gain. However, the measured results showed several discrepancies from the simulated results. This was largely due to the large loss (high tan-delta) associated with the ABS polymer material used in guiding the wave. The performance of the antenna can be improved by replacing this material with a lower loss dielectric. However, this antenna design demonstrated that 3D printing allows the integration of dielectric and metals to form novel structures.

As a further development, the 3D printed dielectric was used to design a reconfigurable antenna through dielectric loading. Cylindrical dielectric pieces with different diameter were placed onto a monopole which enables the frequency of the monopole to be shifted dictated by the size of the ring structure. Furthermore, a novel antenna design is shown which utilizes 3D granule structures that can be physically arranged in any configuration to reconfigure an antenna element, similar to Lego structures. The granule structures can be made both conductive and non-conductive and their combination allows for novel antenna designs. A simple printed patch antenna is also demonstrated with utilizes the 3D printed ABS as a substrate material. The measured and simulated results match very closely. The slight discrepancies noted were largely due to the presence of air gap in between the ABS substrate and the ground plane.

The work of this thesis demonstrated the applicability of 3D printing in the design and fabrication of novel antenna structures. This technology not only allows in the design of complex 3D structures, but also allows in the integration of conductive and non-conductive regions that provides another degree of design flexibility. Overall, 3D printing allows in the design of complex 3D antennas that would have been difficult to fabricate using conventional microfabrication approaches. Thus, this technology proves to be beneficial in the design of antenna elements and their integration in a host of electronic platforms.

Future work

As proven, the capability of 3D printing technology shows that it is a reliable way of fabricating antenna as well as dielectric component for the antenna. Further research will be done to fabricate microwave component such as waveguide, horn antennas, directional couples as well as other microwave devices. Furthermore, novel structures having interwoven metallic and dielectric regions (e.g., dielectric loaded antennas) can be designed which would be difficult to achieve using conventional fabrication approaches. Further work also includes integrating less lossy material for the dielectric components. Furthermore, the granules structure will be fabricated through 3D printing of plastic parts followed by blanket metallization. 3D printing (or additive manufacturing) allows in the fabrication of complex 3D parts which can be metalized through thermal evaporation or electroless plating. A host of structures has been designed and utilized in the assembly of various 3D antenna structures (e.g., monopole, patch and Yagi antennas) and these designs will be presented in this paper. The proposed approach allows in the design of complex antennas that can readily be assembled and tested. This approach opens a new approach to design and test antenna elements prior to mass manufacturing. Also, it can be adopted as an educational tool to train next generation of antenna design engineers.

BIBLIOGRAPHY

BIBLIOGRAPHY

[1] Whittaker, John C. Flintknapping: making and understanding stone tools. University of Texas Press, 2010.

[2] Flenniken, J. Jeffrey. "The past, present, and future of flintknapping: an anthropological perspective." *Annual Review of Anthropology* (1984): 187-203.

[3] Patterson, Leland W., and J. B. Sollberger. "Replication and classification of small size lithic debitage." *The Plains Anthropologist* (1978): 103-112.

[4] Wei, W , Non-traditional machining techniques for fabricating metal aerospace filters , Chinese Journal of Aeronautics , vol 21 , no 5, p.441 - 447

[5] Teti, R , Machining of Composite Materials , CIRP Annals - Manufacturing Technology , vol 51 , no 2, p.611 - 634

[6] F. Müller and J Monaghan Non-conventional machining of particle reinforced metal matrix composite , International Journal of Machine Tools and Manufacture , vol 40 , no 9, p.1351 - 1366

[7] Nagata, Fusaomi, et al. "Robotic sanding system for new designed furniture with free-formed surface." *Robotics and Computer-Integrated Manufacturing*23.4 (2007): 371-379.

[8] Özel, Tugrul. "Computational modelling of 3D turning: Influence of edge micro-geometry on forces, stresses, friction and tool wear in PcBN tooling." *Journal of Materials Processing Technology* 209.11 (2009): 5167-5177.

[9] Oktem, Hasan, Tuncay Erzurumlu, and Ibrahim Uzman. "Application of Taguchi optimization technique in determining plastic injection molding process parameters for a thin-shell part." *Materials & design* 28.4 (2007): 1271-1278.

[10] Larsson, O.; Ohman, O.; Billman, A.; Lundbladh, L.; Lindell, C.; Palmskog, G., "Silicon based replication technology of 3D-microstructures by conventional CD-injection molding techniques,"*Solid State Sensors and Actuators, 1997. TRANSDUCERS '97 Chicago., 1997 International Conference on* , vol.2, no., pp.1415,1418 vol.2, 16-19 Jun 1997

[11] Ye, Hezhou, Xing Yang Liu, and Hanping Hong. "Fabrication of metal matrix composites by metal injection molding—A review." *Journal of materials processing technology* 200.1 (2008): 12-24.

[12] Sachs, Emanuel, et al. "Production of injection molding tooling with conformal cooling channels using the three dimensional printing process." *Polymer Engineering & Science* 40.5 (2000): 1232-1247.

[13] Kodama, Hideo. "Automatic method for fabricating a three-dimensional plastic model with photo-hardening polymer." *Review of Scientific Instruments* 52.11 (1981): 1770-1773.

[14] Hull, Charles. "StereoLithography: Plastic prototypes from CAD data without tooling." *Modern Casting* 78, no. 8 (1988): p38.

[15] Bogue, Robert. "3D printing: the dawn of a new era in manufacturing?."*Assembly Automation* 33, no. 4 (2013): 307-311.

[16] Jacobs, Paul Francis, Rapid prototyping & manufacturing: fundamentals of stereolithography. Society of Manufacturing Engineers; ed, 1992.

[17] Liska, R., M. Schuster, R. Inführ, C. Turecek, C. Fritscher, B. Seidl, V. Schmidt et al. "Photopolymers for rapid prototyping." Journal of Coatings Technology and Research 4, no. 4 (2007): 505-510

[18] Silva, Daniela Nascimento, Marília Gerhardt de Oliveira, Eduardo Meurer, Maria Inês Meurer, Jorge Vicente Lopes da Silva, and Ailton Santa-Bárbara. "Dimensional error in selective laser sintering and 3D-printing of models for craniomaxillary anatomy reconstruction." *Journal of Cranio-Maxillofacial Surgery* 36, no. 8 (2008): 443-449.

[19] Hutmacher, Dietmar W., Thorsten Schantz, Iwan Zein, Kee Woei Ng, Swee Hin Teoh, and Kim Cheng Tan. "Mechanical properties and cell cultural response of polycaprolactone scaffolds designed and fabricated via fused deposition modeling." Journal of biomedical materials research 55, no. 2 (2001): 203-216.

[20] Leong, K. F., C. M. Cheah, and C. K. Chua. "Solid freeform fabrication of three-dimensional scaffolds for engineering replacement tissues and organs."*Biomaterials* 24, no. 13 (2003): 2363-2378.

[21] Meteyer, Simon, Xin Xu, Nicolas Perry, and Yaoyao Fiona Zhao. "Energy and Material Flow Analysis of Binder-jetting Additive Manufacturing Processes."*Procedia CIRP* 15 (2014): 19-25.

[22] Druschitz, A., C. Williams, D. Snelling, and M. Seals. "Additive Manufacturing Supports the Production of Complex Castings." In Shape Casting: 5th International Symposium 2014, pp. 51-57. John Wiley & Sons, Inc., 2013.

[23] Heinl, Peter, Lenka Müller, Carolin Körner, Robert F. Singer, and Frank A. Müller. "Cellular Ti–6Al–4V structures with interconnected macro porosity for bone implants fabricated by selective electron beam melting." Acta biomaterialia 4, no. 5 (2008): 1536-1544.

[24] Klammert, Uwe, Uwe Gbureck, Elke Vorndran, Jan Rödiger, Philipp Meyer-Marcotty, and Alexander C. Kübler. "3D powder printed calcium phosphate implants for reconstruction of cranial and maxillofacial defects." *Journal of Cranio-Maxillofacial Surgery* 38, no. 8 (2010): 565-570.

[25] Mannoor, Manu S., Ziwen Jiang, Teena James, Yong Lin Kong, Karen A. Malatesta, Winston O. Soboyejo, Naveen Verma, David H. Gracias, and Michael C. McAlpine. "3D printed bionic ears." Nano letters 13, no. 6 (2013): 2634-2639.

[26] van Noort, Richard. "The future of dental devices is digital." Dental Materials 28, no. 1 (2012): 3-12.

[27] Hockaday, L. A., K. H. Kang, N. W. Colangelo, P. Y. C. Cheung, B. Duan, E. Malone, J. Wu et al. "Rapid 3D printing of anatomically accurate and mechanically heterogeneous aortic valve hydrogel scaffolds." Biofabrication 4, no. 3 (2012): 035005.

[28] Onuh, Spencer O., and Yahaya Y. Yusuf. "Rapid prototyping technology: applications and benefits for rapid product development." Journal of intelligent manufacturing 10, no. 3-4 (1999): 301-311.

[29] Chapman, Craig B., and Martyn Pinfold. "The application of a knowledge based engineering approach to the rapid design and analysis of an automotive structure." Advances in Engineering Software 32, no. 12 (2001): 903-912.

[30] Campbell, Thomas, Christopher Williams, Olga Ivanova, and Banning Garrett. "Could 3D Printing Change the World?." Technologies, Potential, and Implications of Additive Manufacturing. Washington, DC: Atlantic Council (2011).

[31] Kurczewski, N., “3D Printed Car: NY Daily News Autos gets a ride in the Local Motors “Strati” 3-D printed roadster”, 'NEW YORK DAILY NEWS’, October, 2014.

[32] Griffiths,S.,”Is-best-3D-printer-Machine-creates-exact-replica-face-CHOCOLATE” , Dailymail UK , December , 2013.

[33] Southerland, Deborah, Peter Walters, and David Huson. "Edible 3D printing." In NIP & Digital Fabrication Conference, Society for Imaging Science and Technology, 2011.vol. 2011, no. 2, pp. 819-822.

[34] Periard, Dan, Noy Schaal, Maor Schaal, Evan Malone, and Hod Lipson. "Printing Food." In *Proceedings of the 18th Solid Freeform Fabrication Symposium, 2007, Austin TX*, pp. 564-574.

[35] Schöning, Johannes, Yvonne Rogers, and Antonio Krüger. "Digitally enhanced food." IEEE Pervasive Computing 11, no. 3 (2012): 0004-6.

[36] Plafke, J “The world’s first 3D printed metal gun is a beautiful .45 caliber M1911 pistol” , 'ExtremeTech' , November , 2013,

[37] Hollingsworth, B , World’s First 3D Printed Metal Gun Successfully Fires 600+ Rounds , 'CNSNews.com' , November , 2013

[38] Morelle, R , “Working gun made with 3D printer” , 'BBC World ' , May , 2013.

[39] Lewandrowski, N, “3D Printing for Fashion: Additive Manufacturing and its Potential to Transform the Ethics and Environmental Impact of the Garment Industry”, May, 2014

[40] Franssila S. Introduction to microfabrication. Chichester; Hoboken, NJ: John Wiley and Sons; 2004.

[41] Brown, E.R., "RF-MEMS switches for reconfigurable integrated circuits," Microwave Theory and Techniques, IEEE Transactions on , vol.46, no.11, pp.1868,1880, Nov 1998

[42] Becker, Holger, and Claudia Gärtner. "Polymer microfabrication methods for microfluidic analytical applications." Electrophoresis 21, no. 1 (2000): 12-26.

[43] Guiseppi - Elie, Anthony, Norman F. Sheppard, Sean Brahim, and Dyer Narinesingh. "Enzyme microgels in packed - bed bioreactors with downstream amperometric detection using microfabricated interdigitated microsensor electrode arrays." Biotechnology and bioengineering 75, no. 4 (2001): 475-484.

[44] Waits, C. M., Brian Morgan, M. Kastantin, and R. Ghodssi. "Microfabrication of 3D silicon MEMS structures using gray-scale lithography and deep reactive ion etching." Sensors and Actuators A: Physical 119, no. 1 (2005): 245-253.

[45] Voldman, Joel, Martha L. Gray, and Martin A. Schmidt. "Microfabrication in biology and medicine." Annual review of biomedical engineering 1, no. 1 (1999): 401-425.

[46] Xu, Zhen, Yuan Zhang, Peigang Li, and Chao Gao. "Strong, conductive, lightweight, neat graphene aerogel fibers with aligned pores." ACS nano 6, no. 8 (2012): 7103-7113.

[47] Calle, Carlos I., and Richard B. Kaner. "Graphene-Based Ultra-Light Batteries for Aircraft." (2014).

[48] Novoselov, Konstantin S., V. I. Fal, L. Colombo, P. R. Gellert, M. G. Schwab, and K. Kim. "A roadmap for graphene." Nature 490, no. 7419 (2012): 192-200.

[49] Chen, Zongping, Chuan Xu, Chaoqun Ma, Wencai Ren, and Hui - Ming Cheng. "Lightweight and Flexible Graphene Foam Composites for High - Performance Electromagnetic Interference Shielding." Advanced Materials 25, no. 9 (2013): 1296-1300.

[50] Varchon, François, R. Feng, Joanna Hass, Xuebin Li, B. Ngoc Nguyen, Cécile Naud, Pierre Mallet et al. "Electronic structure of epitaxial graphene layers on SiC: effect of the substrate." Physical review letters 99, no. 12 (2007): 126805.

[51] Echtermeyer, T. J., L. Britnell, P. K. Jasnos, A. Lombardo, R. V. Gorbachev, A. N. Grigorenko, A. K. Geim, A. C. Ferrari, and K. S. Novoselov. "Strong plasmonic enhancement of photovoltage in graphene." Nature communications 2 (2011): 458.

[52] Stankovich, Sasha, Dmitriy A. Dikin, Geoffrey HB Dommett, Kevin M. Kohlhaas, Eric J. Zimney, Eric A. Stach, Richard D. Piner, SonBinh T. Nguyen, and Rodney S. Ruoff. "Graphene-based composite materials." Nature 442, no. 7100 (2006): 282-286.

[53] Garrou, Philip, Christopher Bower, and Peter Ramm, eds. Handbook of 3D Integration: Volume 1-Technology and Applications of 3D Integrated Circuits. John Wiley & Sons, 2011.

[54] Sillon, N.; Astier, A.; Boutry, H.; Di Cioccio, L.; Henry, D.; Leduc, P., "Enabling technologies for 3D integration: From packaging miniaturization to advanced stacked ICs," Electron Devices Meeting, 2008. IEDM 2008. IEEE International , vol., no., pp.1,4, 15-17 Dec. 2008

[55] Vinet, M., P. Batude, C. Tabone, B. Previtali, C. LeRoyer, A. Pouydebasque, L. Clavelier et al. "3D monolithic integration: Technological challenges and electrical results." *Microelectronic Engineering* 88, no. 4 (2011): 331-335.

[56] Chatterjee, R.; Fayolle, M.; Leduc, P.; Pozder, S.; Jones, B.; Acosta, E.; Charlet, B.; Enot, T.; Heitzmann, M.; Zussy, M.; Roman, A.; Louveau, O.; Maitrejean, S.; Louis, D.; Kernevez, N.; Sillon, N.; Passemard, G.; Pol, Victor; Mathew, V.; Garcia, S.; Sparks, T.; Zhihong Huang, "Three dimensional chip stacking using a wafer-to-wafer integration," International Interconnect Technology Conference, IEEE 2007 , vol., no., pp.81,83, 4-6 June 2007

[57] Koester, Steven J., Albert M. Young, R. R. Yu, Sampath Purushothaman, Kuan-Neng Chen, D. C. La Tulipe, Narender Rana, Leathen Shi, Matthew R. Wordeman, and Edmund J. Sprogis. "Wafer-level 3D integration technology." IBM Journal of Research and Development 52, no. 6 (2008): 583-597.

[58] Yuan Xie, "Processor Architecture Design Using 3D Integration Technology," VLSI Design, 2010. VLSID '10. 23rd International Conference on , vol., no., pp.446,451, 3-7 Jan. 2010.

[59] D. Espalin, D.W. Muse, F. Medina, E. MacDonald, R.B. Wicker 3D printing multi-functionality: structures with electronics Int. J. Adv. Manuf. Technol.

[60] Kim, Min-Saeng, et al. "Direct metal printing of 3D electrical circuit using rapid prototyping." *International Journal of Precision Engineering and Manufacturing* 10.5 (2009): 147-150.

[61] MacDonald, E. R. I. C., et al. "3D Printing for the Rapid Prototyping of Structural Electronics." 1-1.

[62] Pease, R. Fabian, and Stephen Y. Chou. "Lithography and other patterning techniques for future electronics." *Proceedings of the IEEE* 96.2 (2008): 248-270.

[63] Leigh, Simon J., et al. "A simple, low-cost conductive composite material for 3D printing of electronic sensors." *PloS one* 7.11 (2012): e49365.

[64] Muth, Joseph T., et al. "Embedded 3D Printing of Strain Sensors within Highly Stretchable Elastomers." *Advanced Materials* 26.36 (2014): 6307-6312.

[65] Sarik, John, et al. "Combining 3D printing and printable electronics."

[66] Ready, Steven, et al. "3D Printed Electronics." *NIP & Digital Fabrication Conference*. Vol. 2013. No. 1. Society for Imaging Science and Technology, 2013.

[67] Garcia, C. R., et al. "Effects of extreme surface roughness on 3D printed horn antenna." *Electronics Letters* 49.12 (2013): 734-736.

[68] Kim, O.S., "Rapid Prototyping of Electrically Small Spherical Wire Antennas," *Antennas and Propagation, IEEE Transactions on* , vol.62, no.7, pp.3839,3842, July 2014

[69] L. Carin, N. Geng, M. McClure, J. Sichina, and L. Nguyen, “Ultra wideband synthetic-aperture radar for mine-field detection,” IEEE Antenna Propag. Mag., vol 41, no.1, pp. 18-33, Feb 1999.

[70] U. Schwarz, M. Helbig, J. Sachs, F. Seifert, R. Stephan, F. Thiel, and M.A. Hein “Physically small and adjustable double-ridged horn antenna for biomedical UWB radar applications,” IEEE ICUWB 2008, May 13, 2008, pp 5-8.

[71] Balanis, Constantine A. *Antenna theory: analysis and design*. John Wiley & Sons, 2012.

[72] Valderas, Daniel. *Ultrawideband Antennas: Design and Applications*. World Scientific, 2011.

[73] Federal Communications Commission Revision of Part 15 of the Commission's Rules Regarding Ultra-Wideband Transmission System from 3.1 to 10.6 GHz, Federal Communications Commission, FCC, ET-Docket, 98153, Washington, DC, 2002.

[74] P. J. Gibson, "The Vivaldi aerial," in Proc. 9th Eur. Microw. Conf., 1979, pp. 01105.

[75] H. Holter, T. H. Chio, and D. H. Schaubert, "Experimental results of 144- element dual-polarized endre tapered-slot phased arrays," IEEE Trans. Antennas Propag., vol. 48, no. 11, pp. 17071718, Nov. 2000.

[76] Lera, De. "A coplanar Vivaldi antenna with wide band balun proposal for the low frequency band of the SKA: approach to the FPA solution." MELECON 2006-2006 IEEE Mediterranean Electrotechnical Conference. 2006.

[77] Ebnabbasi, Khabat, et al. "Taper design of Vivaldi and co-planar tapered slot antenna (TSA) by Chebyshev transformer." Antennas and Propagation, IEEE Transactions on 60.5 (2012): 2252-2259.

[78] Langley, J. D. S., P. S. Hall, and P. Newham. "Novel ultrawide bandwidth Vivaldi antenna with low crosspolarisation." Electronics letters 29.23 (1993): 2004-2005.

[79] Lipson H., Kurman M. ,Fabricated: The New World of 3D Printing, 1st Edition, John Wiley Sons, 2013.

[80] MacDonald, E. R. I. C., et al. "3D Printing for the Rapid Prototyping of Structural Electronics." 1-1.

[81] Xu, Zhe, Svetoslav Kolev, and Emanuel Todorov. "Design, Optimization, Calibration, and a Case Study of a 3D-Printed, Low-cost Fingertip Sensor for Robotic Manipulation."

[82] Garcia, C. R., et al. "Effects of extreme surface roughness on 3D printed horn antenna." Electronics Letters 49.12 (2013): 734-736.

[83] Garcia Lopez, A.; Lopez C, E.E.; Chandra, R.; Johansson, A.J., "Optimization and fabrication by 3D printing of a volcano smoke antenna for UWB applications," Antennas and Propagation (EuCAP), 2013 7th European Conference on , vol., no., pp.1471,1473, 8-12 April 2013

[84] Wang, Zhiming, and Hong Zhang. "Improvements in a high gain UWB antenna with corrugated edges." Progress In Electromagnetics Research C 6 (2009): 159-166.

[85] Guo-Min Yang; Xing, X.; Daigle, A.; Liu, M.; Obi, O.; Stoute, S.; Naishadham, K.; Sun, Nian X., "Tunable Miniaturized Patch Antennas With Self-Biased Multilayer Magnetic Films," *Antennas and Propagation, IEEE Transactions on* , vol.57, no.7, pp.2190,2193, July 2009.

[86] White, C.R.; Rebeiz, G.M., "Single- and Dual-Polarized Tunable Slot-Ring Antennas," *Antennas and Propagation, IEEE Transactions on* , vol.57, no.1, pp.19,26, Jan. 2009

[87] Sivalingam, P.; Sooliam Ooi, "Electronically tunable monopole antenna," Antennas and Propagation Society International Symposium, 2008. AP-S 2008. IEEE , vol., no., pp.1,4, 5-11 July 2008